Republic of Iraq
Ministry of Higher Education
and Scientific Research
University of Babylon
College of Engineering
Mechanical Engineering Department

Influence of Internal Fins using a Nanofluid on Heat Transfer Through a Parabolic Trough Collector

A Thesis

Submitted to the College of Engineering / University of Babylon in Partial Fulfillment of the Requirements for the Degree of Master in Engineering / Mechanical Engineering / Power

By

Mujahid Kalaf Badr Mizeal

Supervised By

Prof. Mr. Farooq Hassan Ali

Ass. Prof. Dr. Mohsin Sheikholeslami

2022 A.D.

قُلْ هَلْ يَسْتَوِي الَّذِينَ يَعْلَمُونَ وَالَّذِينَ لَا يَعْلَمُونَ ۗ إِنَّمَا يَتَذَكَّرُ أُولُو الْأَلْبَابِ

سورة الزمر ، آية (٩)

Supervisor Certification

We certify that the preparation of this thesis, entitled " **Influence of Internal Fins using a Nanofluid Through a Parabolic Trough Collector** " prepared by " ***Mujahid Kalaf Badr***" under our supervision at the Department of mechanical Engineering, College of Engineering, University of Babylon, as a partial fulfillment of the requirements for the degree of Master of Science in Mechanical Engineering (power).

Signature:

Prof. Mr. Farooq Hassan Ali

(First supervisor)

/ /2022

Signature:

Ass. Prof. Dr. Mohsen Sheikholeslami

(Second supervisor)

/ /2022

Dedication

To

- *My dear mother*
- *The soul of my beloved father*
- *All my Supervisors*
- *My brother and sisters*
- *My dear wife*
- *Scholarship friends*

I dedicate this work

Mujahid Kalaf Badr 2022

Acknowledgments

(*In The Name of Allah, The Gracious, The Merciful*)

(*Thanks to Allah for his guidance and help*)

I wish to express my sincere thanks and deep gratitude to my supervisors ***Prof. Farooq Hassan Ali*** *and* ***Prof. Dr. Mohsin Shiehkoeslami*** *for their invaluable help, advice and encouragement during the various stages of the present work.*

I would like to thank the President University of Babylon ***Prof. Dr. Kahtan Aljobory*** *and the head of the department* ***Prof. Dr. Samer Mohammad Abd - Alhaleem*** *and the staff of Mechanical Engineering Department at the University of Babylon especially* ***Prof. Dr. Saba Yasoob*** *for the great cooperation she appeared during the search preparation period.*

My deepest thanks, love and gratitude for all of my family. This work would not have been completed without their love and continuous support.

Mujahid Kalaf Badr Al-Tamimi

٢٠٢٢

Abstract

Current study presents a numerical investigation for three dimensional turbulent flow using the MCRT method to simulate solar radiations as a heat flux and the finite volume method in Ansys Fluent (18.1) to simulate the equations. The fluid in absorber is a synthetic oil having eight hundred index mixed with Aluminum Oxide nanoparticles to enhance the heat transfer process. The study comparing different cases, including different numbers of longitudinal fins of (5mm height, 2mm width) assembled inside the absorber with two arrangements and three particular Reynolds number in addition to test concentration ratio of the heat flux using the MCRT method. The impact of using three different numbers of fins (2, 4 and 6) at two different arrangements ("a" and "b") were presented. The three Reynolds number used in the study (18600, 23000 and 28000). Two Rim angles of the collector are tested (80^{o}) and (120^{o}), results showed that (120^{o}) was achieved high outlet temperature with a concentration ratio (CR=82.47) and the nanofluid volume ratio of (0.04) . The effects on outlet temperature, friction factor, Nusselt number, and then on the performance evaluation criterion (PEC) of the absorber tube are displayed. The results of the study proved that using nanofluid and finned absorber can increase the absorber hydrothermal performance and using (6) fins of arrangement "b" shows better performance in terms of heat transfer than arrangement "a". An enhancement in the PEC reached (6.0845%) at Reynolds number of (18600) and (6) fins with the "b" arrangement compared with the smooth pipe. The conclusions stated that when using high number of internal fins gives better performance and high heat transfer enhancements.

Nomenclature

Latin Symbols

Symbol	Description	Unit
C_p	Specific heat at constant pressure	J/Kg.K
D_i	Inner diameter of pipe	M
F	Friction factor	-
G_k	Rate of turbulent kinetic energy generation	M^2/s^2
K	Thermal conductivity of fluid	W/m.K
TKE	Turbulent kinetic energy	m^2/s^2
Nu	Nusselt number	-
P	Pressure	Pa
Re	Reynolds number	-
S	Modulus of the mean rate of strain tensor	1/s
T	Temperature	K
U	Velocity	m/s
$-\rho\overline{\ddot{u}_i\ddot{u}_j}$	Reynolds stresses	N/m
Pr	prandtle number	[-]
U_{in}	The velocity of the inlet fluid	m/s

Greek Symbols

Symbol	Description	Unit
ε	Turbulent dissipation rate	m^2/s^3
ϕ	Volume fraction	-
ρ	Density	Kg/m^3

ν	kinematic viscosity	m^2/s
M	Dynamic viscosity of fluid	kg/m.s
σ_ε	turbulent Prandtl number for ε	-
σ_K	turbulent Prandtl number for K	-

Abbreviations

Abbreviation	**Description**
PTC	Parabolic Trough Collector
CFD	Computational Fluid Dynamics
FVM	Finite Volume Method
B.C	Boundary Condition
PEC	Performance evaluation criterion
CSP	Concentrated Solar Power

Subscripts

Symbol	**Description**
bf	base-fluid
B	Bulk
nf	Nanofluid
np	nano-particle
t	turbulent kinetic energy
w	Wall

Contents

Chapter One

Introduction

Chapter One: Introduction

1.1 Introduction

In the heat transfer industry there are many types of energy sources like the wind energy, Geo-thermal energy, water falls energy and solar energy . The solar energy power systems also classified into several types such as the photovoltaic systems and concentrating solar power systems (CSP) which contains four main systems (parabolic trough collectors, linear Fresnel's, central receivers and parabolic dish), the main difference that could be noticed of the parabolic dish from the three other types is the mechanism of angle tracking where it is double axis tracking (up -down and left-right) in the parabolic dish while utilizing the single axis mechanism in the other three types [1].

Parabolic Trough Collectors are effective tool for the conservation and transfer of thermal energy where the temperature arriving the absorber being 70 times the temperature of incident on the parabolic trough. The solar energy systems are characterized by using the solar energy which is free cost and also they are free of pollutions products such as CO_2. The recent years witnessed a growing importance in energy conversion systems and their applications in the practical fields.

1.2 Types of solar energy power systems [1]:

Solar energy power systems are critical to the development of industry and the expansion of human electrical demands. The Future of Solar Energy focuses solely on the two well recognized types of technologies: converting solar energy into electricity, photovoltaic (PV) and concentrated solar power (CSP) which also known as solar thermal in their present and conceivable future forms. Because the energy supply facilities often endure several decades, solar power generating technologies

in these classes will predominate. The researchers don't make any climate predictions for two reasons: First, the massively increasing of the solar business from its current is very small scale that results in the developments that it is not claim to be able to anticipate today. Second, it is realized that future solar deployment will be strongly reliant on unknown future market circumstances and public policies, such as measures targeted at reducing global climate change.

1.3 Scope of the Current Work

By reviewing the related studies, it is found that most of them used one or two techniques to enhance the heat transfer rate, while in this study the novelty goes to consider four techniques to enhance the performance of the PTC. These techniques are rim angle of (80º, 120º), number of fins (2,4 and 6), fins arrangements (type "a" and type "b") as well as using AL_2O_3/Syltherm 800 as a Nano fluid with 4% volume ratio of Nano material. In addition to the mentioned techniques, the study consider the Surface plots of the MCRT simulation of the collector for two different Rim angles (80º and 120º) to figure out which angle gives higher temperature to the absorber tube where the volume under the surface could be calculated which represents the amount of heat flux absorbed by the collector.

1.4 Concentrated Solar Power (CSP) technologies:

Figure (1-1) illustrates the three types of concentrated power systems, which are (Parabolic Trough Collectors, Linear Fresnel, and Central Receivers).

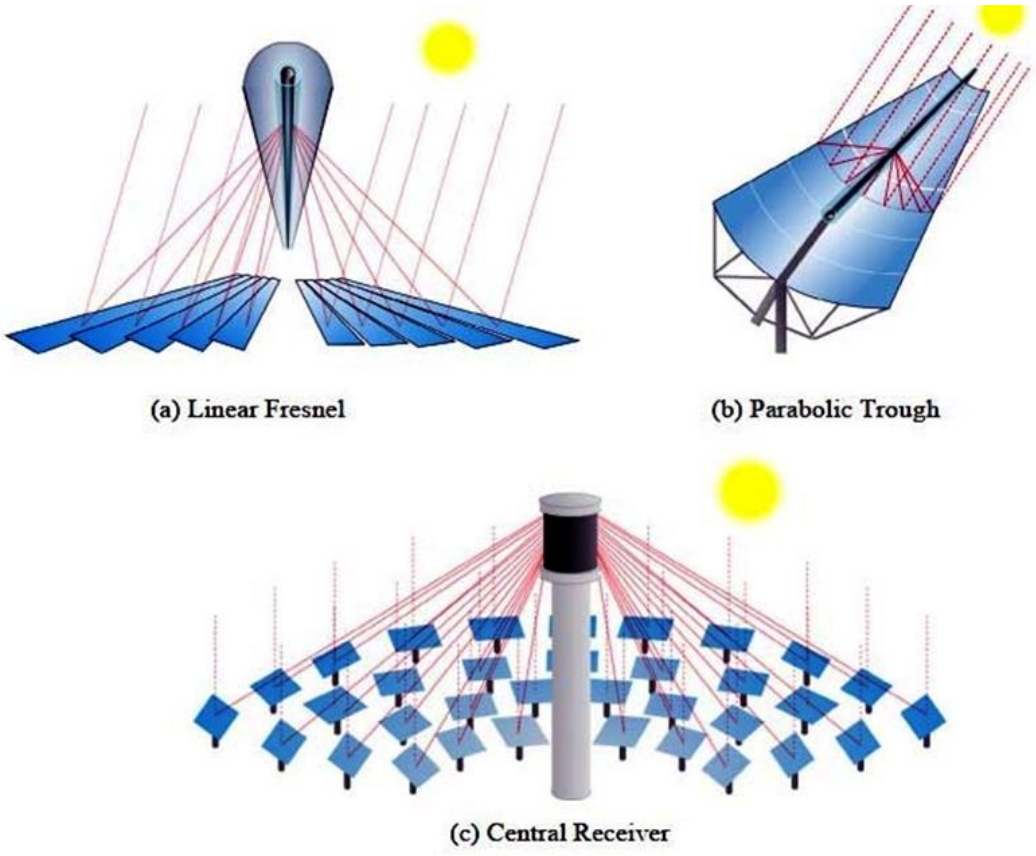

Figure (1-1) Different Types of Concentrated Solar Power

(Nicholas Kincaid et al.) [1]

1.5 Thesis Organization:

The present work concentrated on the following objectives: -

1- Validating of the numerical study results obtained from the current investigation (Nusselt number Nu and heat transfer coefficient h) with results matches of another research by using the Monte Carlo Ray Tracing (MCRT) model in the optimization compute of flow and heat transfer inside the absorber tube.

2- Numerically analyzing of the flow and heat transfer in the absorber tube of the Parabolic Trough Solar Collector (PTSC), figures for the temperature contour, velocity contour and turbulent kinetic energy

contour at the outlet flow of the absorber taken. Numerical results are found for the turbulent flow with three dimensional, steady state system at Reynolds number (Re=18600, 23000 and 28000) in the range. The results were chosen to focus on these cases: -

a- smooth absorber tube.

b- finned absorber with (2, 4, and 6) 5mm height, 2mm width longitudinal fins.

c- two arrangements of "a" and "b".

d- a certain nano-material (Al_2O_3) in the base fluid (Syltherm 800) of a volume fraction (4%).

3- Obtaining the effect of fins usage with the effect of the increasing of the Reynolds numbers on the Nusselt number, T_{out}, friction factor and heat transfer enhancement. The governing equations of incompressible continuity, momentum and energy equations are solved by using the commercial computational fluid dynamics finite volume method " Ansys Fluent 18.1" for computer program with assuming appropriate boundary conditions.

4- Calculating the performance evaluation criteria (PEC) which represented the heat transfer efficiency and the percentage efficiency (PEC%).

Chapter Two

Literature Review

Chapter Two: Literature Reviews

The last recent years (2011 - 2021) witnessed a great interesting of studying and developing the alternative power sources than the traditional sources which used the fossil fuel, The studies that focused on Enhancement of the techniques that used the solar energy is dramatically increased. The Parabolic Trough Collector (PTC) is one of the most efficient techniques took the researchers attention. The physics of the heat transfer to the flowing fluid inside the absorber tube with high Reynolds number had much attention by many researchers with increasing computational abilities of computer programs.

The purpose of present study is to figure out the enhancement achieved in heat transfer between the environment and the heat transfer fluid (HTF) flowing inside the absorber tube of the Parabolic Trough Collector (PTC) by using internal longitudinal fins with the Nano fluid of numerical investigations adopted.

This chapter investigate improvements in the heat transfer of Parabolic Trough Collector studies as well as the parameters affected the enhancement of the PTC's efficiency.

2.1 Numerical and Experimental Studies in Parabolic Trough Collector Systems

In this section, the studies related with the enhancements in performance and heat transfer efficiency of the Parabolic Trough Collectors will be investigated as well as the different parameters related with the performance.

Ricardo Vasquez Padilla et.al (2011) [2] in this research, the 1-D analysis of heat transfer in (PTC) were conducted using a closed envelope

around the absorber with vacuum to reduce dissipation in heat and found that when reducing the dissipation, it gave more enhancement in achievement of the system performance.

F.J. Cabrera et.al (2013) [3] The performance of solar Cooling systems investigated by using parabolic trough collectors (PTC) and flat plate collectors (FPC). The investigation showed that PTC more efficient to increase efficiency and reduce costs than the evacuated tube collectors (ETC) and compound parabolic collectors (CPC) and similar levelized cost of energy for cooling that flat plate collector (FPC).

Y. Wang et.al (2014) [4] studied different parameters of the PTC system such as thermal stresses and thermal deformation that accompanied with the flow. Using the finite element method (FEM), Also investigated numerically the effects of the parameters on the performance of the receiver. The deformations of the absorber and the thermal stress were much more than the glass cover.

Ramchandra G. Patil et.al (2014) [5] The researchers investigated the influence of various parameters on thermal losses in a parabolic solar collector. It was found out that heat loss increased as the wind speed increases and pipe diameter increases, overturned the impact of different parameters on improving the performance of a Parabolic Trough Solar Collector (PTSC) and reducing thermal dissipations. It was discovered that thermal losses depend on pipe diameter and velocity, while it didn't depend on wind speed for a receiver with a peak.

Wang Fuqiang (2015) et.al [6] examined the use of glass cover (GC) with elliptical-circular cross section and its effect on performance of a parabolic circulation collector to reduce the risks of receiver failure and the induced thermal stresses that resulting from the uneven heat flux distribution and cyclic weather. The results showed that the heat flux

distribution through the passage of the elliptical shell over the circular cross-section has been reduced and the efficiency of the system lowered, while the heat flux gradient decreased and the peak flux reduction was up to 32.3%.

Amina Benabderrahmane et.al (2016) [7] offered 3-D numerical study and employed the gathering of two techniques that improved the heat transfer significantly these techniques are the using of rectangular and triangular fins and various types of nanoparticles with a certain concentrations, the enhancement of Nusselt number in the absorber was between (1.3 to 1.8) times of the absorber without fins (smooth), the fraction factor changes range from (1.6 to 1.85) than smooth tube.

Evangelos Bellos et.al (2016) [8] studied different kinds of nanofluids in the PTC in this study at the suitable temperature for each. The results showed that there were variations of the energetic and exergetic from nanofluid to other and .or a certain temperature for each case, as well as the pressurized water was the most proper working fluid for temperature range of 277ºC, whereas for the temperature above 827ºC , the only nanofluids for that was the Helium and carbon dioxide.

Yanjuan Wang et.al (2016) [9] investigated the use of (AL_2O_3)/synthetic oil and compared that with the conventional synthetic oil, demonstrated the effects of using nanoparticles, it was` found that the increasing of AL_2O_3 concentration from (0% to 5.0%) enhanced the performance of the PTC, the maximum temperature and the temperature gradients of the absorber decreased with the increase of the nanoparticle. Moreover diminish the thermal stress and the absorber deformation.

Gong Xiangtao et.al (2017) [10] used pin fin arrangement and adopted the Finite Volume Method (FVM) coupled with the Monte Carlo ray tracing method (MCRT) to investigate the flow characteristics of the

absorber and the heat transfer performance for PTC system. The enhancement of the heat transfer performance was achieved as the numerical results indicated. The overall heat transfer performance was significantly enhanced with the use of pin fin arrays inserting.

E. Bellos and C. Tzivanidiz 2017 [11] studied the behavior of the parabolic trough collector using various nano particles (CuO and Al_2O_3) and the third case examined with Syltherm 800 alone which gave less efficient than the nano fluids cases. The results showed that the heat transfer enhancement was 50% at high levels of temperature. The thermal efficiency increased in case of low flow rate and when maximize the concentration ratio of nano fluid.

Jain Jin et.al (2017) [12] investigated the new method of the symmetry principle and dimensional analysis and thermal performance analysis of (PTC) for applications of solar thermal, investigated different lengths with various particle solar collectors to evaluate the thermal efficiency. It was concluded that the efficiency of the collector has been raised with increasing the Direct Normal Irradiance (DNI) of the sun and decreasing when the air humidity enhanced which means the temperature difference between the receiver fluid and the ambient air (ΔT_a) increasing.

J. Subramani et.al (2017) [13] studied the effect of using TiO_2/DI–H2O (De-Ionized water) nanofluid to enhance the efficiency of the PTC by using different concentrations at a different flow rates and studied the flow and heat transfer characteristics of the nanofluids, the coefficient of the convective heat transfer was improved. It was found that by using TiO_2 as a nanofluid with 0.2 % as concentration ratio leads the efficiency to be maximum enhancement (8.66% higher than the water-based collector) and the heat transfer coefficient to have a considerable rise.

A. Mwesigye and J.P. Meyer (2017) [14] investigated the optimum thermodynamic and thermal operating conditions of the PTSC using various Nano fluids which are (AL_2O_3-Therminol VP-1, silver-Therminol VP-1 and copper-Therminol VP-1), the influence of the use of Nano fluids on system efficiency shows that the Using nanofluids will make heat transfer better and improves the thermodynamic performance which depend on the inlet temperature. The thermal efficiency was increased by (5%) when the concentration ratio of the Nano fluids raised from (88 to 113) at the same flow rate. In addition to that the highest thermal performance with silver/therminol VP-1, and the lower thermal performance was shown with Al2O3-Therminol VP-1.

Evangelos Bellos et al (2018) [15] investigated different arrangements of the internal extended surfaces and the best number of them in the absorber of the PTC which gives most heat transfer and thermal efficiency improvement. It was concluded from the results that the internal extended surfaces should be placed in the lower portion of the absorber were the heat flux being biggest amount at that part. For good performance, (3) fins should be utilized in the lower part rather than the upper part of the absorber which gives lower improvement of the performance.

Q. Wang et.al (2018) [16] studied the way of getting heat energy by using the range of temperatures between (673K to 823K), and to reduce the heat losses, a radiation shield (RS) used for the high temperatures to improve the thermal performance of the receiver. When absorber temperature exceeding (823K), a superior performance was showed for the solar receiver without solar selective absorbing coating on the outer surface of the RS. When the temperature of the absorber reached (823K), the percentage of heat loss reduction with solar selective absorber coating was less than of without selective absorbing coating.

Q. Wang Et.al (2018) [17] investigated how to reduce heat dissipation from the absorber when the PTC operating at high temperature ranges, and Since there is an irregularity of solar irradiation arrived the tube so inner Transparent Radiation Shield (TRS) used for that purpose. Numerically studied, the model satisfied consistency with experimental results. A good performance was observed for the absorber rather than classical receiver.

Man. Fan et.al (2018) [18] discussed the fluctuation of the Monte Carlo Ray Tracing (MCRT) method in the optical simulation, to reduce the fluctuation and runtime as the Monte Carlo ray tracing takes longer runtime and Higher computing cost. For parameters exerted effects on the simulation results. An optimized MCRT model was suggested by the iteration method being combined with the MCRT method. The model used has the advantages such as improve the accuracy, reduce the fluctuation and relieve the runtime of MCRT method.

D.Korres et.al (2018) [19] studied the enhancements of thermal efficiency and the enhancement in the heat transfer coefficient using a nanofluid in compound parabolic collector with range of temperature (298K up to 573K). There was a significant enhancement in the overall efficiency up to 2.76% with the nanofluid used. The flow was laminar and the nanofluid of Syltherm 800/CuO with 5% volumetric ratio of nanoparticle, the enhancement of the exergy efficiency was up to 2.6%.

A. Amine et.al (2018) [20] examined the development of a model using Direct Steam Generation (DSG) process with different real working conditions, so can replace the synthetic oil in the future studies and experimental. By investigating the comparative of the effect of various parameters on the thermal gradient around the absorber tube. It was shown from the analysis that the highest thermal gradient exist in the superheated

region and the risk of thermal bending also exist with the damage risk and thermal bending.

Ze-Dong Cheng et.al (2018) [21] displayed the applications of the optical efficiency fitting formulas for the parabolic trough collectors and the computing methods of these formulas, in addition to the combining of the Monte Carlo ray-tracing method with the population based particle swarm optimization algorithm. It was discovered that the calculation time will be reduced as a consequence of the optimization process and the system being efficient with optimized parameters and it was useful for the simulation by reducing 90% of the particle swarm optimization computing time that was less than (10^{-7} second) as a time of the annual optical efficiency.

Pablo D Tagle-Salazar et.al (2018) [22] studied and analyzed heat dissipation in solar receivers and discovered that the use of coating for absorber pipes reduced thermal losses and improved collective performance. The investigation focused on the effect of using alumina nanoparticle combined with water on the thermal efficiency estimations of the solar collector. The experiments showed that utilizing nanoparticles can play a major role for developing the efficiency of the system. the study used the Engineering Equation Solver (EES) as a software for the model simulation.

Chun Chang et.al (2018) [23] analyzed the convective heat transfer of the molten salt and the flow in the parabolic trough collector using a concentric and eccentric rods inserted in the receiver to introduce turbulence and obtain the enhancement of the overall heat transfer performance and the reliability. It was found that both concentric and eccentric rod insert could effectively enhance the performance of the heat transfer. The Nusselt number was 1.10 to 7.42 times over the normal

receiver when the diameter of the concentric rod increasing, but for a certain dimensionless diameter bigger than 0.8 the integrated performance factor decreased significantly with the increase of Reynolds number. For the eccentric rod both of the integrated performance factor and the performance evaluation criteria decreased with increasing of Reynolds number under a certain dimensionless eccentricity.

M Vahabzadeh et.al (2019) [24] used the annular porous medium as well as the additional particles of high thermal conductivity nanoparticle Al_2O_3 (Alumina) for various parameter values like degree of concentration and Reynolds number and studied the enhance in heat transfer inside the receiver. It was found that the parameters such as (pressure drop , heat transfer and thermal efficiency) increased with the increase of volume fraction and Reynolds number. The overall efficiency increased by 5% and 14% , the exegetics efficiencies by 7% and 15% when the inlet temperature were 500 and 600 K respectively.

E. Bellos and C. Tzivanidis (2018) [25] studied the most common ways of improving the performance of (PTC) by using different nanoparticles (Cu, CuO, Fe_2O_3, TiO_2, Al_2O_3 and SiO_2) with synthetic oil (Syltherm 800) at different flow rates 50 to 300 L/min using the Engineering Equation Solver for the developed thermal model. The temperature at the inlet was (27ºC to 377ºC) and the volume fraction of 6% noticing the best improvements when reducing the flow rates, rising the inlet temperature and enlarging the volume fraction of the Nano fluids. found that the thermal efficiency enhancement was 31%, 54% and 74% for Cu with 2%, 4% and 6% as a concentrations ratios respectively.

E. Bellos and C. Trivanidis (2019) [26] A special technique used to increase the effectiveness of the collector by reducing optical losses at the trough end. Used the steady-state conditions overall analysis and the yearly

optical enhancements evaluations with use of the focal distance to the length ratio of 0.236 were found 21.7%. the optical enhancements were 8.% in June, 24.2% in September and 77.1% in December. The final results showed that the use of an extra booster gives a thermal and optical improvements at greater angles of incident .

Ramesh K. Donga and Suresh Kumar (2019) [27] presented the thermal and optical analysis for PTSC system with surface slope error of mirror and absorber tube misalignment, the factors affecting the PTSC's thermal efficiency were examined using the Finite Volume Method. It was discovered that the factors like absorbent tubes misalignment (15mm in two directions), mirror positioning and absorber tube diameter (70mm and 80mm where taken) are the factors which influenced on the collector thermal efficiency. The overall collector efficiency decreased by 11% when using 70mm diameter tube and absorber dislocation in the slope error presence.

F. Razmmand et.al (2019) [28] Investigated the effects of adding nanoparticles to the pure water numerically in order to avoid reaching the critical heat flux point through the receiver tube of the PTC system which leads the troubles of thermal fluctuating and failure of the absorber. The use of pure water gives less heat transfer than of using a nanoparticle with different volume concentrations, and specifically Al and Au will give almost twice times the critical length (the distance at which the critical heat flux occurs). Used 2% as a volume ratio of Au-H_2O and Al-H_2O showed 2.7 and 2.3 times the critical length for the pure water.

M.M. Heyhat et.al (2019) [29] studied the main experimental examination used the Nano fluid and metal foam in separate mean, and their combination and studying their influence on the thermal performance of direct absorption parabolic trough solar collector (DAPTSC). The better

mixing of the flow and the superior properties can lead to lower thermal losses. The results showed that both Nano fluid and metal foam were good absorbers. Furthermore, the maximum temperature difference was found with the combination of the metal foam and Nano fluid.

Recep Ekiciler et.al (2020) [30] investigated different hybrid nanofluid at turbulent flow in a (PTC) absorber, various volume fractions also used. The results of the study proved that all Hybrid nanofluids offer notability over the base fluid (Syltherm 800). Ag–ZnO/Syltherm 800, Ag–TiO2/Syltherm 800, and Ag–MgO/Syltherm 800 hybrid nanofuids with 1.0%, 2.0%, 3.0%, and 4.0% nanoparticle volume fractions were used as

working fluids. The hybrid nanofluid Ag-MgO/Syltherm 800 with 4% nanoparticle volume concentration found to be the most efficient as a working fluid.

Bellos Evangelos et.al (2020) [31] Investigated the thermal enhancement in PTC. Studied three different types of collectors (evacuated tube receiver, the non-evacuated tube and the bare tube without cover). The investigated systematic parametric. The results showed that with the cases of higher heat losses will get the maximum enhancements and most of the performance enhanced with the use of Nanofluids in the bare tube rather than the non-evacuated tube receiver and the evacuated tube receiver. The values of thermal enhancement was 17.11%, 12.30% and 12.24% respectively.

Table (2-1) Tabulating of the numerical and experimental studies in the literature review

The Reference	**Type of the Work**	**Remarks**
Ricardo V. Padilla , 2011 [2]	Numerical	PTC / Receiver with evacuated envelop
F.J. Cabrera, 2012 [3]	Numerical	PTC / refrigeration and air-conditioning applications
Yanjuan Wang , 2015 [4]	Numerical	PTC / SRT method and FEM
Ramchandra G. Patil ,2014 [5]	Numerical	PTC / non evacuated receiver
Wang Fuqiang, 2015 , [6]	Numerical	PTC / MCRT, effects of a glass cover (GC) on heat flux distribution
B. Amina , 2016, [7]	Numerical	PTC / Longitudinal fins and Nano fluid
Evangelos Bellos , 2016, [8]	Numerical	PTC / Different working fluids investigated
Yanjuan Wang, 2016 , [9]	Experimental	PTC / Applications of nano fluid on PTC performance
Gong Xiang 2017 [10]	Numerical	PTC / Pin Fins
Evangelos Bellos 2017 [11]	Numerical	PTC / various nano fluids
Jian Jin 2017, [12]	Numerical	PTC / combining Monte-Carlo ray-tracing method with finite-element is developed to analyse the performance of PTCs
J. Subramani , 2017, [13]	Numerical and Experimental	PTC / Turbulent regime, TiO_2/Di-H_2O

Aggrey Mwesigye , 2017 , [14]	Numerical	PTC / Different Nano fluids and concentrations
Evangelos Bellos , 2018, [15]	Numerical	PTC / Longitudinal Fins
Qiliang Wang . 2018 [16]	Numerical	PTC / Radiation Shield
Qiliang Wang. 2018 [17]	Numerical	PTC / Inner radiation shield
Man Fan, 2018 [18]	Numerical	PTC / MCRT method
Dimitrios Korres, 2018 [19]	Numerical	PTC / compound parabolic collector with laminar flow
Ahmed Amine Hachicha , 2018 [20]	Numerical	PTC / Direct steam generation
Ze-Dong Cheng , 2018 [21]	Numerical	PTC / combining the Monte Carlo ray-tracing methodology with the population based particle swarm optimization algorithm
Pablo D. Tagle-Salazar , 2018, [22]	Numerical and Experimental	PTC / Alomina-water nanofluid, Heating applications
Chun Chang , 2018 ,[23]	Numerical	PTC / Three Dimensions, Rods in the receiver and molten salt as (HTF)
M. V. Bozorg , 2019, [24]	Numerical	PTC / Internal annular porous structure and synthetic oil–Al2O3 nanofluid
Evangelos Bellos and Tzivanidis 2019, [25]	Numerical	PTC / use of various nanoparticles, flow rate and inlet temperatures
Evangelos Bellos , 2018 [26]	Numerical	PTC / Various Nano particles
Ramesh K. Donga,2019 [27]	Numerical	PTC / thermal performance of a

		parabolic trough collector with absorber tube misalignment and reflector slope error
Farhad Razmmand , 2019 , [28]	Numerical	PTC / Steam direct generation, critical heat flux
M. M. Heyhat , 2019 , [29]	Experimental	PTC / utilizing of Nano fluid and metal foam porous medium
Recep Ekiciler-2020 [30]	Numerical	PTC / Hybrid fluids
Evangelos Bellos. 2020 [31]	Numerical	PTC/ Nano fluid

Chapter Three

Theoretical work

Chapter Three: Theoretical Work

3.1 Introduction

This chapter deals with the CFD numerical analyses of three dimensional turbulent flow and heat transfer in a circular pipe (absorber) of the PTC, which show the velocity, temperature, Turbulent Kinetic Energy (TKE) distribution, coefficient of heat transfer, Nusselt number (Nu) and friction factor (*f*). The effect of the rim angle of the reflector on the outlet temperatures, As well as the Performance Evaluation Criteria (PEC). The PEC of the Parabolic Trough Solar Collector (PTSC) must be determined using the present model which can predict the optimization of the heat transfer in the absorber.

3.2 Model description of present study:

In this study, the simple design of the receiver tube used in the Parabolic Trough Solar Collector (PTSC) numerical analysis as shown in Figure (3-2) that is neglecting the effect of the supports were considered as well as the central rod effect. The inner and outer diameters of the tube are (D_i=66mm) and (D_o=70mm) respectively. The length of the tube as a model simulated is 1500mm. The number of fins studied are (2, 4 and 6) respectively with a certain arrangement ("a" arrangement) and the same number repeated with another arrangement ("b" arrangement) as shown in figure (3-1). The variables of the study are Reynolds number, number of fins, arrangement of fins and reflector rim angle. The results of parameters for each case such as Nusselt number, friction factor and performance evaluation criteria (PEC) will be numerically investigated and to be compared to each other so as to recognize which values will be useful and resulting in best heat transfer enhancement to be considered, all the

parameter values that discussed in the last paragraph will calculated for each fin number category taken with different Reynolds numbers (18600, 23000 and 28000). The height of the internal fins used to enhance the heat transfer is (5mm). The considered heat flux direct normal irradiation DNI is (1000W/m²), The choice of direct normal irradiation (DNI= 1000 W/m2) in the present study is because it is very close to the readings recorded in the Babylon province during the Summer season, the solar global pyranometer measurement is 1031 W/m2 (Sabah A., (2018)) [48].

Using the Alumina (Al_2O_3) as a nanomaterial (nanoparticles) with volume ratio (4%) and the Syltherm 800 as a base fluid. The model drawn using the solid work program.

Fin arrangement		
	Type (a)	Type (b)
n=2	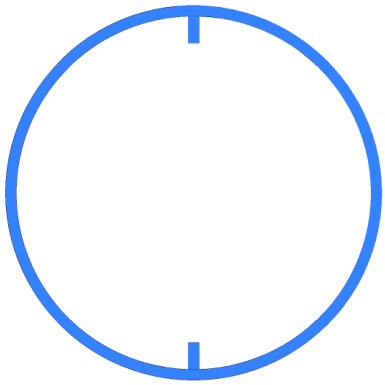	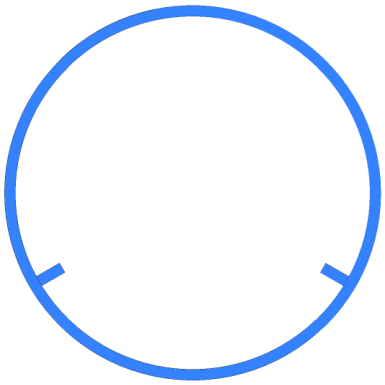
n=4	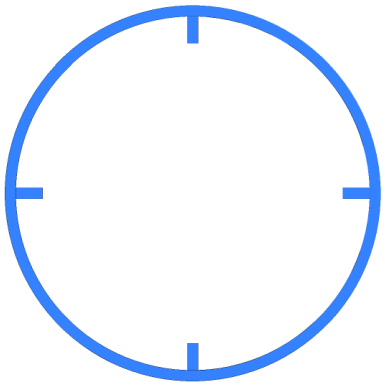	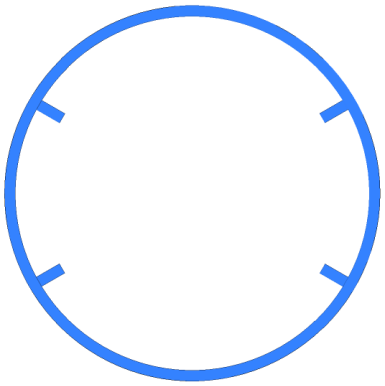

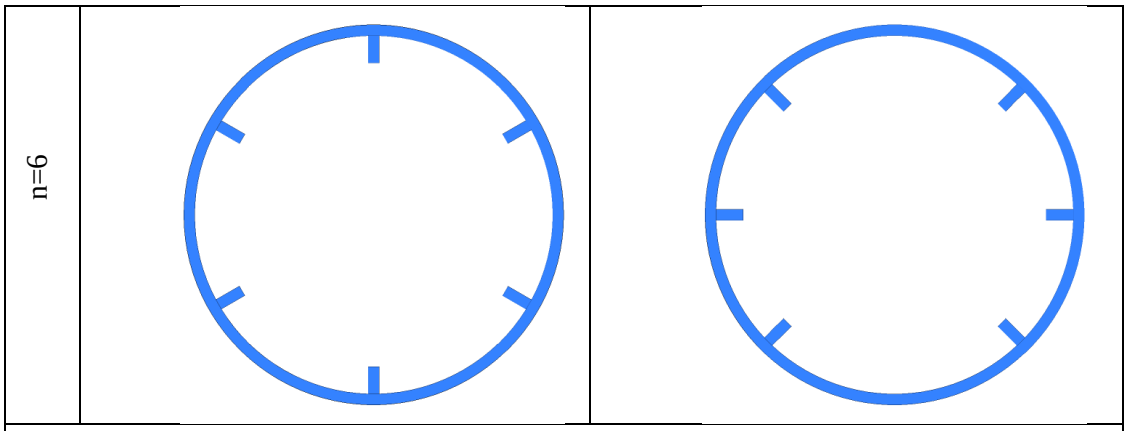

Figure (3-1) The studied absorber tube with different number and arrangement of fins.

3.3 Estimation of Heat Flux Concentration around the Absorber Tube

There are several ways to find the distribution of heat flux around the pipe as below :

1) Utilizing ANSYS FLUENT software for pure radiation heat transfer
2) Utilizing Sol-trace to extract the heat flux. The basic method of this software is based on the Monte Carlo method which is utilized in the present study.

The software tool called Sol-Trace developed by the National Renewable Energy Laboratory (NREL) for concentration modeling of Solar Power Systems (CPS) and optical performance analyzing.

The Sol-Trace can be used to model many general optical systems as well as the solar applications. The code of the Sol-Trace uses the Monte-Carlo ray-tracing methodology to select a number of rays that need to be traced. The Sol-Trace also suitable for modeling the Linear Fresnel, Parabolic Trough Collectors, Point Focus Optical systems (solar furnaces and dishes) and power tower geometries as well as analyze their performance. Sol-Trace specifically written for windows 2000 as

environment of operation. The methods of ray tracing coupled with memory capabilities and the speed of the windows 2000 operating conditions provide for rapid and accurate results. The minimum required software practically is windows 2000 OS, a 700MHZ Intel Pentium class processor, 128M system memory and a 1024x768 display (1280x1024 is preferable). The rays number and the geometry (project size) specify the speed of the process and the code can run on slower systems with less memory. The code utilizes ray tracing methodology (Spencer and Murty , 1962) [51].

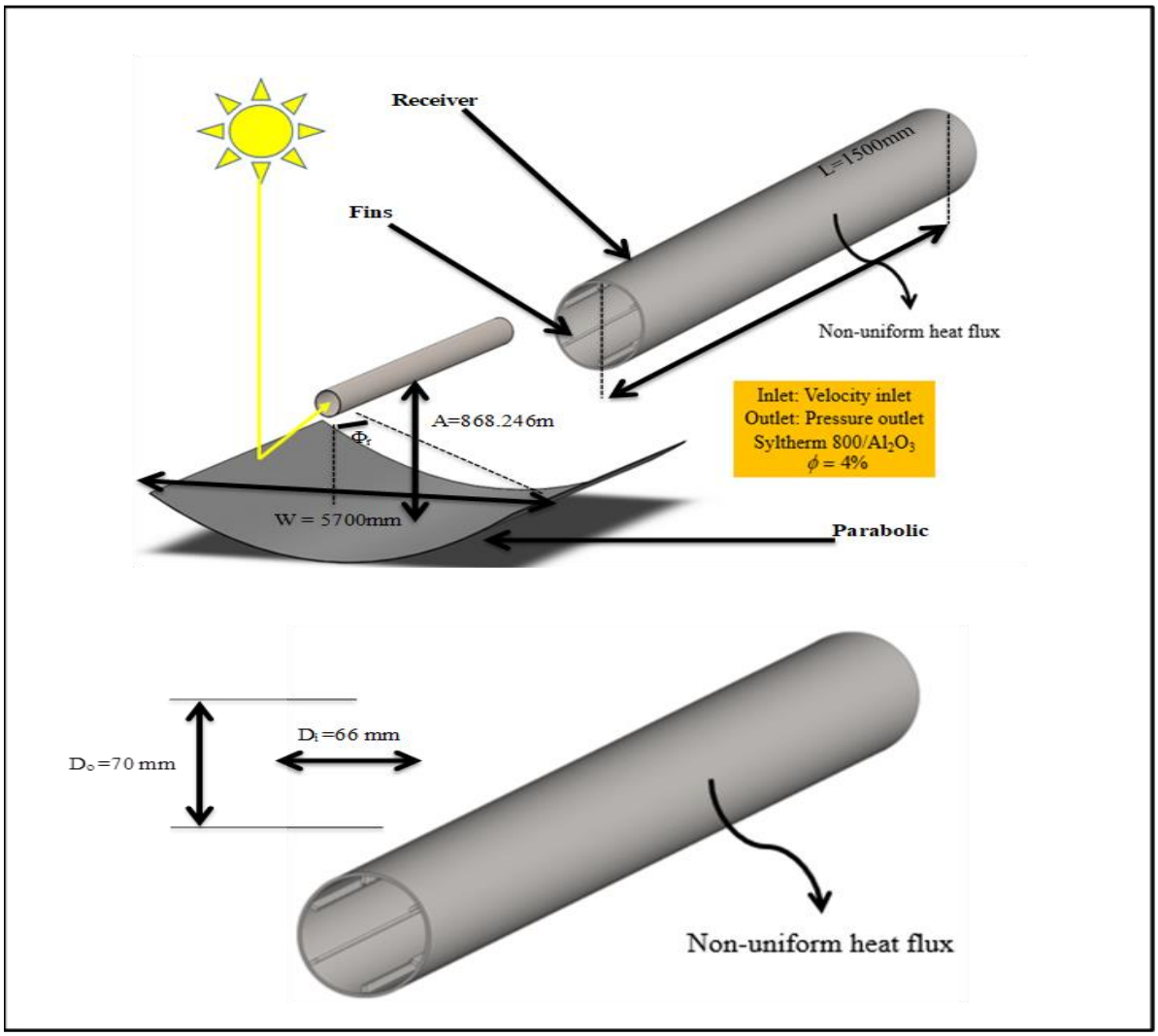

Figure (3-2) The model of parabolic collector and boundary conditions.

3.4 Parabolic Trough Collector System description [22]

Figure (3-2) shows that the PTC system contains a curved mirror, steel structure, a receiver, and a tracking system. The focused and reflected light from the curved mirrors went into an absorber tube in the collector's focal line. The receiver is of tube shape, a fluid is heated up to about 400ºC and flowing through the absorber tube. When the thermal characteristics and shape of PTC are understood, it is possible to estimate the amount of energy gained and the fluid's thermal performance under various environmental circumstances. In order to calculate thermal losses, you must have this information. PTC's study of heat transfer. A description of the collector is provided so that you may understand how the PTC model works.

The line passes through the focal point and the vertex is called the axis. This is calculated by measuring the angle between a focus and the rim (edge) of the parabola as it passes through the axis. Reflection length of the reflector multiplied by distance from edge to edge gives the aperture area. Aperture normal to the focus point, and parallel to the axis, are used to design the collector shape, which concentrates incoming solar energy. Using a driving mechanism, the solar collector trough rotates to face the un to gather as much energy as possible. To maintain the sun's rays aligned with the axis, the tracking mechanism works. Trough collectors cycle with the sun; therefore, they are generally lined along meridians from dawn to sunset. The receiver tube is coated with an optically selective coating to help it absorb most of the incident solar light while releasing very little heat radiation. The receiver tube is enclosed in a glass envelope to minimize heat loss.

For the best performance, the envelope should be very transparent to incoming solar radiation and highly opaque to minimize the amount of heat

radiation radiated from the tube's wall. In order to limit convective heat transmission between the tube and the envelope, the annular space between the tube and the envelope should be emptied. Direct and indirect radiations are both components of solar radiation. Concentrating collectors only collect direct normal irradiance (DNI), the radiation that comes straight from the sun and is not diffused by the surrounding environment. These collectors are unable to concentrate the irradiance that is coming from the indirect (diffuse) source. The only irradiance component of DNI normal to the aperture that PTC may concentrate is the aperture normal irradiance (ANI).

The following are the PTC's performance parameters:

1. An aperture-to-receiver-area ratio is known as a concentration ratio. It provides information about the collector's maximum temperature.
2. Optical efficiency: the proportion of total solar energy incident on the collecting surface that is absorbed by the absorber.
3. In terms of thermal efficiency, this is how much of the total energy incident on the collection area is converted into heat as it leaves the collector. The parabolic trough solar collector system's thermal efficiency is tied to its optical efficiency.

3.5 Numerical Method and Verification

In the current work, the ANSYS Fluent program (18.1) used in order to perform simulation for the first time and solved the three dimensions of fluid flow and heat transfer problem in the absorber of the Parabolic Trough solar Collector. The settings of the Ansys Fluent Solver shown in Table (6) in Appendix (B). A Computing Fluid Dynamics (CFD) module in

ANSYS Fluent based upon the finite volume method to solve the partial differential equations which are governing the problem domain, (continuity, momentum and energy equations).

To ensure of accuracy of mesh grid, the examination was carried out by taking a different number of elements for absorber tube as shown in figure (3-3).

3.6 Computational Fluid Dynamic (CFD) Techniques

Because of the fast development achieved in the fluids flow and the heat transfer applications, it is being necessary to find a software technique to simulate the practical reality numerically. The Software consists of certain languages that programmed the data which make the computer proceed various tasks. Instructions are written in a higher-level language, that can easily use by human programmers, as well as, then transmitted into low - level mechanism code, which the computer can directly knew the Arithmetic Operators and Algorithms to Compute the Equations. The start Days of Mathematical Software was at 1948, the Computer scientist programmed the small scale experimental machine (SSEM) to do mathematical calculations with machine code. This first part of software needed 52 minutes to compute the divisor of 2 to the power of 18 as written in **Timeline of Computer History [32].**

In the late 1950's and beginning of 1960's of the twenty first century, The computer languages like (Fortran) was appear and had an acceptable deal with numbers, (COBOL) report include a very good English - grammar and (BASIC) concentrated on supporting, directly forward mathematical solution, with use of matrix arithmetic. These languages are advanced by the obvious goal to be able to describe algorithms, were meant for

appointing numerical calculations. In 1970, Pascal became an effective language of programs. C programming language was used instead of Pascal in 1980, which is also utilized for numerical investigation. A derivative famous as subject Pascal program was available on the Macintosh in 1985 as part of the MacApp application, or application framework, then pascal was displaced by C++ and Java and then Apple's famous as a fundamental development language in the initial of 1990's. Extensions for the Pascal concepts guide to the languages Oberon and Modula-2, and then developed into Delphi on the Microsoft Windows as shown by **Jinxu (2019) [33]** and in **History of programming languages [34]**.

Microsoft was produced Visual Basic in 1991. In 2000, MATLAB were capable of plotting of data, matrix treatment, plotting of functions, running of algorithms, linking with programs written by other languages and construction of operator interfaces. Today start to use the FORTRAN of Formula Translation system, these were involved (integer, real, logical variables, and double -accuracy numbers) as shown in **A Brief History of MATLAB [35]**.

The development of mathematical program was started by Stephen Wolfram in the year of 1980. Now wide version of Mathematical are obtainable for a variety computer system including Apple Macintosh, MS-DOS, NEXT, Microsoft windows, sun, Hewlett – Packard / Apollo, Sony, and other computer systems. The mathematical software is the first stage of the numerical analysis of application problem and consists a number of functions

- Numerical computations.
- Computer graphics.
- Symbol computations.

The graphical tools of the numerical analysis techniques are used to have mathematical patterns for many applications of (Civil, electrical

,chemical and mechanical Engineering) take in roughly a complex for continuous face of structure or process such as solid mechanics, fluid flow mechanics, torsion analysis, stress analysis, heat transfer applications, magnetism, electricity, quantum mechanics and relativistic mechanics as shown in **Numerical analysis [36]** .

3.7 Numerical Computational Fluid Dynamic CFD Formulation

Computational fluid dynamics CFD is a branch of fluid mechanics, which employs numerical analysis and algorithms to fix complex problems that involve fluid flows. The visualization technique of CFD is employed by engineers to forecast and styling for a better display of the free-stream of fluid flow (liquids or gases), and heat transfer within the boundary conditions with accurate results, CFD is the progress of computer programs supplies approximate numerical solution that refers to the colors at the grid- point match to the number computed for the related flow properties , the CFD Module matches to an finite resolution practical video camera. The first CFD computing was in the 1957 and the first dealings was by a variance of numerical methods for simulate 2-D fluid flows, were the method of Particle-in-cell, as showed by **Brackbill and Ruppel (1986)[37]** , Vorticity stream function way, which showed by **Donna Calhoun (2002)[38]** and another method of Marker-and-cell, as explained by **Santosl .et al (2002)[39]** .

The limitation of CFD are explained as below: -

- analyses of complex dynamics, will need a lot of engineering approximations that produce numerical errors such as modelling shortcuts like unconverted mesh, and turbulence models.
- The complexity of the algorithms works in it which need good acknowledgement of what is happening with relating practically

behaviors and set the right boundary conditions for the numerical model.

There are many kinds of CFD methods. Each application has the appropriate type of method. Some of those methods that used are: -

- Finite volume method (FVM), that used for high Reynolds numbers of turbulent flows.
- Finite element method (FEM), which has more steady than the Finite volume method , need more memory and has delayer resolution times than the FVM.
- Finite difference method (FDM), which is used for overlapping grids.
- Boundary element method : the boundary is divided into to the surface mesh.
- High-resolution scheme, which is used for second and higher-order of numerical schemes.
- Large eddy simulation, that is used for turbulent models.

3.8 Finite Volume Method

(H K VERSTEEG and W MALASEKERA 2007) [40]

The integration of the formal control volume can be used as the base develop the numerical method which is the volume method or (control volume method). Considering the transport process of pure diffusion and the steady state. The steady diffusion governing equation could be derived from transport equation

$$\frac{\partial(\rho\varphi)}{\partial t} + div\ (\rho\varphi \mathrm{u}) = \mathrm{div}(\Gamma\ grade\ \varphi) + S_{\varphi} \quad [40] \qquad (3.1)$$

Where the general variable (φ) is the conservative form representing all equations of fluid flow, containing the scalar values like temperature and pollutant concentration.

for property φ after deleting the convective and transient terms obtaining:

$$div(\Gamma\, grade\ \varphi) + S_{\varphi} = 0 \quad [40] \qquad (3.2)$$

the integration of the control volume is the first step of the finite volume method which differs from all other CFD techniques. Leads to the form:

$$\int_{cv} div\,(\Gamma\, grad\ \varphi)dV + \int_{cv} S\, dV = \int_{A} \mathrm{n}\,.\,(\Gamma\, grad\ \varphi)dA + \int_{cv} S\varphi\, dV = 0 \qquad (3.3)$$

[40]

the needed approximation of the techniques to obtain the discretized equation by dealing with one-dimensional diffusion equation of the steady state. Then the method extended to two-dimensional and three-dimensional diffusion problems. When the fluid flow being a main effected role the effect of the convection must be took in account. Always the diffusion occurs beside the convection so the combined diffusion and convection must be examined.

The steady diffusion-convection eq. could be derived from eq. (3.3) after eliminating the transient term

$$div\ (\rho\varphi \mathrm{u}) = \mathrm{div}(\Gamma\, grade\ \varphi) + S_{\varphi} \quad [40] \qquad (3.4)$$

by integration through the control volume obtain:

$$\int_{A} \mathrm{n}\,.\,(\rho\varphi u)dA = \int_{A} \mathrm{n}\,.\,(\Gamma\, grad\ \varphi)dA + \int_{cv} S\varphi\, dV \quad [40] \quad (3.5)$$

The equation above representing the flux balance within the control volume where the net convective flux is the left side term and the net diffusive flux and the destruction or generation of the property φ is the right hand side in the control volume.

The calculation of the transported property value φ is the principal problem in the discretization of the convective terms within the control volume faces and the convective flux across the boundaries.

The distribution of the transported quantity affected by the diffusion process along the gradient if the quantity in all direction, on the other hand the influence of the convection spreads is only in the flow direction. Ansys Fluent Software

1- First, in this section, by clicking on the Check option, the mesh is verified.

In the Type section, select the Pressure based option, in the Velocity Formulation section, select the Absolute option, and in the Time section, select the Steady option (because the solution is not time dependent). The software also shows the input in blue and the output in red.

2- Models: In this section, the Energy option is activated because the energy equation needs to be solved.

3- In this case, the K-epsilon option is selected. In the K-epsilon Model section, the Realizable option is selected. The Enhanced Wall Treatment option is usually selected in the Near-Wall Treatment section. Then, in the Enhanced Wall Treatment Options section, select the Thermal Effects option to observe the temperature effects on the wall.

4- Materials: In the Fluid section, to define the desired fluid, the fluid properties of Sylterm 800 - Al_2O_3 are entered manually. These numbers are obtained from the existing relations. Also, the properties of steel are imported.

5- Cell Zone Conditions: In this section, click on the domain and in the Material Name section, select the sylterm800-al_2O_3 option. Choose steel for the solid fin and the solid pipe.

3.9 Geometry Simulation

In the current study, the finite volume method on the Ansys Fluent (18.1) is utilized to solve the Navier-stokes equations numerically for the flow and heat transfer inside circular pipe. SOLIDWORKS is used to draw

the geometry of fined absorber tube with different number of fins (n) and two arrangements ("a" and "b"). The governing equations for the three-dimensional, turbulent flow of

Syltherm 800/Al_2O_3 nanofluid inside the absorber. The physical parameters for the flow and heat transfer rate inside the circular cylinder studied and their boundary conditions in the current study are assumed. See **(AppendixA)**.

3.9.1 Solid Work Steps

To draw a parabolic finned tube with Syltherm 800-Al_2O_3 as a heat transfer fluid with the parameters bellow (matches to the reference [49]):

Table (3- 1) Dimensions Parameters of (PTC) system

Parameter	Value
Inner diameter	66 mm
Outer diameter	70 mm
Length of tube	1500 mm
Height of fins	5 mm
Width of fins	2mm

1- Create the geometry by creating a new sketch and selecting the plane, and then extrude it along the axis.
2- Draw a circle with a diameter of 70mm.
3- Enter the length amount of 1500 mm, which is equal to the length of the pipe.
4- In the second sketch, draw the inner diameter of the pipe to 66 mm and extrude as before.
5- The third sketch is about drawing the fins, which is very simple, first we draw a circle with a diameter of 66 mm and then a rectangle.

6- Select the drawn rectangle. Next, by using the circular sketch pattern option, select the number and location of the fins.

7- In the fourth Sketch, to make the mesh more precise, we draw a square under the fins between the inner and outer diameters, and extrude as before. This is done only to improve the mesh structure.

3.10 Mathematical Formulation

3.10.1 Governing equations

The governing equation for the present study of the steady state, viscous, turbulent incompressible and three - dimensional in the Cartesian coordinate system flow are the Navier – stokes equation and the thermal energy equation.

In the present study, the governing equations for the flow of the three-dimensional in the planner of the Cartesian coordinate are described by means of the following assumptions: -

a) The flow is considered three-dimensional, steady, incompressible, and turbulent flow.
b) The circular tube walls are considered stationary (no slip condition) .
c) The wall of the tube is well treated to optimize the absorbed solar energy.
d) Constant properties of the working fluid (Nanofluid) as well as the tube walls properties.
e) The thermo-physical properties are assumed constant**.**

The governing equation of the steady state three - dimensional, viscous , laminar, 3-D and incompressible flow are the Navier – stokes equation and the thermal energy equation in the Cartesian coordinate system**.**

In order to simplify the mathematical calculations of the present study, there are several assumptions made about the flow operating conditions, the

fluid flow is turbulent, steady state, incompressible and single phase flow across the absorber (where the fluid is only in its liquid state). The supporters heat transfer and gravitational are negligible.

To simulate the behavior of the heat transfer and fluid flow in the parabolic through solar collector, considering the three-dimensional governing equations (continuity, momentum and energy equation) are employed. In simulating the turbulent flow regime of heat transfer and fluid flow, the k-ε turbulence model is used. According to the research in the field of flow simulation in solar collectors, this model has many advantages such as the ability to describe the flow near the wall. The equations that considered to describe the flow field and heat transfer in the absorber pipe were presented as follows ANSYS Fluent Theory Guide [41]:

Continuity Equation [4]

$$\frac{\partial(\rho \ddot{u}_i)}{\partial x_i} = 0 \tag{3.6}$$

Momentum Equation [4]

$$\frac{\partial}{\partial x_j}\left(\rho_{nf}\ddot{u}_i\ddot{u}_j\right) = -\frac{\partial \ddot{p}}{\partial x_j} + \frac{\partial}{\partial x_j}\left(\mu_{nf}\left(\frac{\partial \ddot{u}_i}{\partial x_j} + \frac{\partial \ddot{u}_j}{\partial x_i}\right) - \frac{2}{3}\mu_{nf}\frac{\partial \ddot{u}_i}{\partial x_i}\delta_{ij} - \rho_{nf}\overline{\ddot{u}_i\ddot{u}_j}\right) \tag{3.7}$$

Energy Equation [4]

$$\frac{\partial}{\partial x_i}\left(\rho_{nf} Cp T \ddot{u}_i\right) = \frac{\partial}{\partial x_i}\left(\left(\ddot{\Gamma} + \ddot{\Gamma}_t\right)\frac{\partial T}{\partial x_i}\right), \ddot{\Gamma} = \left({}^{\mu_{nf}}/_{Pr_{nf}}\right), \ddot{\Gamma}_t = \left({}^{\mu_t}/_{Pr_t}\right) \tag{3.8}$$

Where the term $(-\rho_{nf}\overline{\ddot{u}_i\ddot{u}_j})$ is:

$$-\rho_{nf}\overline{\ddot{u}_i\ddot{u}_j} = \left(\frac{\partial u_i}{\partial x_j} + \frac{\partial u_j}{\partial x_i}\right)\mu_t - \frac{2}{3}\rho_{nf}K\delta_{ij} - \frac{2}{3}\mu_t\frac{\partial \ddot{u}_k}{\partial x_k}\delta_{ij} \tag{3.9}$$

Where : $\mu_t = \frac{1}{\varepsilon}K^2 C_\mu \rho_{nf}$

In this study, the k-epsilon Realizable turbulence model with enhanced wall treatment was used to model the turbulence. According to this model, the modeled transport equations for k and ε are formulated as follows ANSYS Fluent Theory Guide [41]:

$$\frac{\partial}{\partial x_j}\left(\rho_{nf} K \ddot{u}_j\right) = \frac{\partial}{\partial x_j}\left[\left(\mu_{nf} + \frac{\mu_t}{\sigma_k}\right)\frac{\partial K}{\partial x_j}\right] + G_k - \rho_{nf}\varepsilon \tag{3.10}$$

Where

k: Turbulent kinetic energy

ε: Turbulent dissipation

$$\frac{\partial}{\partial x_j}\left(\rho_{nf} \varepsilon \ddot{u}_j\right) = \frac{\partial}{\partial x_j}\left[\left(\mu_{nf} + \frac{\mu_t}{\sigma_\varepsilon}\right)\frac{\partial \varepsilon}{\partial x_j}\right] + \rho_{nf} C_1 S\varepsilon - C_2 \rho_{nf}\frac{\varepsilon^2}{K + \sqrt{\nu\varepsilon}} \tag{3.11}$$

Here, the production of turbulent kinetic energy is represented by G_k and has the very exact model for all k-ε models like in the following:

$$G_k = -\rho_{nf}\overline{\ddot{u}_\iota \ddot{u}_\jmath}\frac{\partial u_j}{\partial x_i} \tag{3.12}$$

The Cμ isn't constant on empirical relations and is continual in the realizable k-ε. in Ref [33], the complete resolution of Cμ is stated the constant models for the realizable k-ε in:

Table (3- 2) constant models for realizable k-ε

$C_1 = \max\left[0.43, \frac{\lambda}{\lambda+5}\right]$,	$\lambda = S\frac{K}{\varepsilon}$,	$S \equiv \sqrt{2S_{ij}S_{ij}}$,	$C_2 = 1.9$,
$\sigma_k = 1$,	$\sigma_\varepsilon = 1.2$		

The properties of the nanofluid can be calculated according to equations (3.13) to (3.16), using the properties of the base fluid (bf) and of the nanoparticles (np). The density of the mixture is given by equation (3.13) M.AYATOLLAHI et. al [42] and the specific heat capacity according to equation(9) [43],[2],[25]

$$\rho_{nf} = \rho_{bf}(1-\phi) + \rho_{np}\phi \tag{3.13}$$

$$C_{p,nf} = \frac{\rho_{bf}(1-\phi)}{\rho_{nf}}.C_{p,bf} + \frac{\rho_{np}(\phi)}{\rho_{nf}}.C_{p,np} \tag{3.14}$$

The thermal conductivity of the nanofluid is calculated according to the Maxwell equation, W. Yu and S.U.S. Choi [44], Kincaid et. al [1],[30],[7],[11]:

$$k_{nf} = \frac{k_{np} + 2k_{bf} - 2\phi\left(k_{bf} - k_{np}\right)}{\frac{k_{np}}{k_{bf}} + 2 + \phi.\frac{k_{bf} - k_{np}}{k_{bf}}} \tag{3.15}$$

The mixture viscosity is calculated according to equation (3.16) [45],[25]:

$$\mu_{nf} = \mu_{bf}(1 + 2.5\phi + 6.5\phi^2) \tag{3.16}$$

The Nusselt number (Nu) and Reynolds number (Re) can be found using the next equations [49]:

$$Nu = \frac{hD_i}{k}, Re = \frac{\rho u D_i}{\mu} \tag{3.17}$$

the Nusselt number can be determined based on Colburn correlation [49] as:

$$Nu = 0.023 \cdot Re^{0.8}.Pr^{0.4} \quad (3.18)$$

The calculations of the physical parameters (density, viscosity, specific heat and conductivity) are listed in Table (7) in appendix B.

The heat transfers between the absorber and the heat transfer fluid is modeled using the heat transfer coefficient (h), where it can be calculated as below [49]:

$$h = \frac{q^{"}}{(T_w - T_b)} \quad (3.19)$$

The flow's friction factor (*f*) is computed as follows. The following formula employs the pressure drop (ΔP) determined from the CFD study in each situation [49].

$$f = \frac{2D_i.\Delta P}{\rho.u_m^2.L} \quad (3.20)$$

The Performance Evaluation Criterion (PEC), which reflects the heat transfer coefficient enhancement under "constant pumping work circumstances," may be used to evaluate the flow augmentation. The reference example with a smooth absorber tube is denoted by the subscript "0." Yunus. A and Cengel [46]:

$$PEC = \frac{\left(\frac{Nu}{Nu_0}\right)}{\left(\frac{f}{f_0}\right)^{1/3}} \quad (3.21)$$

3.10.2 Boundary Conditions

In this section, if the naming in the mesh section is done correctly, for example, Inlet is written, the software will automatically consider this line as velocity inlet. The boundary conditions is explained as bellow :

1- In the Inlet section and in the Momentum section, select the absolute speed and enter the input speed in the x direction according to the problem data in turbulent flow at $3.6 m/s$. At the bottom, in the turbulent intensity section, enter the current turbulence intensity is (5%), which obtained by entering the Reynolds number in the formula for turbulence intensity ($I = 0.1 * Re^{-0.125}$).
2- In the Turbulent Viscosity Ratio section, a value of 10 is entered. And in the Thermal section, the temperature enters 300 K.
3- In the Outlet section, the software considers the output as a pressure outlet. Since there is a variable flux in the outer wall, call the variable flux profile in the Heat flux section.

To call the profile, the file option is selected, then the read option and then the profile option is selected. And then in the Boundary conditions section for wall heat flux is called next to the heat flux option.

The boundary conditions are necessary limitations that are assumed to surround the domain in the numerical analysis of the problems. The purpose of the Boundary conditions is to simplify the partial differential equations to enable resolved. also to know whether the computational problems are good placed. There are two type of boundary conditions surrounding the domain containing the flow: -

1- Flow boundary conditions surrounding the domain:

- No_ slip boundary conation

2- Thermal boundary condition surrounding the domain:

- Dirichlet BC or 1st kind (specified constant temperature),
- Neumann BC or 2nd kind (specified heat flux)

In the present work, the boundary condition surrounding the computational domain: -

Uniform velocity and temperature fields are given at the absorber tube's entrance as:

$$u(x, y, 0) = 0 \tag{3.22}$$

$$v(x, y, 0) = 0 \tag{3.23}$$

$$w(x, y, 0) = w_{in} \tag{3.24}$$

$$T(x, y, 0) = T_{in} = 300K \tag{3.25}$$

Where (u, v, w) and (w_{in}) are velocities in x, y and z directions, and uniform velocity in z direction, respectively. The boundary condition on the outlet of the receiver tube is assumed to be fully-developed, hence $\partial u/\partial z = \partial v/\partial z = \partial w/\partial z = \partial T/\partial z = 0$ (at the outlet).

3.11 The procedure of the numerical solution.

The procedure of the algorithm solution can be summarized. The governing equation, which contain the components of the velocity and temperature are numerically analyzed. The algorithm solution is iterative, the requisites stages In the update of the numerical solution are as follows:

1-Indicate the physics parameter of the fluid flow and the heat transfer rate, also indicate the case of the steady state solution.

2- Draw the geometry of the computational domain, which contain the fined absorber tube.

3-Indicate the governing equations of the continuity, momentum and energy equation.

4-Indicate the equations of the Nusselt Number, which represented of the heat transfer rate.

5-Indicate the equations of the friction coefficient.

6-Assume and apply the suitable boundary conditions.

7- The continuity, momentum and energy equations are solved by using the finite volume method. The solution is explained as bellow:

a- In the Methods section and the Spatial Discretization menu, the Second Order Upwind option is selected for Momentum to solve the pressure more accurately. For turbulent kinetic energy, turbulent dissipation rate, and Energy, First Order Upwind is selected.

b- In the Controls section, there are coefficients called Under Relaxation, which remain the software default.

c- In the Monitor section, in the Residual section, all residuals enter 0.0001, except for the energy equation, which enters 1E-6.

d- Initialization is the initial solution. Initial solutions enter the project through the Hybrid Initialization option.

e- In the Run Calculation section, the value of Number of Iterations is entered as 1000 and then the Calculate option is clicked.

3.11.1 Mesh building

Normal CFD technique need a mesh which arrange the boundaries of the computational domain. The building of the computational mesh is appropriate to the discretized solution for the three dimensional momentum and energy equations. A good mesh is the last point of the total number for the cells generation, It is basis to have sufficient number of cells for a good determination but memory desires growth to the increasing for the number of cells, Thus, the triangular elements is chosen with the free mesh in the present work.

In order to have correct numerical results, a grid individuality study performed. To find the size of the most acceptable mesh, grids are independently tested for five meshes were used for fin number (n=6) at "a" fin arrangement with several shape elements (1.802.403, 2.978.117,

3.249.036 , 3.547.878 , 4.496.551) respectively as illustrated in Figure (3-3). The Nusselt number and friction factor have been estimated for each mesh element number for the absorber tube at Reynolds number equal to (28000) and heat flux equal to 1000 kW/ m^2 and the results were compared. The values of both friction coefficient and Nusselt number where noticed the same for the last three numbers of elements, they equal to (Nu =490, f = 0.0335), so the considered element number of the mesh is (4.496.551).

1. draw a square under the fins between the inner and outer diameters.
2. Enter the design modeler and call the geometry by using the Import external geometry option.
3. First Boolean, reduce the volumes by using the Boolean option, in the Tool body section, we select all volumes except the outer diameter.
4. Second Boolean: Define a Boolean again and select all the fins and walls in the Tool body option, In the Target section, select the inner diameter volume, and click on generate option
5. Click on the inside diameter volume and select the Fluid option. Because the walls and other places are solid and there is only fluid inside the pipe.
6. After separating the volumes, we enter the mesh section.
7. To mesh, first in the Sizing section, the Relevance Center was changed to Fine, and also in the Quality section, smoothing to High, and in the Mesh Metric, the Skewness option is selected to see the accuracy of the mesh.
8. Because the flow is turbulent, the boundary layer mesh must be applied. Then, by right-clicking on the Mesh, in the Insert section, the Inflation option is selected. Because the shape is 3D, the fluid domain in the direction of the tube is selected for the Geometry section and the Apply option is clicked.

9. in the Definition section in the Boundary section, all the pages around the fluid are selected (both at the input and at the output, which is equal to 24 pages).
10. In the First Layer Height section, enter the height of the first layer a small number. In the internal flow, the following equation is used to obtain the height of the first cell.
11. First edge sizing: To improve the mesh using the Edge sizing option, first select the pages between the fins at the inlet and outlet of the pipe, which are 12, and in the Type field, select the Element size and enter 0.002.
12. Second edge sizing: Again, by creating a new Edge sizing, this time for the fins, we will act as before and select 24 pages at the input and output. Also, in Edge sizing 3, in the longitudinal direction, we select all the existing lines, which are 36 pages around the pipe.
13. Finally, we name the pages.
14. By selecting the Named Selections option, the desired pages will be named. One of the front or back pages of the tube is named Inlet and the other is called Outlet. Also, the cylindrical plate, the surrounding walls, were named wall heat flux.
15. For the fluid domain, first click on the Body option and then the inner part of the cylinder is selected and named Fluid.

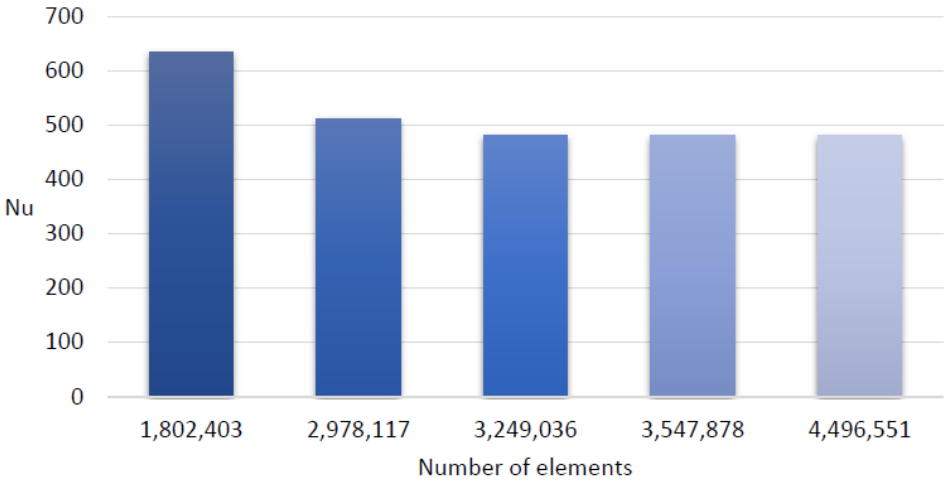

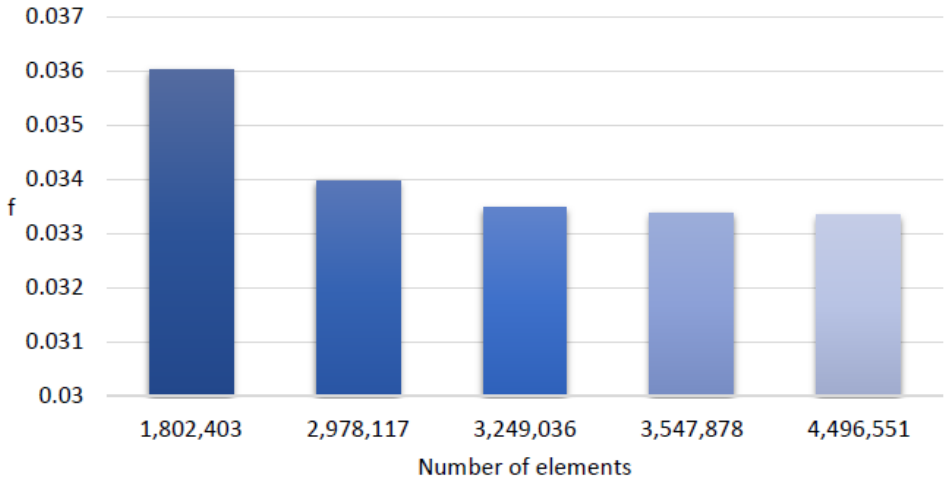

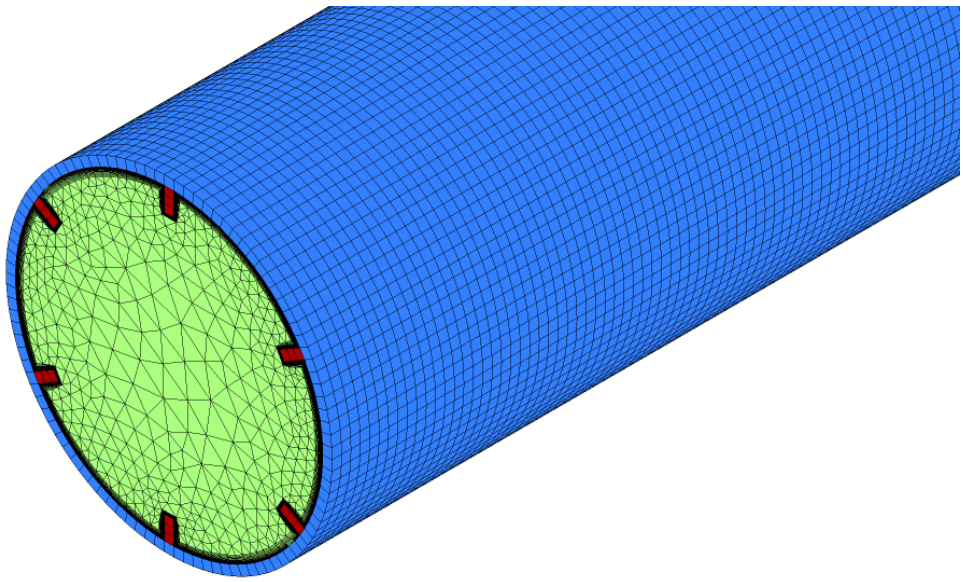

Figure 3-3 Mesh dependence studies for n=6 and Re=28000 at "a" fin arrangement and sample pictures of the mesh.

3.12 Nanotechnology:

Nanotechnology deals with a matter having dimensions of the order of a billionth of a meter. From the advent of nanotechnology, people realized that certain materials can exhibit different properties based on its size and shape. It all started after the famous lecture, "There is plenty of room at the bottom" given by Richard Feynman on December 29, 1959. Nanomaterial are intermediate between macroscopic solid and of atomic and molecular systems. Nanomaterial have certain properties which make them different from that of the bulk materials, including large fraction of surface atoms, high surface energy, spatial confinement, **Ibrahim Khan et al. (2017) [47]**. The properties of the Nanomaterial used in the current study (Al_2O_3) listed in Table (2) in Appendix (B) **E. Bellos and C. Tzivanidis [11]**.

3.12.1 Characteristics of alumina (Al_2O_3):

1- Hard, wear-resistant.
2- Excellent dielectric properties from DC to GHz frequencies.
3- Resists strong acid at elevated temperatures.
4- Good thermal conductivity.
5- Excellent size and shape capability.
6- High strength and stiffness.
7- Available in purity ranges from (94% to 99.8%) for the most demanding high temperature applications.
8- Properties of Al_2O_3 found in table (2) in Appendix (B).

3.13 SYLTHERM 800 Heat Transfer Fluid:

SYLTHERM 800 fluid is a highly stable, long-lasting, silicone fluid designed for high-temperature liquid phase operation. It has a recommended operating temperature range of -40°F (-40°C) to 750°F (400°C). Operating continuously at the upper end of this range, SYLTHERM 800 fluid exhibits low potential for fouling and can often remain in service for 10 years or

more. The fluid is essentially odorless and is low in acute oral toxicity. **Dow Oil and Gas[50]**.

The properties of the working fluid (Syltherm 800) are listed in table (4) in Appendix B.

SYLTHERM 800 fluid features include:

- Low fouling potential
- Low freeze point
- High-temperature stability
- Long life
- Noncorrosive
- Low acute oral toxicity

Chapter Four

Results and Discussion

4. Chapter Four: Results and Discussion

4.1 Introduction

The numerical results and the discussions related to them are displayed in this chapter such as (outlet velocity, outlet temperature distribution, TKE, Nusselt number, friction factor, heat flux distribution, heat transfer coefficient and performance evaluation criteria PEC). The numerical results of the flow and heat transfer inside the absorber tube of the PTC are obtained using the Finite Volume Method (FVM), and validated with another previous researches in the recent years for two parameters (heat flux and heat transfer coefficient). The comparison is considered between the present numerical results and the previous studies results, finally the recommendations for the future studies were discussed.

4.2 Monte Carlo Ray-Trace (MCRT) model of the present parabolic trough collector:

The Monte Carlo Ray-Trace Method in Radiation Heat Transfer and Applied Optics offers the most modern and up-to-date approach to radiation heat transfer modelling and performance evaluation of optical instruments. The Monte Carlo ray-trace (MCRT) method is based on the statistically predictable behavior of entities, called rays, which describe the paths followed by energy bundles as they are emitted, reflected, scattered, refracted, diffracted and ultimately absorbed. The characterize work in this study is the Rim angle of the reflector, where the angles chosen are either 80º or 120º as tested, since the Rim angle of 120º achieved high outlet temperature as it is obvious in Fig. (4-1) while the Monte Carlo ray tracing model records heat flux density higher than in case of 80º and where achieved the concentration ratio of (82.47), so the used model of the solar reflector was with 120º**.**

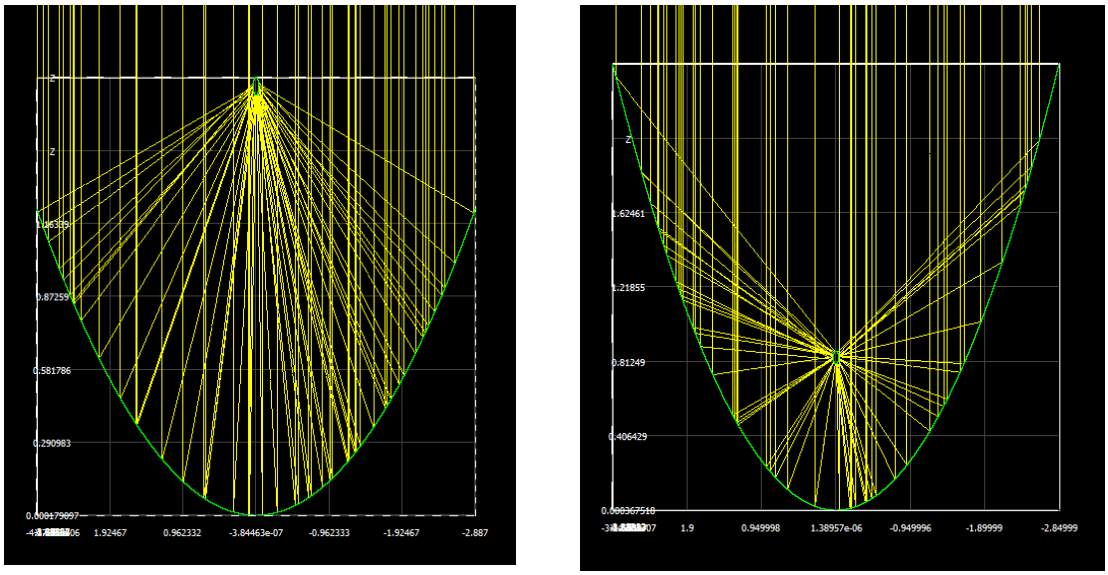

Figure. (4-1) MCRT model of the present parabolic trough collector.

4.3 Validation of numerical results

Two validations are conducted in this study, the first validation considered the distribution of heat flux (Validation of MCRT result) on the outer surface of the absorber and the validation is compared with Wang 2015 [4] as shown in Figure (4-2) where it signified the good agreement between the current results and those obtained from Wang 2015 [4] that used a rim angle of (80.2º) and the concentration ratio is (82). The main similarity between both studies that have the DNI equal to (1000 W/m^2), the HTF inlet temperature (300 K) and the inlet velocity (3 m/s), the concentration ratios of the reference study is (82) and the working fluid flow inside the absorber was Syltherm 800.

The second validation conducted for the heat transfer coefficient as shown in Figure (4-3). The validation is done with M. Malekan et al. (2019)[49] for different Reynolds numbers (30.000, 60.000, 120.000, 250.000) respectively. It is noticed that the values of the heat transfer coefficients (h) at each Reynolds number are very close for both the present

study and the reference study which depend the properties of (working fluid is CuO/Therminol 66, volume ratio of ϕ=4%, Dout=70mm, Din=66mm, I_{top}=680 W/m^2, I_{bottom}=9739.8 W/m^2). The validation shows good agreement which signifies accepted the results of the present study.

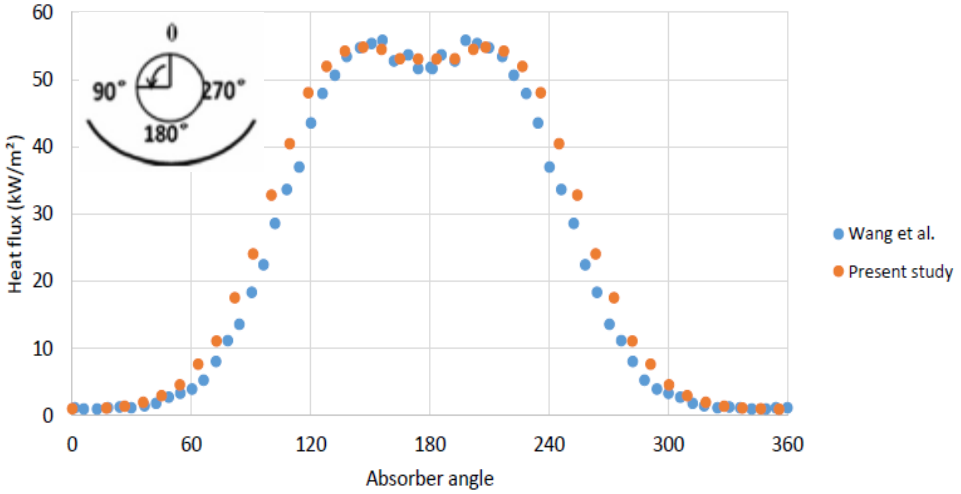

Figure (4-2) Validation of MCRT results.

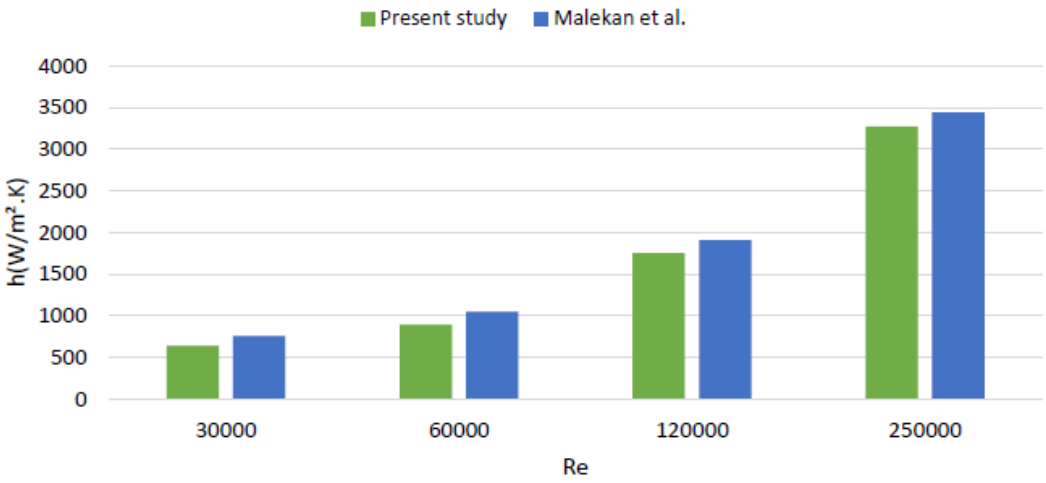

Figure (4-3) Validation of heat transfer coefficient results.

4.3 Surface plots of the MCRT simulation:

It is known that the solar radiation incident on the reflector will reflect to the absorber which it lies in the focal position, the ray paths which represent the directions of the reflected solar radiation towards the absorber will distribute with a non-uniform manner, creating the heat flux

distribution on the reflector shown in Fig. (4-4). The heat flux reflected on the absorber can be illustrated as in the surface plot of the MCRT simulation which shows more heat flux values occurred through the reflecting surface to the absorber tube surface when Rim angle equal 120° compared to the plot of 80º. The heat flux value started from (22000 w/m²) at (x= -0.1), then it increased to (45000 w/m²) when (x= -0.075) then it decreased till it reaches (zero) at the point (x=0) which represent the shadow of the absorber on the reflector, then the plot is repeated itself due to match.

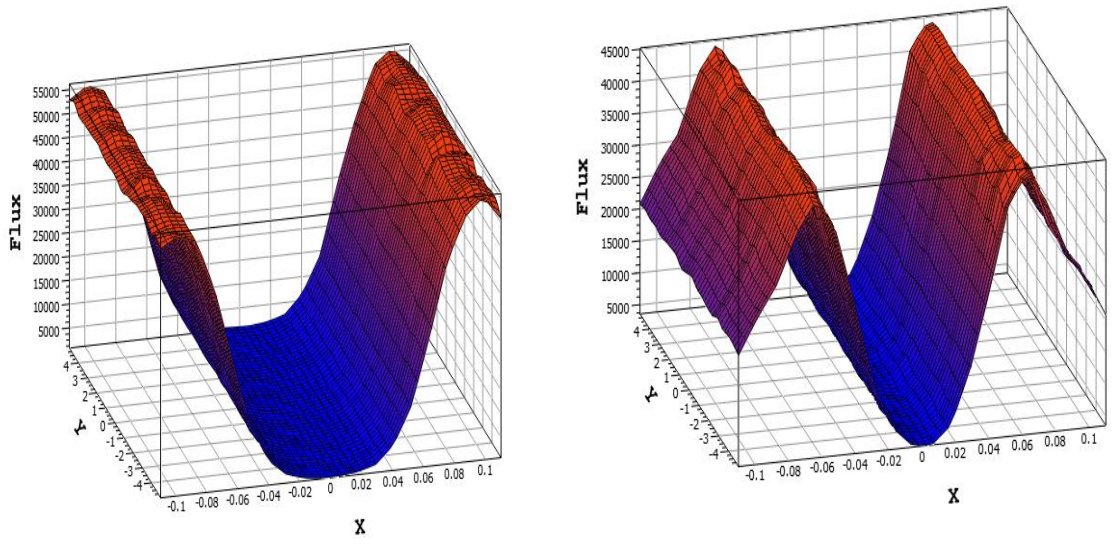

Rim angle=80° ***Rim angle=120°***

Figure (4-4) Surface plots of the MCRT simulation.

4.4 velocity contour characteristics:

The inlet velocity in this study is in (m/s) varies depending on the Reynolds values, discussing the velocity contour of the fluid at outlet region of the absorber based on three different Reynolds number (18600, 23000 and 28000) with two different arrangements "a" and "b" for each

fins number which are (2, 4 and 6 respectively) as shown in fig. (4-5).

Starting with Re=18600, when using two fins the velocity roughly stay the same value when changing the arrangement from "a" to "b", also the same behavior occur when using 4 and 6 fins.

Now moving horizontally in Figure (4-5) to notice that the velocity increased with increasing the number of fins from 2 to 4 and then to 6 fins the maximum outlet velocity achieved is (3.458m/s) at center of pipe.

At Re=23000, when using two fins the velocity will not change when changing the arrangement from "a" to "b", also the same behavior occur when using 4 and 6 fins. Also the outlet velocity reached the maximum value when changing the number of fins from 2 to 4 and then to 6 fins and the maximum outlet velocity will be (4.32599m/s).

Finally at Re=28000, when using two fins the velocity will not change when changing the arrangement from "a" to "b" , also the same behavior occur when using 4 and 6 fins.

And also the outlet velocity reached the maximum value when changing the number of fins from 2 to 4 and then to 6 fins and the maximum outlet velocity will be (5.208m/s).

The higher outlet velocity achieved is (5.208 m/s) when the Reynolds number being (28000) and (6 Fins) than the other cases of (2 and 4 Fins), that occur because of the cross sectional area reduction according to the increasing of Fins number, where it is obvious that the velocity decrease from center towards the circumferential of the absorber.

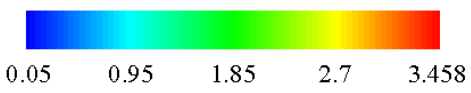

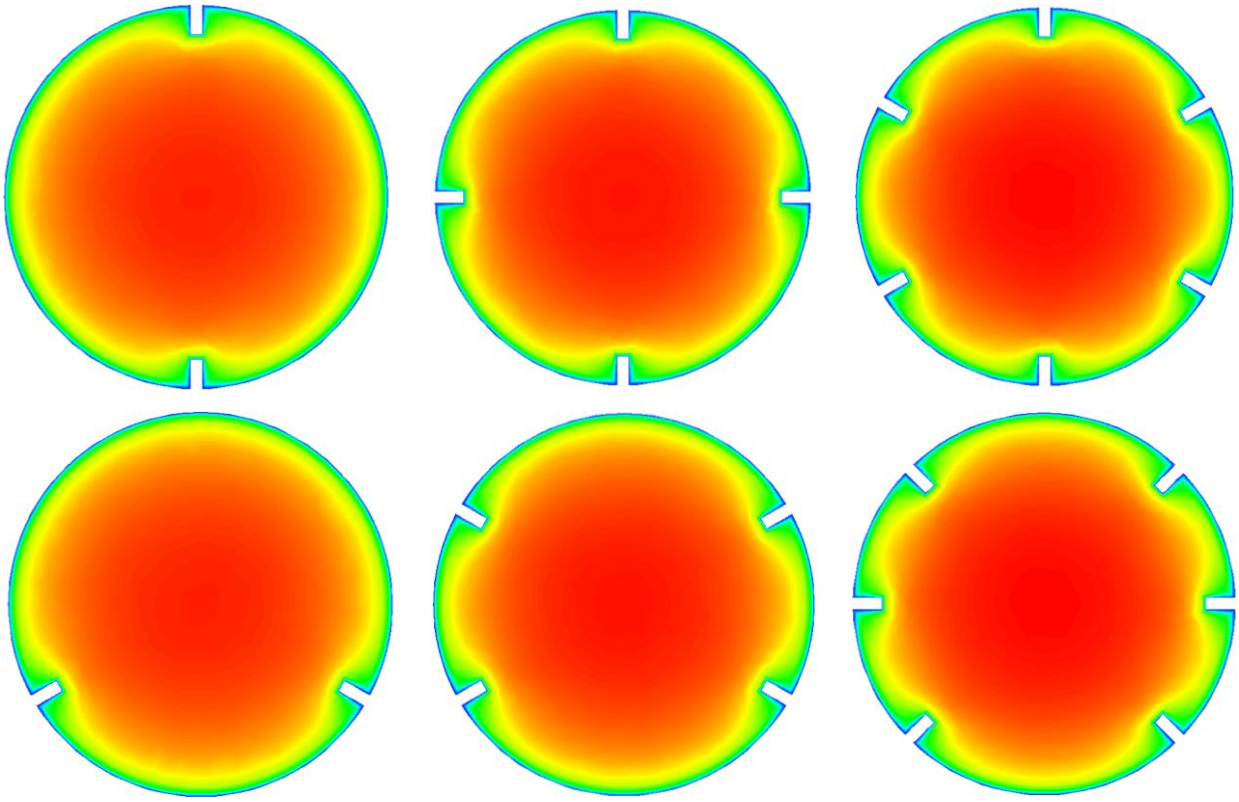

a) Re=18600

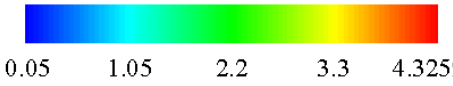

2 4 6

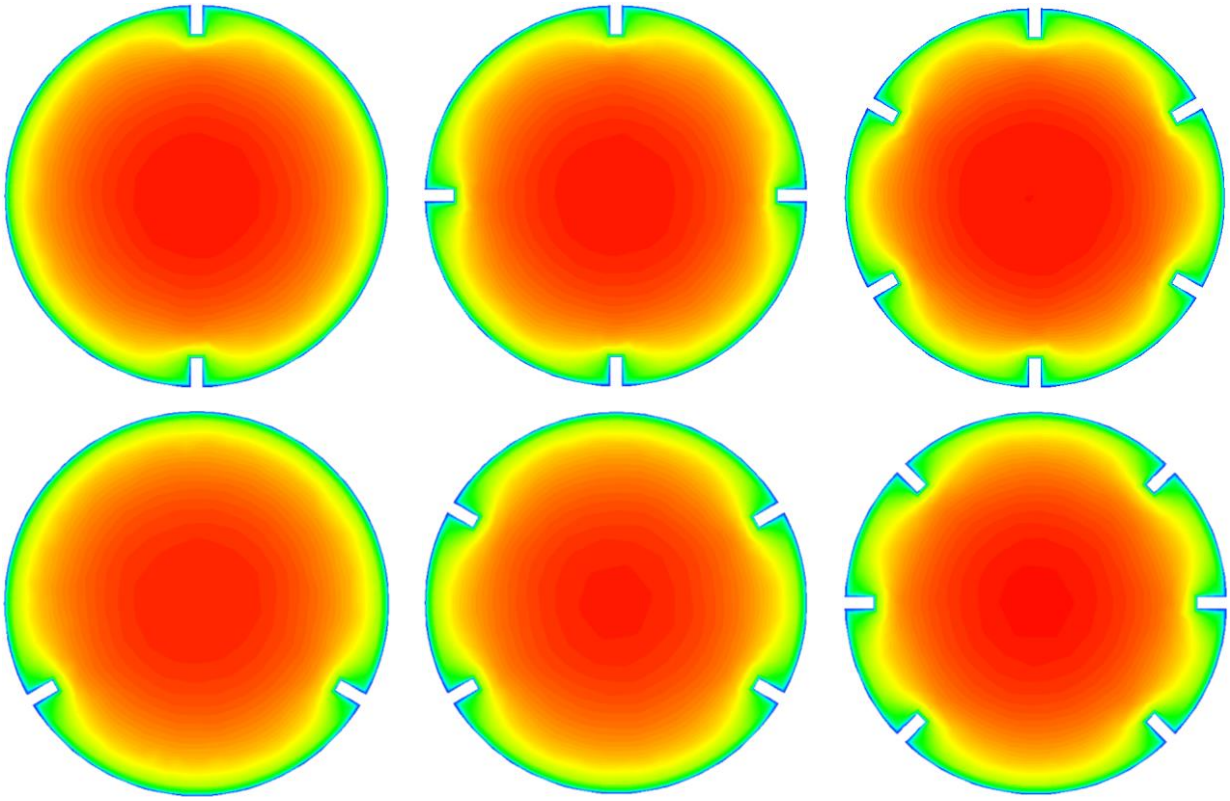

b) Re=23000

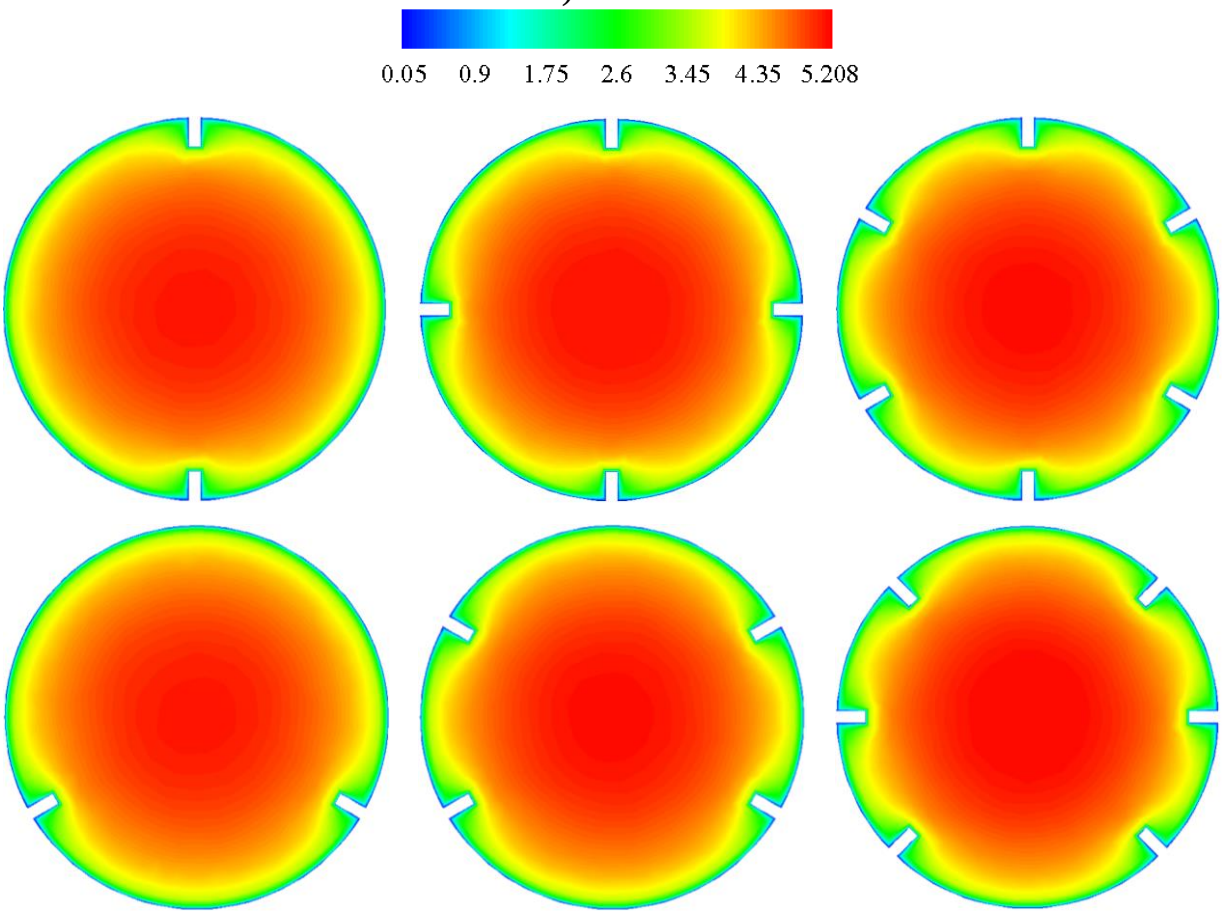

c) Re=28000

Figure (4-5) V_z for different number of fin and arrangements and Re at outlet.

4.5 The Temperature distribution characteristics

To explain the distribution of temperature along the absorber and the flowing fluid, the temperature contour is presented at the outlet section. the parameters that have main effect on the heat transfer rate between the heat flux on the surface and flowing Nano fluid are Reynolds number (Re=18600,23000 and 28000), number and arrangement of the longitudinal fins. The other parameters are fixed such as the nanoparticle volume concentration ($\varphi = 0.04$), the inlet temperature condition (Tin=300K). The temperature rises from the inlet to the outlet along the tube. As the process of heat transfer occurs by convection between the walls of the tube and the fluid along the stream. The maximum temperature appears on the

distribution label in the temperature contour represents the temperature of the solid surface, while the minimum temperature on the distribution label represents the nano fluid temperature.

4.6 Temperature distribution for different number of fins and arrangements and Re at absorber outlet:

For the best performance of the heat transfer in the absorber tube and in order to choose the best studied case among many cases which deals with different Reynolds numbers (13600, 23000 and 28000), different fin numbers (2,4 and 6) and two different arrangements ("a" and "b"). Figure (4-6) illustrates the temperature distribution in the heat transfer fluid (HTF) inside the absorber and on the absorber wall surface at outlet region, it could be observing that the highest outlet temperature recorded for the flow was with Reynolds number (18600) and of arrangement (a) which is (352.578K), while the lowest fluid outlet temperature was with Reynolds number of (28000) and arrangement (a) was (300.231 K). The two temperatures mentioned above not represented the preferred case for good enhancement that the study is looking for.

The best outlet fluid temperature must be the highest as much as possible to give the sign of the enhancement in the absorber performance, so the (300.444 K) at Reynolds number (18600) arrangement (b), at the same time the lowest absorber wall surface temperature was found (335.501 K) at Re (28000) and arrangement (b).

Although there are another temperature recorded which were represented the wall surface of the absorber and the flowing fluid at the intermediate values of Re (23000), these temperatures are not useful for estimating the enhancement. The best heat transfer occurs when increasing the number of fins and Reynolds number which lead to increase the

turbulence, as a consequence of that, the heat transfer coefficient will increase thus Nusselt number increase too.

It could be concluded that the case of Reynolds number equal to (28000) , fin number n=6 and arrangement "b" represent the best case which give better heat transfer performance.

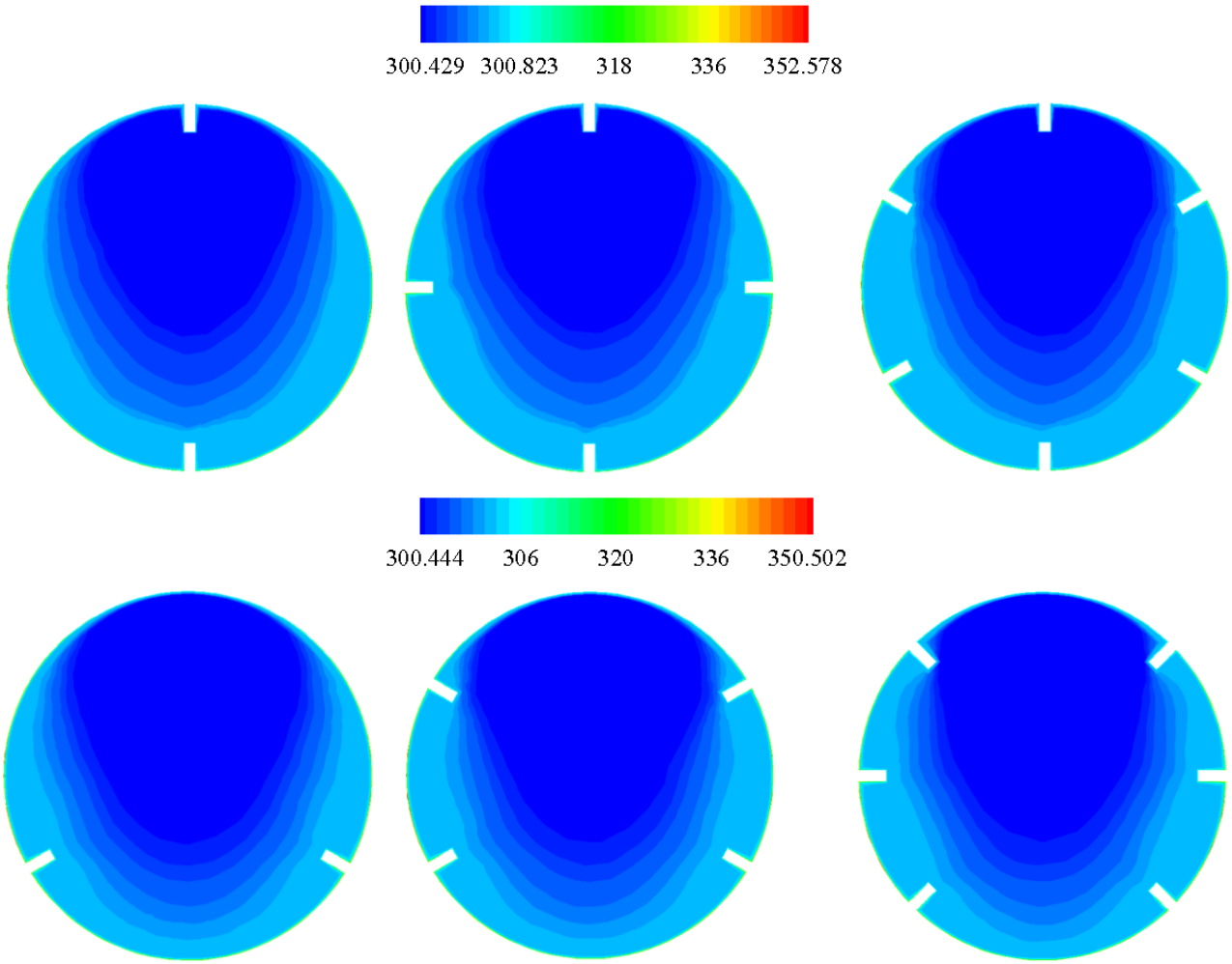

a) Re=18600

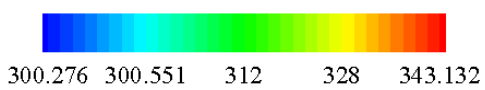

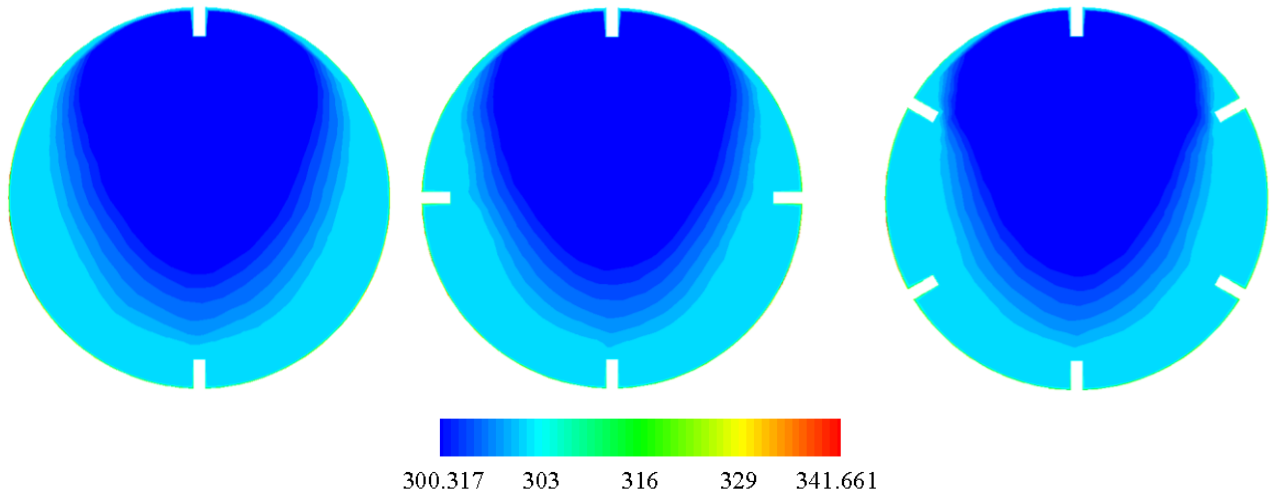
300.317
303
316
329
341.661

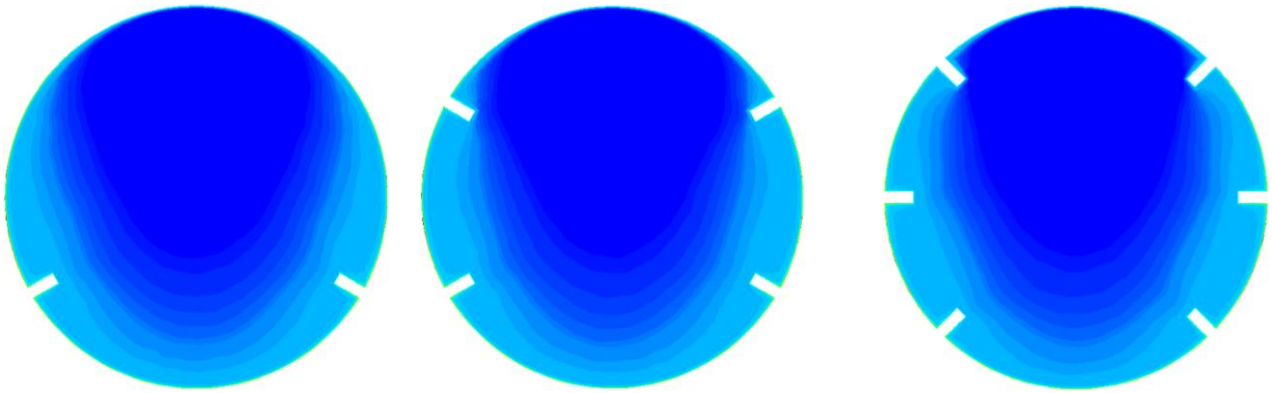

b) Re=23000

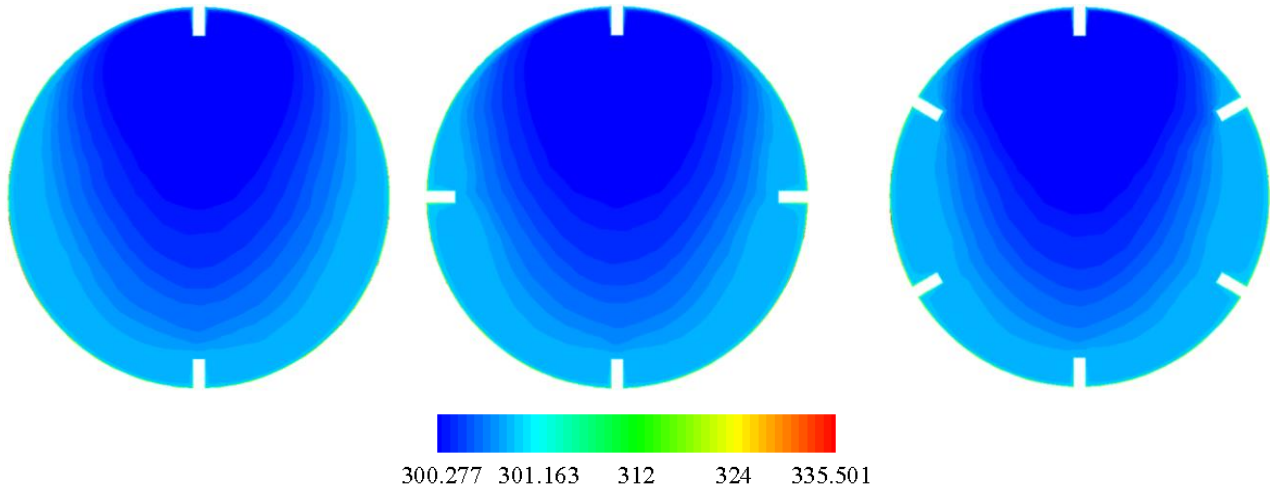
300.231
302
313
325
336.58

300.277
301.163
312
324
335.501

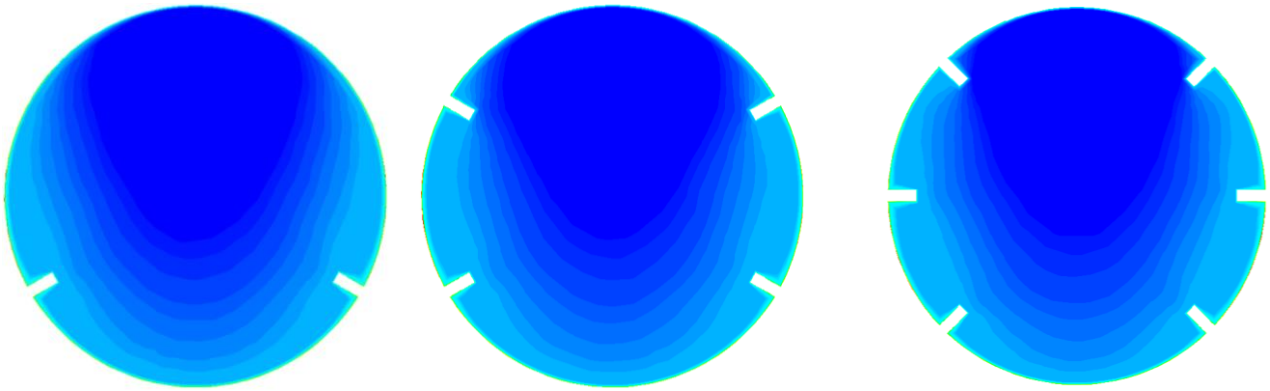

c) Re=28000

Figure. (4-6) T for different number of fin and arrangements and Re at outlet.

4.7 TKE for different number of fins, arrangements and Re at outlet

Figure (4-7) illustrated the Turbulent Kinetic Energy (TKE) of the heat transfer fluid flows inside the absorber tube.

When Re =18600, the TKE increased with the increase of the number of fins for "a" arrangement, and TKE change when compared with arrangement "b" where it slightly increase from "a" to "b" for the same number of fins.

When Re=23000 and Re=28000, the TKE behave with the same manner as in Re= 18600, but the values of TKE have clear increasing when increase the Re for the same set of the three different fin number when comparing arrangement "a" of Re=18600 with arrangement "a" of Re=23000.

Moving from (Re=23000) to (Re=28000), although the TKE increase from (0.16297 to 0.223) respectively, but the red region area decrease slightly at the places that are close to the inner wall surface.

It is obvious that the highest values of (TKE) was (0.223) occurs in the flow of the Reynolds number of (28000) and (6 Fins) with "b" arrangement, and the regions close to the absorber inner wall surface close to the Fins showed highest (TKE) values than the other regions which

represented with the red color, the high turbulence happen because of the non-uniform shape at the fins regions.

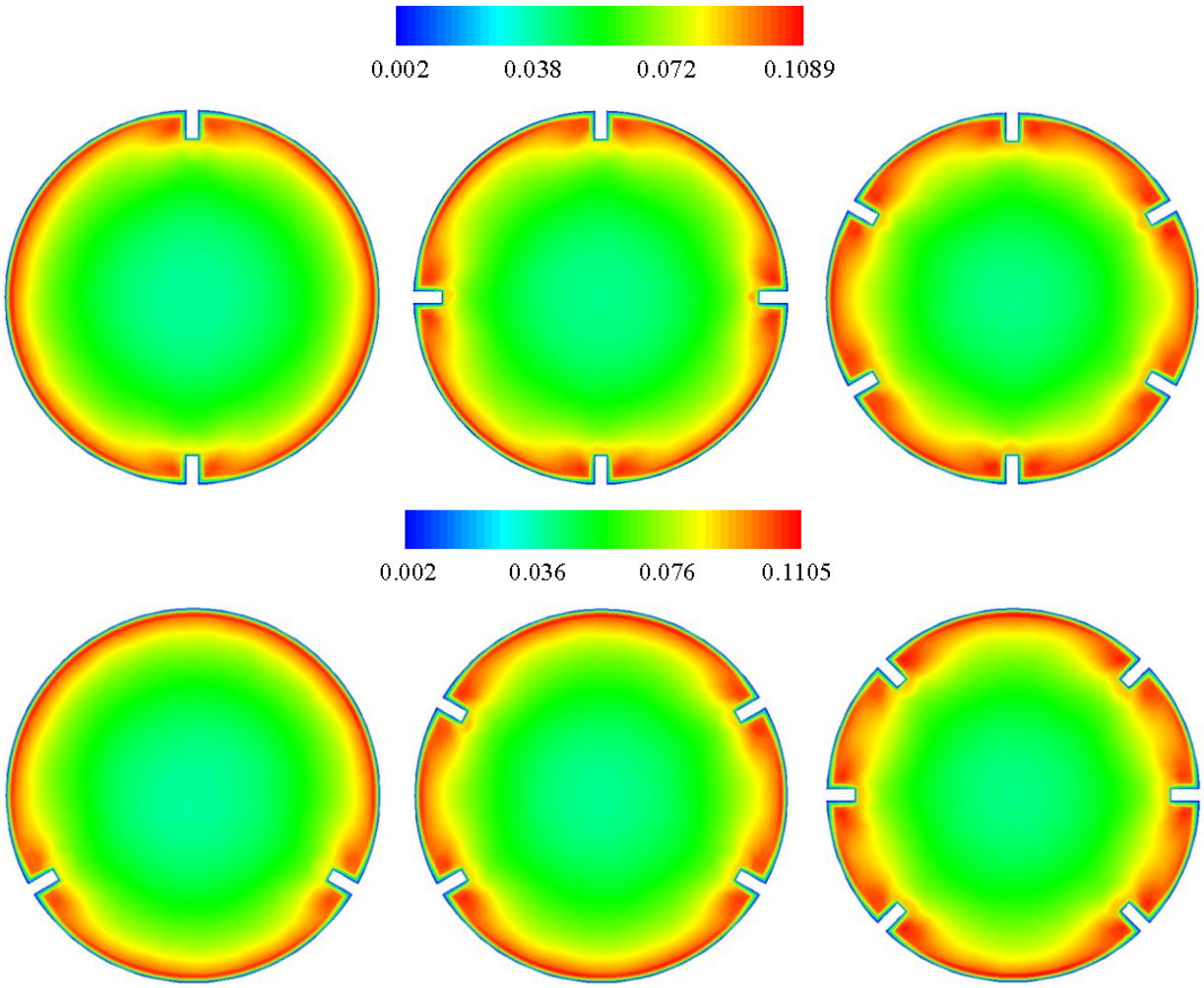

a) Re=18600

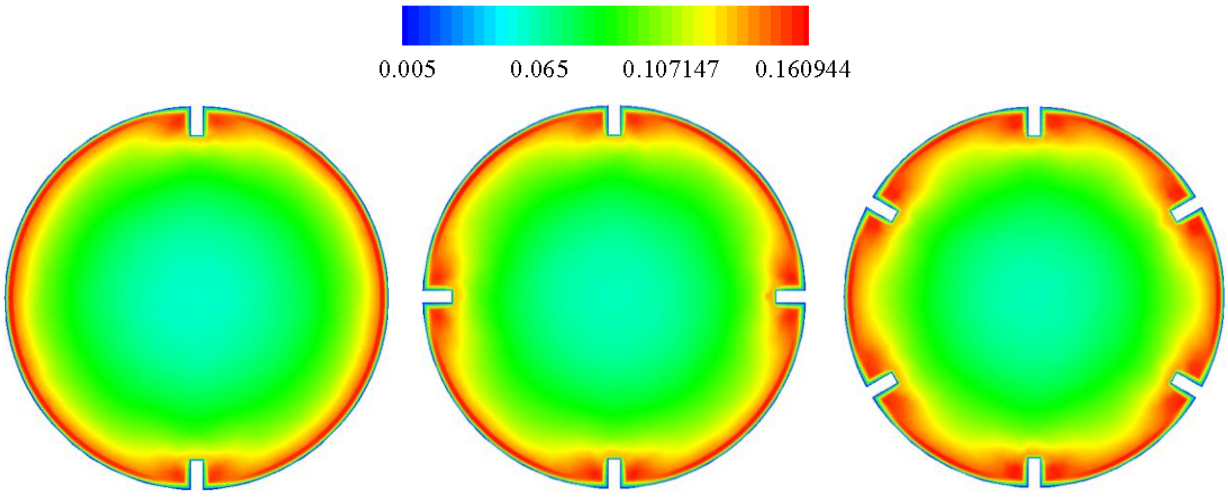

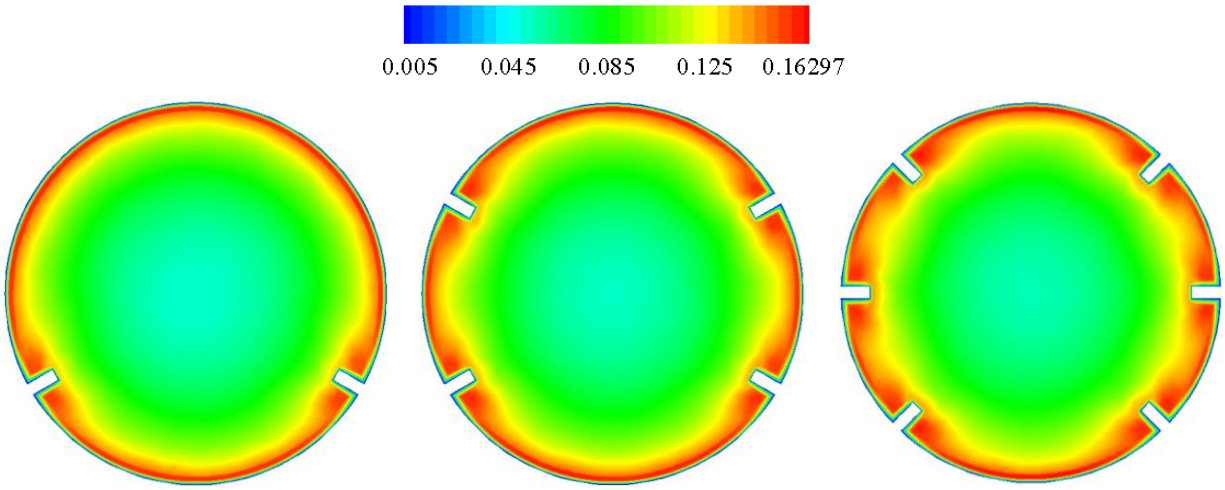

b) Re=23000

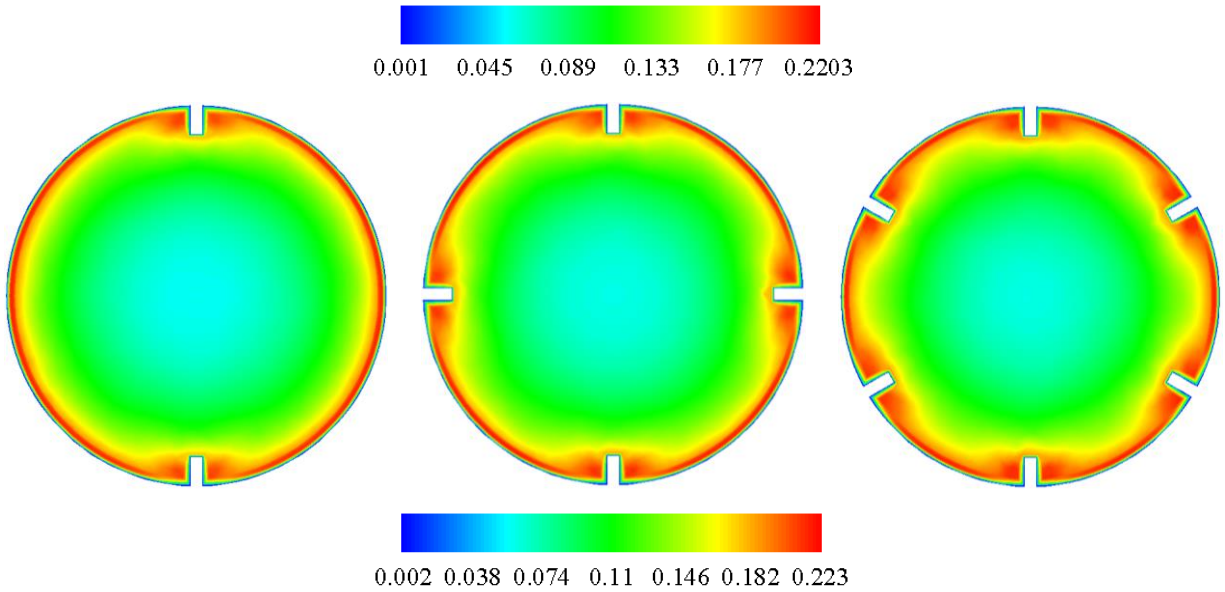

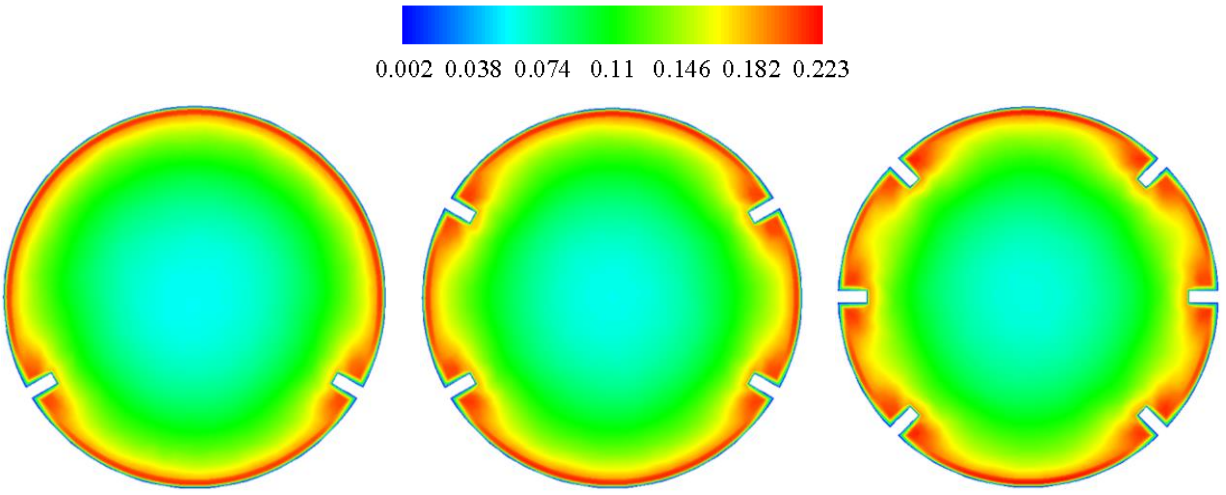

c) Re=28000

Figure.(4-7) TKE for different number of fin and arrangements and Re at outlet.

4.8 Effect of Rim angle on the outlet temperature

As tested for the heat flux concentration ratio of the collector which gave the preferable value of the Rim angle (120º). Fig. (4-8) showed the effect of Rim angle on the outlet temperature of the heat transfer fluid (HTF) for three different Reynolds numbers (18600, 23000 and 28000). At Re (18600) the outlet temperature is higher when Rim angle (120º) than when the Rim angle is (80º) and the same thing repeated at Re (23000 and 28000).

The results discussed above are acceptable for each Reynolds number since the heat flux reflected on the absorber increasing with the bigger Rim angle (120º) according to the high concentration ratio, then the heat transfer from the absorber wall to the flowing fluid increase, as a result of that the outlet temperature increased.

When the Reynolds number change from small value to bigger value, the outlet temperature (Tout) decrease because of the low velocity of the working fluid give more mass flow rate which carrying the heat to transfer from the absorber walls to the fluid itself.

The difference between the outlet temperatures in case of the low Re (18600) and high Re (28000) are very small values and ranging from (300.52K to 300.35K), so the difference is (0.17 K). At low Reynolds number (Re=18600), the difference of outlet temperature between the rim angles (120º and 80º) is about (0.02). At the moderate Reynolds number (Re=23000)), the difference of outlet temperature between the rim angles (120º and 80º) is about (0.019), at high Reynolds number (Re=28000) , the difference of outlet temperature between the rim angles (120º and 80º) is about (0.015). These results indicated that effect of increasing Reynolds number on temperature distribution for different rim angles is weak, so that rim angle of 120º can be used for different Reynolds number.

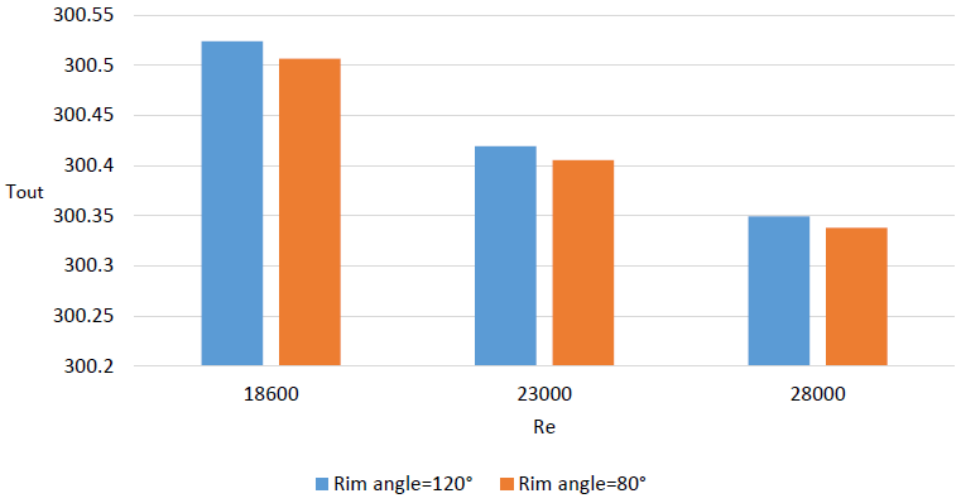

Figure (4-8) T_{out} results for different rim angle.

4.9 The Effect of Reynolds Number and Number of fins on Results of Friction Factor (f)

Figure (4-9) illustrate the results of friction factor (*f*) for different Re and number of fins (n) at "a" fin arrangement. The reason of choose arrangement "a" only is that when using arrangement "b" will give similar results of "a" arrangement as shown in fig. (4-10). The friction factor decreased with the increase of Reynolds number as it has inverse proportion with the square mean velocity due to equation (14) and this help to increase the performance of the absorber tube and then the heat transfer efficiency.

$$f = \frac{2D_i \cdot \Delta P}{\rho \cdot u_m^{\,2} \cdot L} \qquad (14)$$

For each Re, the friction factor increase with the increment of the fin number from 2 to 4 then to 6, where the velocity in this case is constant as the Re constant, so the increment of (n) will cause the area of friction between the fluid and solid surface to be increase resulting in the increasing of friction factor (f).

For each fin number (n), the value of friction factor (*f*) slightly decreased with the increase of Re because the high velocities accompanied

with the high Re number which lead to overcoming the surface friction. In general the friction factor decreasing with increasing of Re for each set of the three different number of fins (n) as obvious in fig. (4-10) .

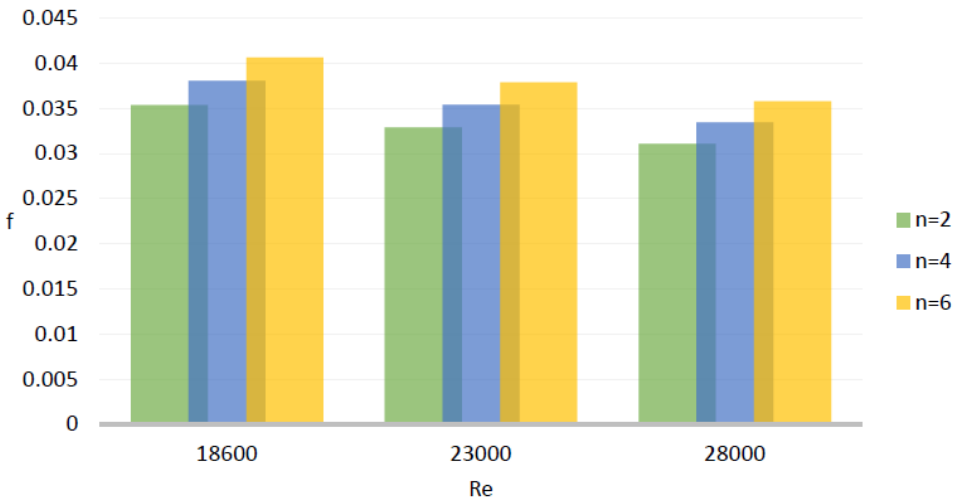

Figure (4-9) f results for different n and Re at "a" fin arrangement.

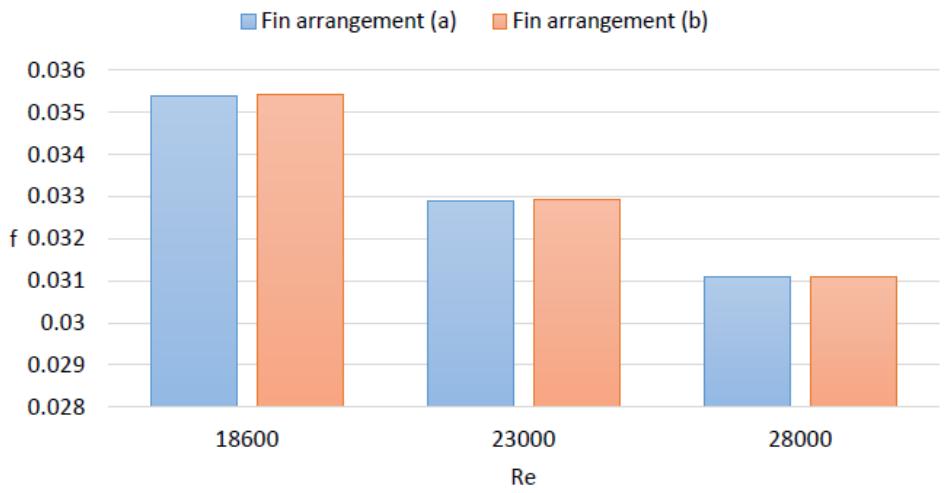

a) n=2

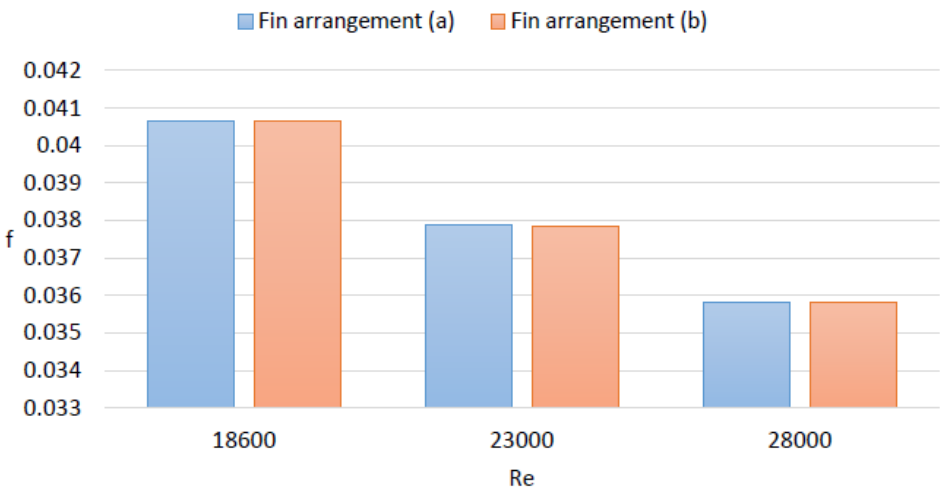

b) n=6

Figure (4-10) f results for different fin arrangements.

4.10 The Effect of Reynolds Number and Number of fins on Results of Nusselt number (Nu)

Since the Nusselt number is direct proportional with the heat transfer coefficient (h) and the use of the longitudinal fins as well as the nano material lead to increasing of (h), at the same time the contact area increased between the flowing fluid and the inner wall surface of the absorber tube also increased, resulting in more heat transfer between the contact surfaces.

$$Nu=\frac{hDin}{K}$$

In fig. (4-11), at Re=18600 the Nusselt number (Nu) increase with the increase of the number of fins and the same thing occur at Re= (23000, 28000).

The Nusselt number (Nu) also increase with the Re increasing for each set of the fin numbers at arrangement "a".

To compare the Nusselt number (Nu) of arrangement "a" and arrangement "b", move to figure (4-12) which contained three separate diagrams with fin number n of (2, 4 and 6) respectively.

For n=2, Re=18600 the Nusselt number is higher at arrangement "b" than its value at arrangement "a", and so the values of Nu in case of Re=23000 and Re=28000 being higher for "b" arrangement than the "a" arrangement. Since the heat flux distribution around the absorber surface is non-uniform therefore the arrangement of fins in case "b" distributes the fins in the hottest region therefore the heat transfer rate was enhanced.

The same behavior exactly appears when discussing the cases of n=4 and n=6.

The overall look at figures (4-11) and (4-12) it could be concluded that the highest Nu occur at Re= 28000 with arrangement "b" and number of fins (n=6) where it almost reach (500 w/m²) as well as

The high value of Nusselt number when increasing the fin number signified the enhancement in the heat transfer efficiency of the absorber tube by using the longitudinal fins.

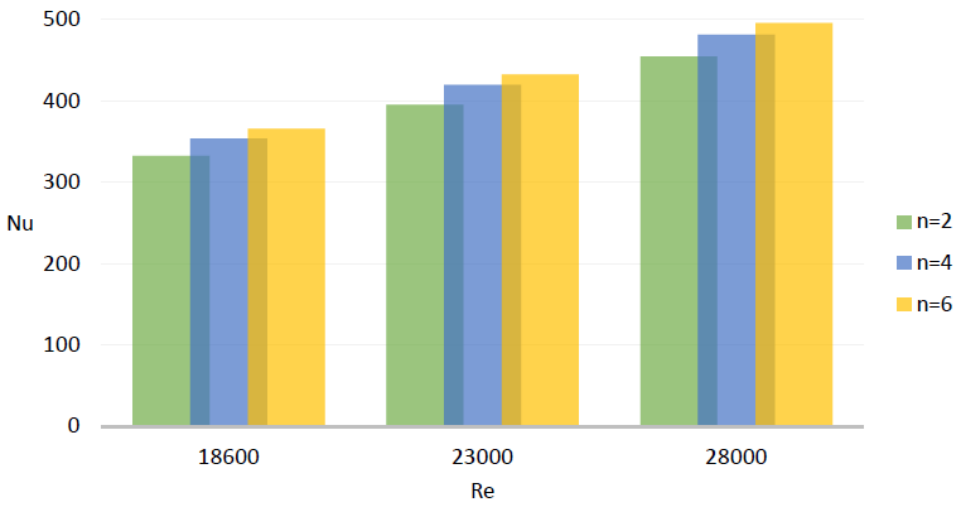

Figure.(4-11) Nu **results for different n and Re at "a" fin arrangement.**

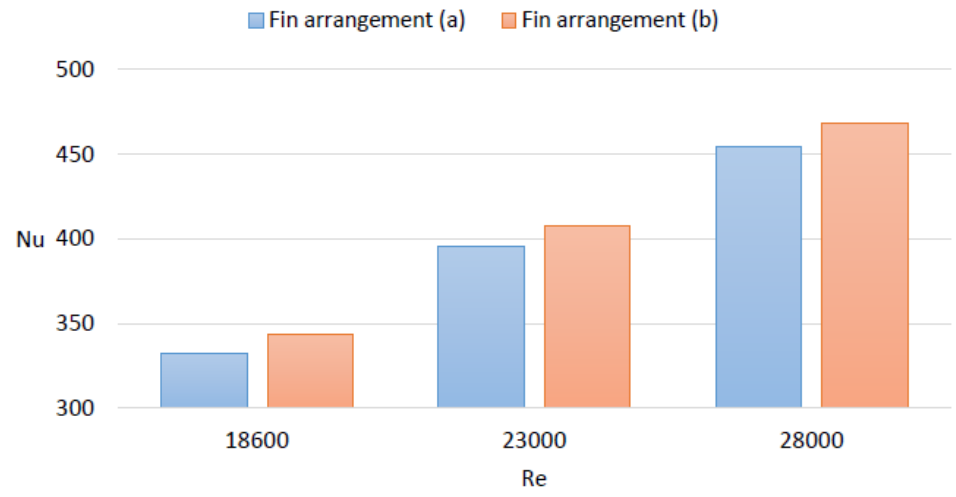

a) n=2

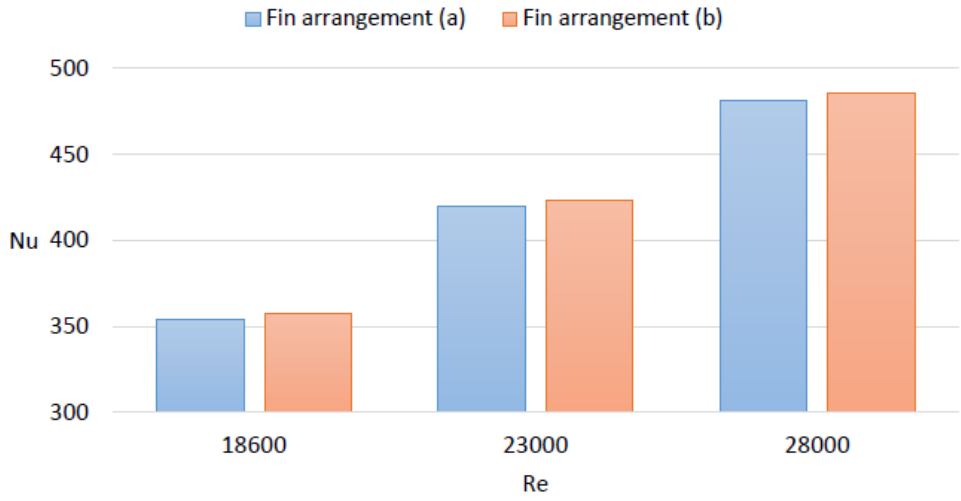

b) n=4

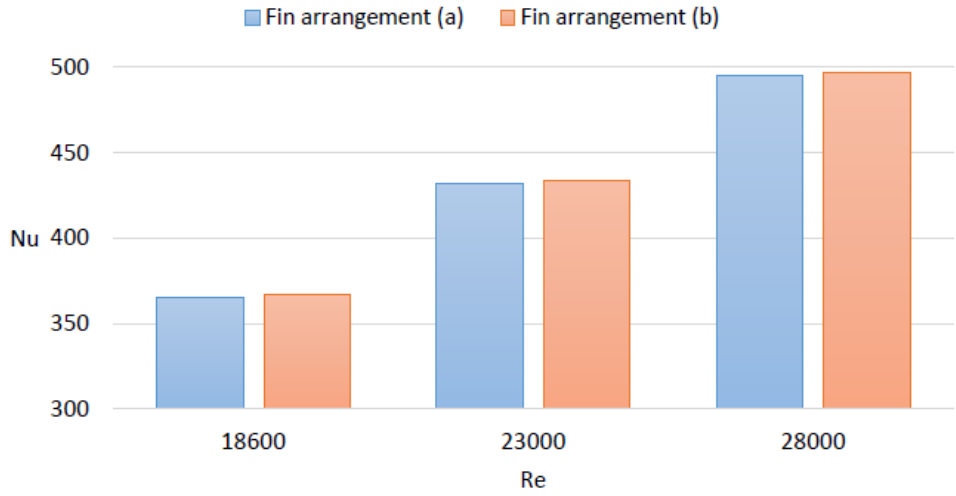

c) n=6

Figure. (4-12) Nu ***results for different fin arrangements.***

4.11 Performance Evaluation Criterion (PEC)

There were multy effects of both Nusselt number (Nu) and the friction factor (*f*) that employed to measure the overall hydrothermal behavior of absorber tube using Performance evaluation criterion (PEC) as expressed in Eq. (19) which expresses the heat transfer coefficient enhancement under ‘‘constant pumping work conditions’’. The subscript ‘‘0’’ means the reference case with smooth absorber tube.

$$PEC = \frac{\left(\frac{Nu}{Nu_0}\right)}{\left(\frac{f}{f_0}\right)^{1/3}} \tag{19}$$

Fig. (4-13) shows the variation of the thermal performance factor versus Reynolds number for three different numbers of longitudinal fins (2, 4, 6) at “a” fin arrangement in the absorber tube, it can be observed that the thermal performance factor values are greater than unity over the entire Reynolds number range and slightly decrease with the increase in the number of Reynolds at same fin number. Additionally, when the fin number increases the thermal performance factor increases at the same Reynolds number, this implies that the increase in pressure loss can be balanced by the improvement in the heat transfer when using of finned tube comparison to the smooth tube.

To understand the role of the two fins arrangement studied, fig. (4-14) showed three separate diagrams each one represented the relation between the performance evaluation criteria (PEC) and Reynolds number for two different arrangements of the longitudinal fins supported in the absorber tube "a" and "b", each case studied with fixed number of fins (2, 4 and 6).

For n=2, arrangement "a" the PEC almost stayed constant when Re increased and still more than unity in its value. While the PEC slightly decreased for n=2 and at arrangement "b" when Re increased.

It was noticed that the same behavior repeated in the second and third diagrams with little difference in PEC values for each case, as well as the highest PEC achieved with case of n=6, arrangement "b" and Re=18600 which is roughly equal (1.060845).

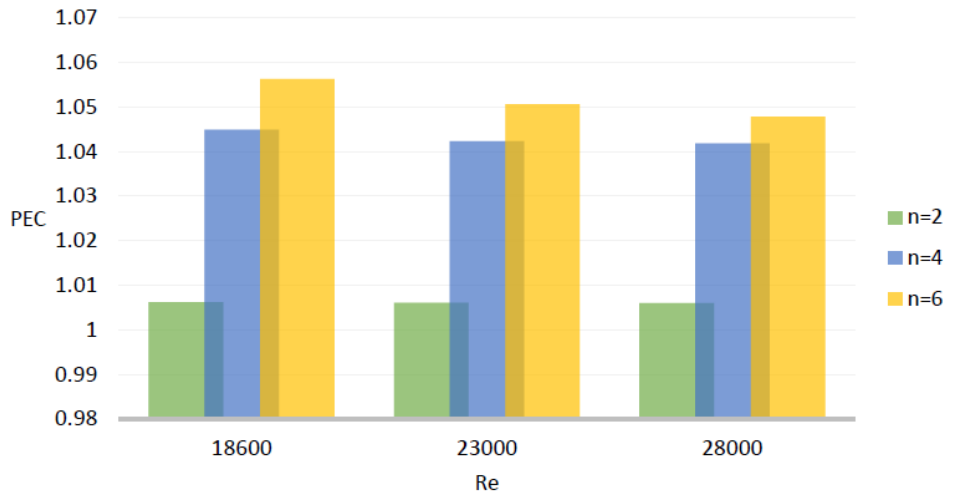

***Figure (4-13)** PEC results for different n and Re at "a" fin arrangement.*

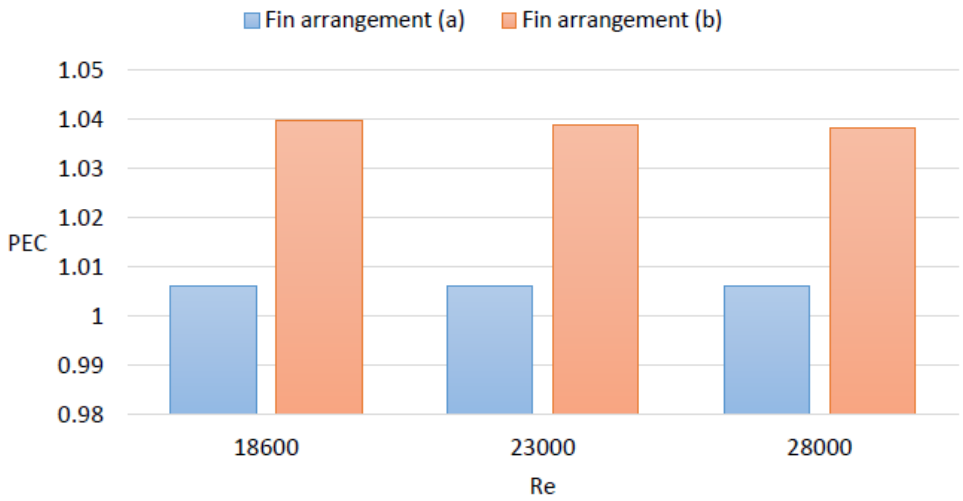

a) n=2

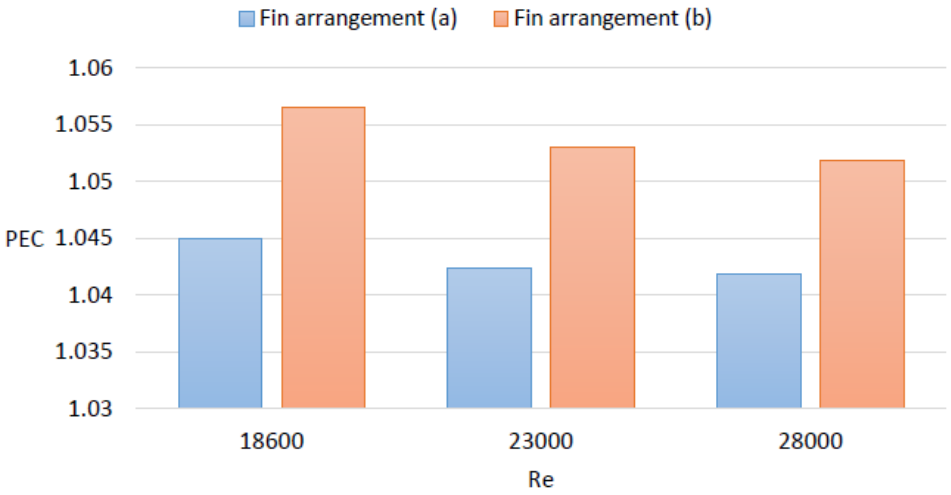

b) n=4

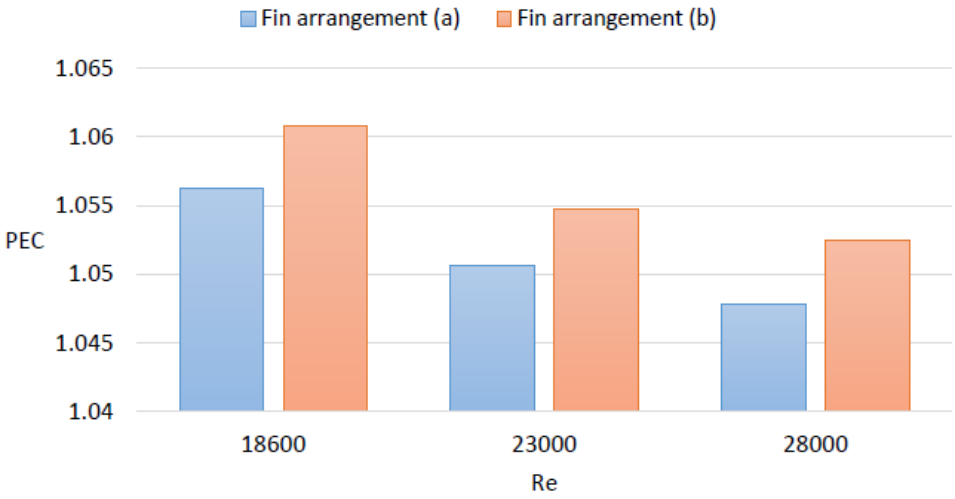

c) n=6

Figure (4-14) *PEC* ***results for different fin arrangements.***

4.12 The Effect of the Volume Fraction and the Re on the Nusselt Number

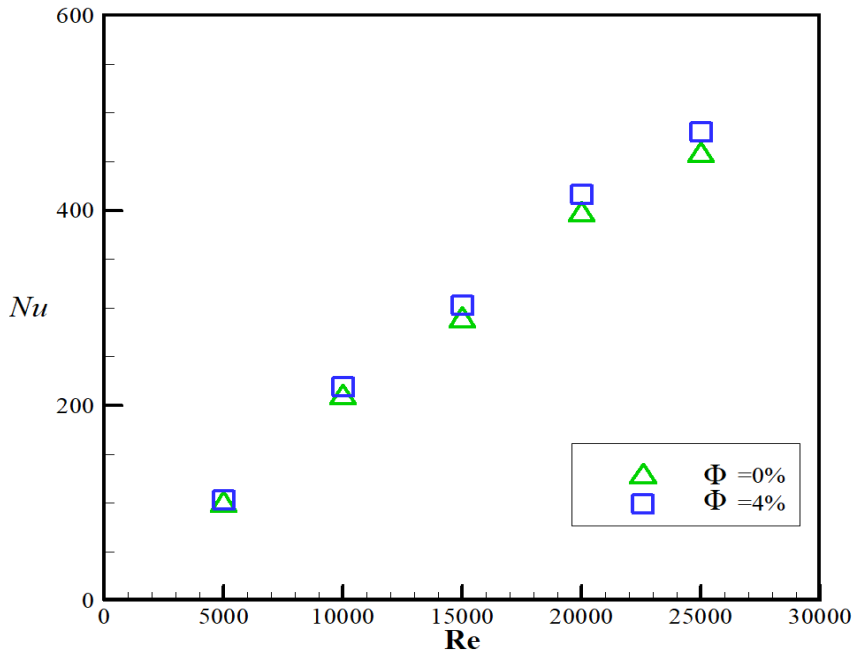

Figure (4-14) Influence of adding nanoparticles to base fluid

There is an important point including the usage of high Reynolds number which is higher than 15000, the explanation for this point is that at the low values of Re (5000 to 10000), the Nusselt number not increased significantly even when changing the nanomaterial volume fraction from (0% to 4%), while the increasing in (Nu) being higher when comparing between the nano material volume fractions (0% and 4%) at Re values higher than 15000 as it is illustrated in Fig. (4-14). The increase of the of the volume fraction lead to higher thermal conductivity (k) as well as to higher heat transfer coefficient (h), at the low Reynolds number values the increase in (k) is more than the increase in (h) so the change in Nu value is low, this behavior can be concluded because of the higher viscosity achieved when increasing the volume fraction. When increasing the Reynolds to high values the effect of the viscosity will be less than the heat transfer coefficient (h). The conclusion is that the increase of the heat

transfer coefficient and Nusselt number are more affected with the Reynolds number than the volume fraction.

4.13 The Results of the Performance Evaluation Criteria (PEC)

These results are very important to consider in the resent study which are giving high absorber performance indication and they are an evidence of that enhancement. All the situations discussed and studied are listed with the values related and tabulated in table (5) in appendix (B) which obtained from both Figures (4-12) and (4-13).

.

Type a	Re	Nu	PEC	% PEC		Type b	Re	Nu	PEC	% PEC
n=2	18600	332.5452	1.006248	0.624827		n=2	18600	343.6914	1.039775	3.977505
	23000	395.133	1.0061	0.61			23000	407.8759	1.038862	3.886228
	28000	454.4474	1.006002	0.60021			28000	468.593	1.038278	3.827791
n=4						n=4				
	18600	353.8505	1.04493	4.492976			18600	357.5639	1.056541	5.654115
	23000	419.3878	1.042387	4.238677			23000	423.502	1.05304	5.304024
	28000	481.4866	1.041876	4.187558			28000	485.9193	1.051858	5.185773
n=6						n=6				
	18600	365.583	1.05626	5.625958			18600	367.1191	1.060845	6.084535
	23000	432.2544	1.050615	5.061474			23000	433.8904	1.054766	5.47663
	28000	495.3455	1.047871	4.787076			28000	497.0725	1.05253	5.252954

Chapter Five

Conclusions and Suggestions for Future Work

5 Chapter Five: Conclusions and Suggestions for Future Work

5.1 Conclusions

In this study, heat transfer was enhanced by using a comparison between two rim angles (80º and 120º) and three different number of steel longitudinal fins (5mm height x 2mm width) mounted on the inner wall surface of the absorber tube, also using nanofluid (Al_2O_3 / Syltherm 800) with volume fraction not exceed (4%) as well as the technique of changing the arrangements in two different manners as "a" and "b" arrangements. A numerical analysis conducted with (18) cases depending on the varieties in the parameters such as Reynolds number, fins arrangements ("a" and "b") and number of fins (2,4, and 6). The use of fins increase the drop in pressure and the friction factor, but on the other hand the heat transfer coefficient increased with the help of the Nano material. Moreover the technique of testing the better heat flux concentration ratio using the Monte Carlo Ray Tracing (MCRT) method and changing the Rim angle added additional performance enhancement. The comparison between the smooth tube and the finned tube displayed an increase of Nusselt number (Nu) against the friction factor which lead to the enhancement of Performance Evaluation Criteria (PEC =1.060845) and the percentage of PEC to (PEC% = 6.084535%) which represents heat transfer coefficient enhancement. There is an important point concerning the usage of high Reynolds number which is higher than 15000, the explanation for this point is that at the low values of Re (5000 to 10000), the Nusselt number did not increase significantly even when changing the nanomaterial volume ratio from (0% to 4%), while the increasing in (Nu) is obvious when comparing between the nanomaterial volume ratios (0% and 4%) at Re values higher than 15000 as it is illustrated in Fig. (4-14).

The numerical results of analyzing the flow and heat transfer in the absorber tube for different parameters can be detailed as below:

1- The outlet fluid temperature T_{out} has the biggest value when Re=18600, while it has moderate value at Re=23000, and the lowest value achieved at Re=28000.
2- T_{out} has the biggest values for rim angle=120^{o} than rim angle=80^{o} for all three Reynolds numbers.
3- The friction factor has the maximum values when using (6 fins) rather than using (2 or 4 fins).
4- The friction factor has the maximum values when Re=18600 rather than (Re=23000 or 28000) for all the fin number categories mentioned.
5- The friction factor value doesn't change when using different fins arrangements for the same number of fins and Re (changing the arrangements of fins not affecting on the friction factor).
6- Nusselt number has the maximum values (Re= 28000 rather than Re=18600 and 23000), as same as when (n=6 rather than n=2 or 4 fins), that is due to the heat transfer coefficient enhancement.
7- Nusselt number has the maximum values with the arrangement "b" for all Re and n values mentioned in point (6).
8- The Performance Evaluation Criteria (PEC) has the maximum value when (n=6 rather than n=2 or 4), also when Re=18600 with arrangement "b".

5.2 Suggestions for Future Work

It is possible to obtain the highest heat transfer enhancement using the same absorber tube, therefore, there are many suggestions for the coming work in the future depend on the results of the present work as bellow: -

1- Conducting the experimental work for the same Circumstances of the present study.

2- Developing the shape of the circular absorber to the new Geometry that is contained a helical absorber.
3- The future studies can use the fins made of porous medium.
4- Developing the new Geometry of absorber tube utilizing hybrid Nano fluid with utilizing the same options tested in the present study.
5- Suggesting to utilize different shapes of longitudinal fins such as a helical shape fins.
6- The future studies can concentrate on the Rim angle and to develop its effect on the concentration ratio.

References

6 References

[1] N. Kincaid, G. Mungas, N. Kramer, M. Wagner, and G. Zhu, “An optical performance comparison of three concentrating solar power collector designs in linear Fresnel, parabolic trough, and central receiver,” *Appl. Energy*, vol. 231, no. June, pp. 1109–1121, 2018, doi: 10.1016/j.apenergy.2018.09.153.

[2] R. V. Padilla, G. Demirkaya, D. Y. Goswami, E. Stefanakos, and M. M. Rahman, “Heat transfer analysis of parabolic trough solar receiver,” *Appl. Energy*, vol. 88, no. 12, pp. 5097–5110, 2011, doi: 10.1016/j.apenergy.2011.07.012.

[3] F. J. Cabrera, A. Fernández-García, R. M. P. Silva, and M. Pérez-García, “Use of parabolic trough solar collectors for solar refrigeration and air-conditioning applications,” *Renew. Sustain. Energy Rev.*, vol. 20, pp. 103–118, 2013, doi: 10.1016/j.rser.2012.11.081.

[4] Y. Wang, Q. Liu, J. Lei, and H. Jin, “Performance analysis of a parabolic trough solar collector with non-uniform solar flux conditions,” Int. J. Heat Mass Transf., vol. 82, pp. 236–249, 2015, doi: 10.1016/j.ijheatmasstransfer.2014.11.055.

[5] R. G. Patil, S. V Panse, and J. B. Joshi, “Optimization of non-evacuated receiver of solar collector having non-uniform temperature distribution for minimum heat loss,” Energy Convers. Manag., vol. 85, pp. 70–84, 2014, doi: 10.1016/j.enconman.2014.05.047.

[6] F. Wang, J. Tan, L. Ma, and C. Wang, “Effects of glass cover on heat flux distribution for tube receiver with parabolic trough collector system,” Energy Convers. Manag., vol. 90, pp. 47–52, 2015, doi: 10.1016/j.enconman.2014.11.004.

[7] B. Amina, A. Miloud, L. Samir, B. Abdelylah, and J. P. Solano, “Heat transfer enhancement in a parabolic trough solar receiver using longitudinal fins and nanofluids,” J. Therm. Sci., vol. 25, no. 5, pp. 410–417, 2016, doi: 10.1007/s11630-016-0878-3.

[8] E. Bellos, C. Tzivanidis, and K. A. Antonopoulos, “A detailed working fluid investigation for solar parabolic trough collectors,” Appl. Therm. Eng., 2016, doi: 10.1016/j.applthermaleng.2016.11.201.

[9] Y. Wang, J. Xu, Q. Liu, Y. Chen, and H. Liu, “Performance analysis of a parabolic trough solar collector using Al2O3/synthetic oil nanofluid,” Appl. Therm. Eng., vol. 107, pp. 469–478, 2016, doi: 10.1016/j.applthermaleng.2016.06.170.

[10] G. Xiangtao, W. Fuqiang, W. Haiyan, T. Jianyu, L. Qingzhi, and H. Huaizhi, “Heat transfer enhancement analysis of tube receiver for parabolic trough solar collector with pin fin arrays inserting,” *Sol. Energy*, vol. 144, pp. 185–202, 2017, doi: 10.1016/j.solener.2017.01.020.

[11] E. Bellos and C. Tzivanidis, “Parametric investigation of nanofluids utilization in parabolic trough collectors,” Therm. Sci. Eng. Prog., vol. 2, pp. 71–79, 2017, doi: 10.1016/j.tsep.2017.05.001.

[12] J. Jin, Y. Ling, and Y. Hao, “Similarity analysis of parabolic-trough solar collectors,” Appl. Energy, pp. 1–8, 2017, doi: 10.1016/j.apenergy.2017.04.065.

[13] J. Subramani, P. K. Nagarajan, O. Mahian, and R. Sathyamurthy, “Efficiency and heat transfer improvements in a parabolic trough solar collector using TiO2 nanofluids under turbulent flow regime,” *Renew. Energy*, vol. 119, pp. 19–31, 2018, doi: 10.1016/j.renene.2017.11.079.

[14] A. Mwesigye and J. P. Meyer, “Optimal thermal and thermodynamic performance of a solar parabolic trough receiver with different nanofluids

and at different concentration ratios," *Appl. Energy*, vol. 193, pp. 393–413, 2017, doi: 10.1016/j.apenergy.2017.02.064.

[15] E. Bellos, C. Tzivanidis, and D. Tsimpoukis, "Optimum number of internal fins in parabolic trough collectors," *Appl. Therm. Eng.*, vol. 137, no. March, pp. 669–677, 2018, doi: 10.1016/j.applthermaleng.2018.04.037.

[16] Q. Wang, H. Yang, X. Huang, J. Li, and G. Pei, "Numerical investigation and experimental validation of the impacts of an inner radiation shield on parabolic trough solar receivers," *Appl. Therm. Eng.*, vol. 132, pp. 381–392, 2018, doi: 10.1016/j.applthermaleng.2017.12.112.

[17] Q. Wang, H. Yang, M. Hu, X. Huang, J. Li, and G. Pei, "Preliminary performance study of a high-temperature parabolic trough solar evacuated receiver with an inner transparent radiation shield," *Sol. Energy*, vol. 173, no. December 2017, pp. 640–650, 2018, doi: 10.1016/j.solener.2018.07.065.

[18] M. Fan *et al.*, "An optimized Monte Carlo ray tracing optical simulation model and its applications to line-focus concentrating solar collectors," *Appl. Energy*, vol. 225, no. May, pp. 769–781, 2018, doi: 10.1016/j.apenergy.2018.05.067.

[19] D. Korres, E. Bellos, and C. Tzivanidis, "Investigation of a nanofluid-based compound parabolic trough solar collector under laminar flow conditions," *Appl. Therm. Eng.*, vol. 149, pp. 366–376, 2019, doi: 10.1016/j.applthermaleng.2018.12.077.

[20] A. Amine, I. Rodríguez, and C. Ghenai, "Thermo-hydraulic analysis and numerical simulation of a parabolic trough solar collector for direct steam generation," *Appl. Energy*, vol. 214, no. October 2017, pp. 152–165, 2018, doi: 10.1016/j.apenergy.2018.01.054.

[21] Z. D. Cheng, X. R. Zhao, and Y. L. He, "Novel optical efficiency formulas for parabolic trough solar collectors: Computing method and applications Ze-Dong," *Appl. Energy*, vol. 224, no. May, pp. 682–697, 2018, doi: 10.1016/j.apenergy.2018.05.033.

[22] P. D. Tagle-Salazar, K. D. P. Nigam, and C. I. Rivera-Solorio, "Heat transfer model for thermal performance analysis of parabolic trough solar collectors using nanofluids," *Renew. Energy*, vol. 125, pp. 334–343, 2018, doi: 10.1016/j.renene.2018.02.069.

[23] C. Chang *et al.*, "Enhanced heat transfer in a parabolic trough solar receiver by inserting rods and using molten salt as heat transfer fl uid ☆," *Appl. Energy*, vol. 220, no. March, pp. 337–350, 2018, doi: 10.1016/j.apenergy.2018.03.091.

[24] M. V. Bozorg, M. Hossein Doranehgard, K. Hong, and Q. Xiong, "CFD study of heat transfer and fluid flow in a parabolic trough solar receiver with internal annular porous structure and synthetic oil–Al2O3 nanofluid," *Renew. Energy*, vol. 145, pp. 2598–2614, 2020, doi: 10.1016/j.renene.2019.08.042.

[25] Bellos, E., & Tzivanidis, C. (2019). Thermal efficiency enhancement of nanofluid-based parabolic trough collectors. Journal of Thermal Analysis and Calorimetry, 135(1), 597–608. https://doi.org/10.1007/s10973-018-7056-7

[26] Bellos, E., & Tzivanidis, C. (2019). Investigation of a booster secondary reflector for a parabolic trough solar collector. *Solar Energy*, *179*, 174–185. https://doi.org/10.1016/j.solener.2018.12.071

[27] R. K. Donga and S. Kumar, "Thermal performance of parabolic trough collector with absorber tube misalignment and slope error," *Sol.*

Energy, vol. 184, no. March, pp. 249–259, 2019, doi: 10.1016/j.solener.2019.04.007.

[28] F. Razmmand, R. Mehdipour, and S. M. Mousavi, "A numerical investigation on the effect of nanofluids on heat transfer of the solar parabolic trough collectors," *Appl. Therm. Eng.*, vol. 152, pp. 624–633, 2019, doi: 10.1016/j.applthermaleng.2019.02.118.

[29] M. M. Heyhat, M. Valizade, S. Abdolahzade, and M. Maerefat, "Thermal efficiency enhancement of direct absorption parabolic trough solar collector (DAPTSC) by using nanofluid and metal foam," *Energy*, vol. 192, 2020, doi: 10.1016/j.energy.2019.116662.

[30] R. Ekiciler, K. Arslan, O. Turgut, and B. Kurşun, "Effect of hybrid nanofluid on heat transfer performance of parabolic trough solar collector receiver," *J. Therm. Anal. Calorim.*, no. 0123456789, 2020, doi: 10.1007/s10973-020-09717-5.

[31] E. Bellos, C. Tzivanidis, and Z. Said, "A systematic parametric thermal analysis of nanofluid-based parabolic trough solar collectors," *Sustain. Energy Technol. Assessments*, vol. 39, no. February, p. 100714, 2020, doi: 10.1016/j.seta.2020.100714.

[32] Timeline of Computer History. Available at the website address https://www.computerhistory.org/timeline/1948/

[33] Jinxu Zhao, Bruno Oliveira and Tom Schrijvers. "A Mechanical Formalization of Higher-Ranked Polymorphic Type Inference." Proc. ACM Program. Lang, 2019; vol:3. pp. 1-29

[34] History of programming languages. (19 / 3 / 2020) . Available at the website address https://en.wikipedia.org/wiki/History_of_programming_languages

[35] A Brief History of MATLAB. (2018). Available at the website address https://www.mathworks.com/company/newsletters/articles/a-brief-history-of-matlab.html

[36] Numerical analysis. (19 / 3 / 2020) . Available at the website address https://en.wikipedia.org/wiki/Numerical_analysis

[37] J. U. Brackbill & H. M. Ruppel. FLIP "A method for adaptively zoned, Particle-In-Cell calculations of fuid flows in two dimensions." J. Comp. Phys ,1986; vol :65. pp. 314-343.

[38] Donna Calhoun . "A Cartesian Grid Method for Solving the Two-Dimensional Stream function Vorticity Equations in Irregular Regions." Journal of Computational Physics,2002; vol :176. pp. 231–275.

[39] F. L. P. Santos1, V. G. Ferreira, M. F. Tomé, A. Castelo, N. Mangiavacchi and S. McKee. "A marker-and-cell approach to free surface 2-D multiphase flows." Int. J. Numer. Meth. Fluids, 2012; vol :70 , issue: 12. pp. 1–16

[40] H K VERSTEEG and W MALASEKERA. An introduction to computational Fluid Dynamics, The Finite Volume Method (2007), Available at the website address Versteeg_H_K_,_Malalasekera_W_Introduction_To_Computational_Fluid.pdf

[41] Fluent Ansys, "Ansys Fluent Theory Guide," *ANSYS Inc., USA*, vol. 15317, no. November, pp. 724–746, 2013.

[42] Kasaeian, A. B. (2012). Convection Heat Transfer Modeling of Ag Nanofluid Using Different Viscosity Theories. *IIUM Engineering Journal*, *13*(1). https://doi.org/10.31436/iiumej.v13i1.149

[43] Khanafer, K., & Vafai, K. (2011). A critical synthesis of thermophysical characteristics of nanofluids. *International Journal of Heat and Mass Transfer*, *54*(19–20), 4410–4428. https://doi.org/10.1016/j.ijheatmasstransfer.2011.04.048

[44] W. Yu and S. U. S. Choi, "The role of interfacial layers in the enhanced thermal conductivity of nanofluids: A renovated Maxwell model," *J. Nanoparticle Res.*, vol. 5, no. 1–2, pp. 167–171, 2003, doi: 10.1023/A:1024438603801.

[45] G. Batchelor, The effect of Brownian motion on the bulk stress in a suspension of spherical particles, J. Fluid Mech. 83 (1977) 97–117

[46] Yunus A. Cengel, Afshin J. Ghajar. Heat and Mass Transfer Fundamental and Application 2015.

[47] Khan, I., Saeed, K., & Khan, I. (2019, November 1). Nanoparticles: Properties, applications and toxicities. *Arabian Journal of Chemistry*. Elsevier B.V. https://doi.org/10.1016/j.arabjc.2017.05.011

[48] Sabah A. Abdul Ameer Experimental and Theoretical Study of Absorption Cooling System Integrated with Solar Concentrated Collector (2018).

[49] M. Malekan, A. Khosravi, S. Syri, Heat transfer modeling of a parabolic trough solar collector with working fluid of Fe3O4 and CuO/Therminol 66 nanofluids under magnetic field, Applied Thermal Engineering 163 (2019) 114435.

[50] Dow Oil and Gas, "Syltherm 800 Heat Transfer Fluid," pp. 1–28, 1997.

[51] SPENCER, G. H., MURTY, M. V. R. K. General Ray-Tracing Procedure. DOI:10.1364/JOSA.52.000672

Appendix (A)

ANSYS fluent Steps performed for calculating flow and heat transfer inside circular absorber tube

7 Appendix (A): ANSYS fluent Steps performed for calculating flow and heat transfer inside circular absorber tube

Parabolic fined tube with Sylterm800-Al2O3 as a heat transfer fluid

Parameter	Value
Inner diameter	66 mm
Outer diameter	70 mm
Length of tube	1500 mm
Height of fins	5 mm
Width of fins	2 mm

Solid works

1. How to draw a pipe with a fin in SolidWorks:

First, we create the geometry we want to draw in SolidWorks by creating a new sketch and selecting the plane, and then we extrude it along the axis.

To create a new sketch, left-click on the desired plane and select new sketch.

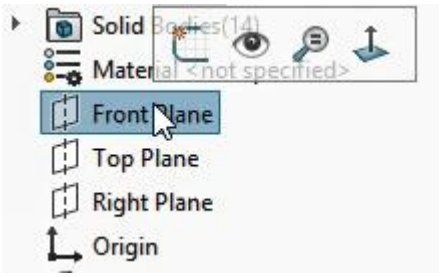

1.1.

In the first sketch, we first draw a circle with a diameter of 70 mm

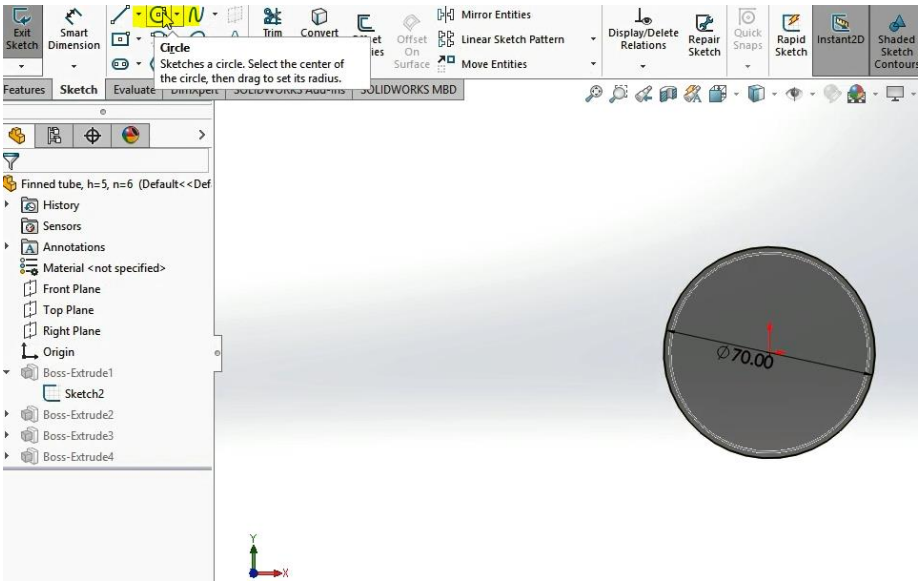

Then, by selecting the Extrude option from the top of the screen, in the direction of the pipe axis, we enter the length in the opened window in the amount of 1500 mm, which is equal to the length of the pipe.

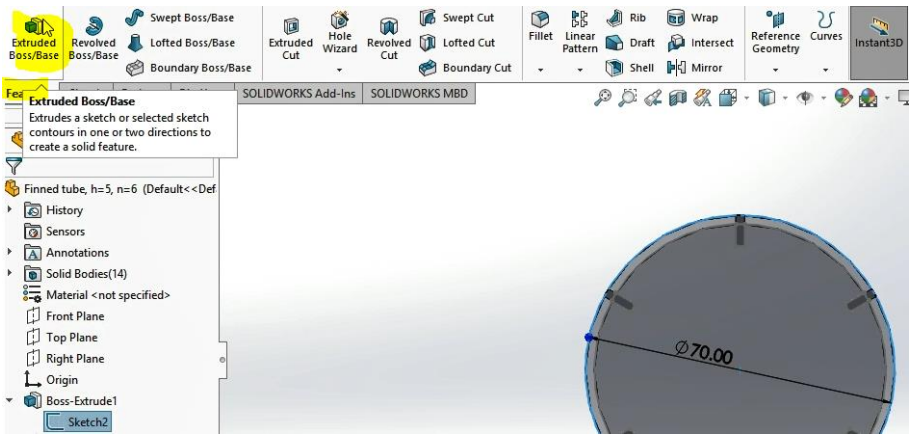

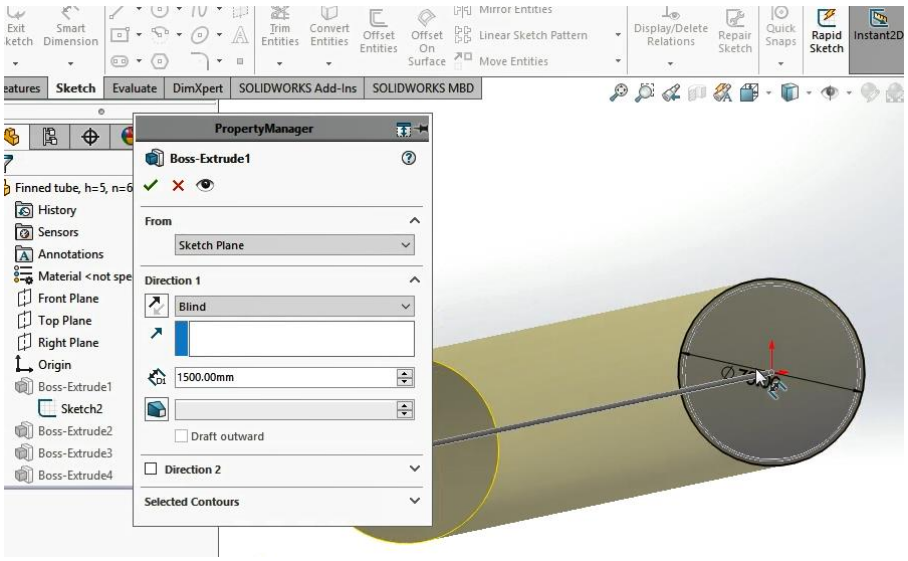

1.2.

In the second sketch, draw the inner diameter of the pipe to 66 mm and extrude as before.

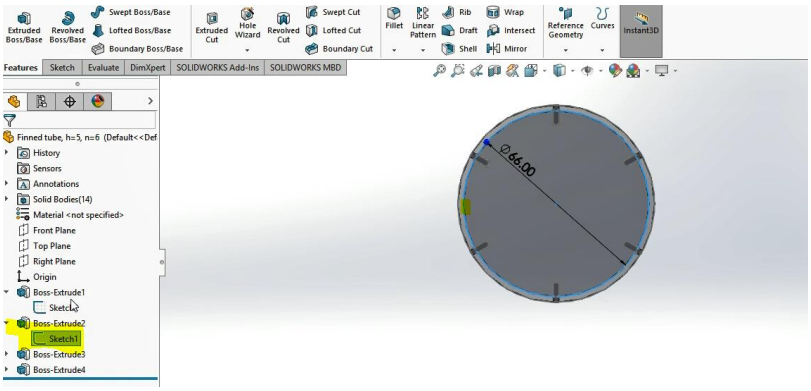

1.3.

The third sketch is about drawing the fins, which is very simple, first we draw a circle with a diameter of 66 mm and then a rectangle. Then select the drawn rectangle. Next, by using the circular sketch pattern option, select the number and location of the fins in the opened window.

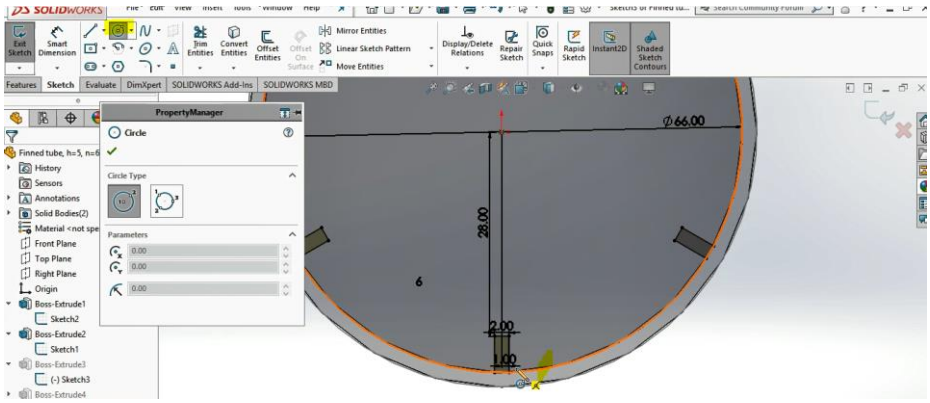
PropertyManager
Circle
Circle Type
Parameters
Ø66.00
28.00
2.00
1.00
6

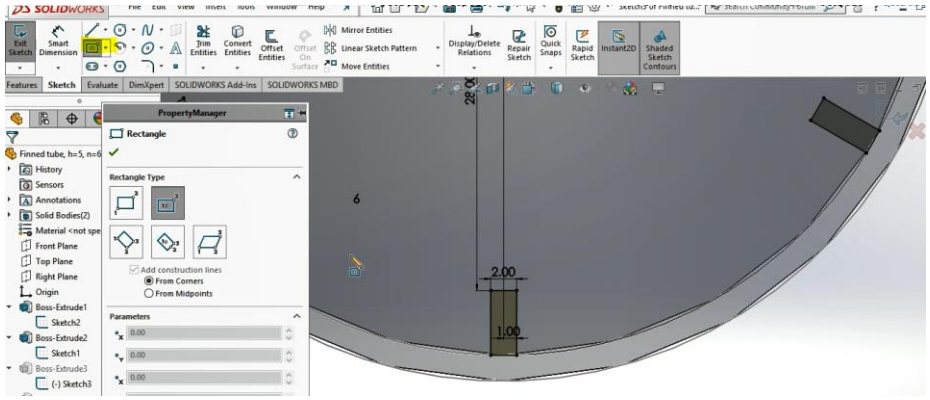
PropertyManager
Rectangle
Rectangle Type
Add construction lines
From Corners
From Midpoints
Parameters
28.00
2.00
1.00
6

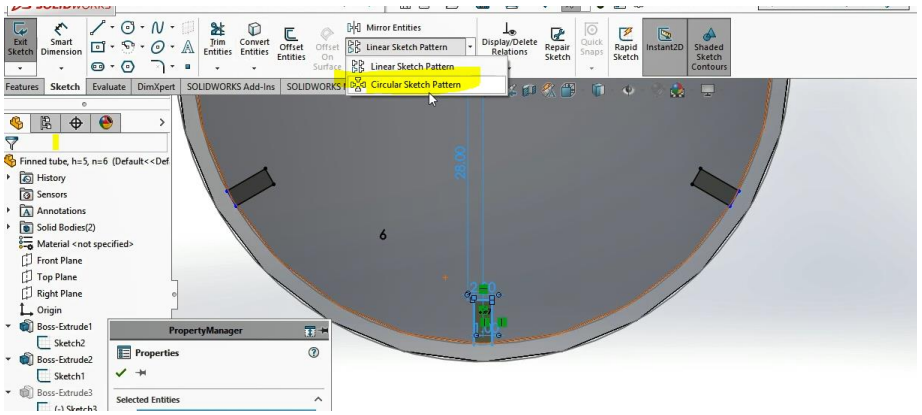
Mirror Entities
Linear Sketch Pattern
Circular Sketch Pattern
Move Entities
PropertyManager
Properties
Selected Entities
28.00
6

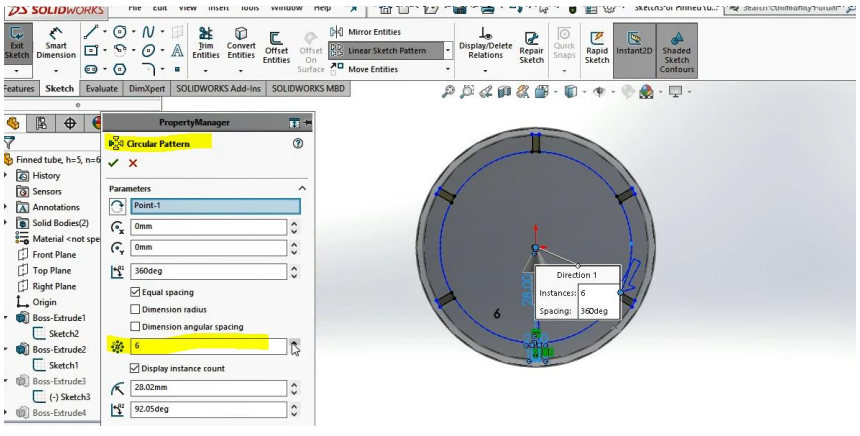
PropertyManager
Circular Pattern
Parameters
Point-1
0mm
0mm
360deg
Equal spacing
Dimension radius
Dimension angular spacing
6
Display instance count
28.02mm
92.05deg
Direction 1
Instances: 6
Spacing: 360deg
28.00
6

Then we extrude as before

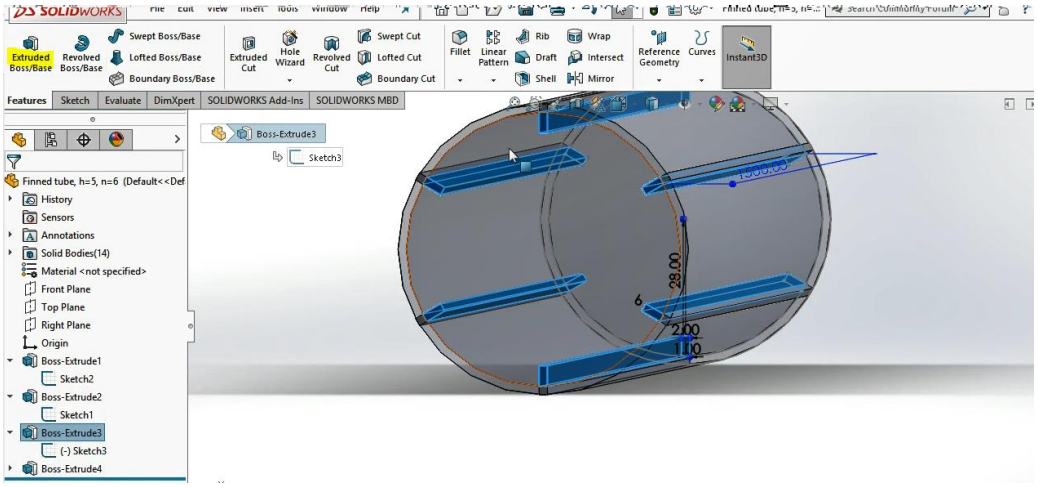

1.4.

In the fourth Sketch, to make the mesh more precise, we draw a square under the fins, i.e. between the inner and outer diameters, and extrude as before. This is done only to improve the mesh structure.

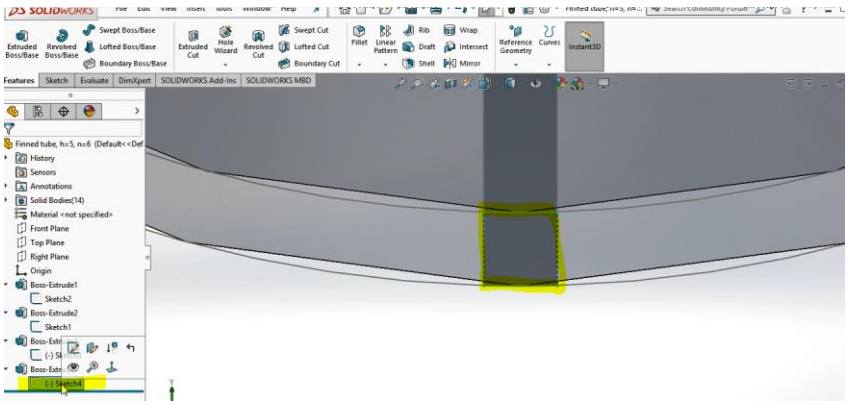

We output from SolidWorks either in .step or .x_t

ANSYS fluent

2. Design modeler:

Enter the design modeler and call the geometry by using the Import external geometry option

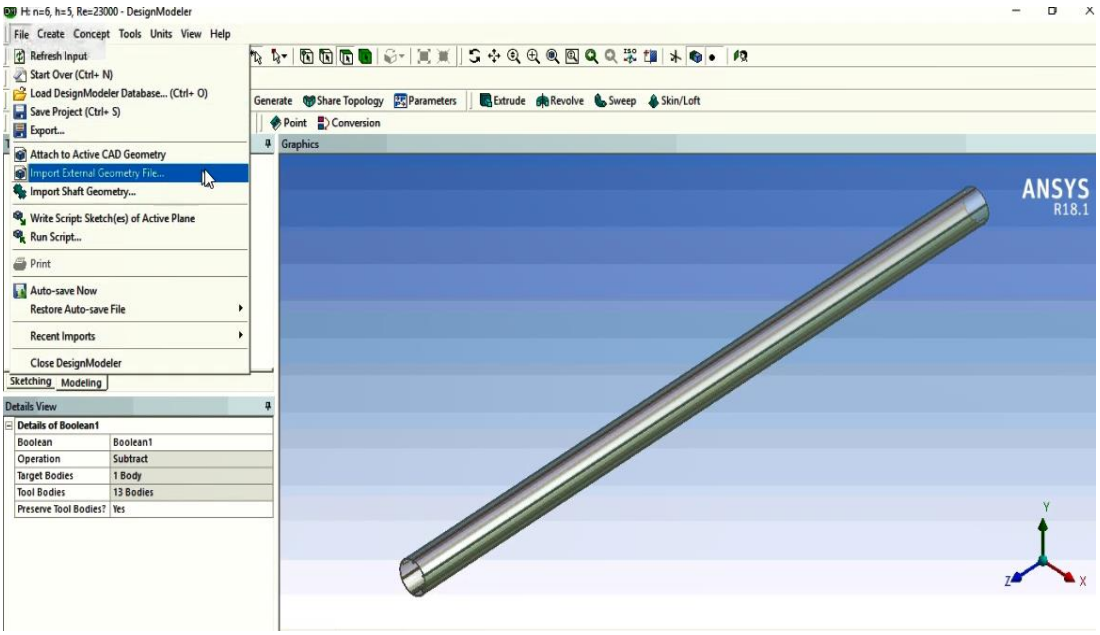

First Boolean:

First, reduce the volumes by using the Boolean option.

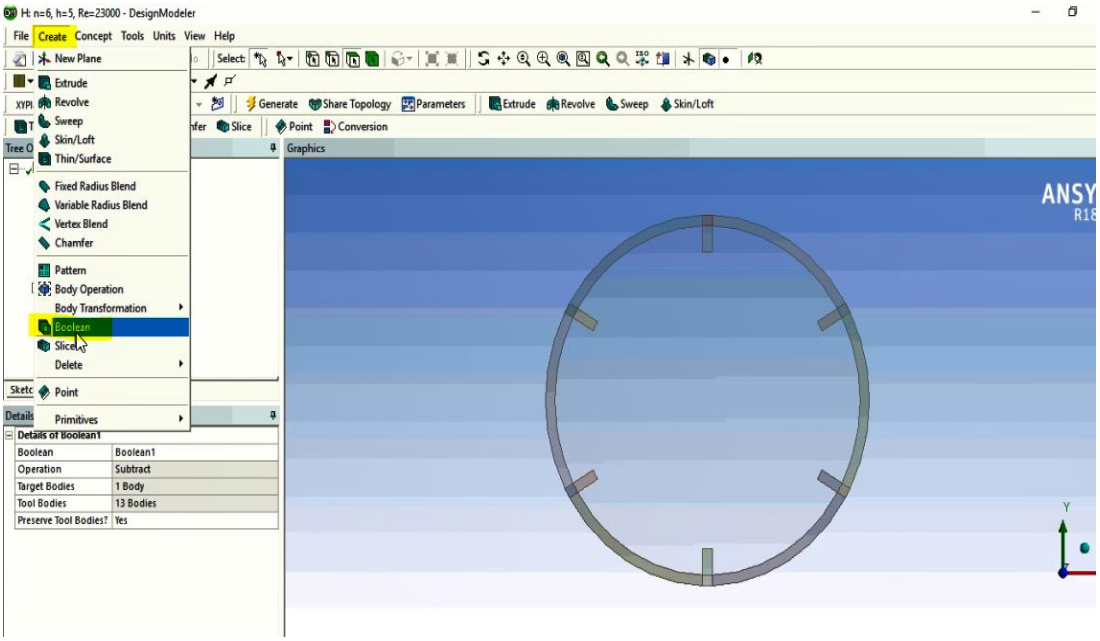

First, in the Tool body section, we select all volumes except the outer diameter

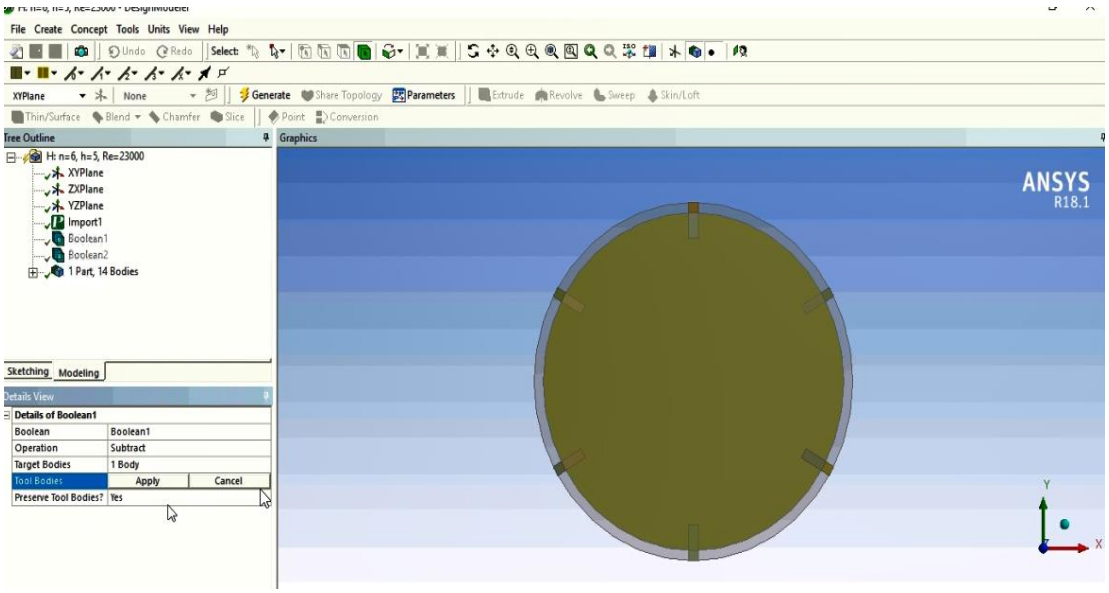

In the Target section, select the outer diameter volume

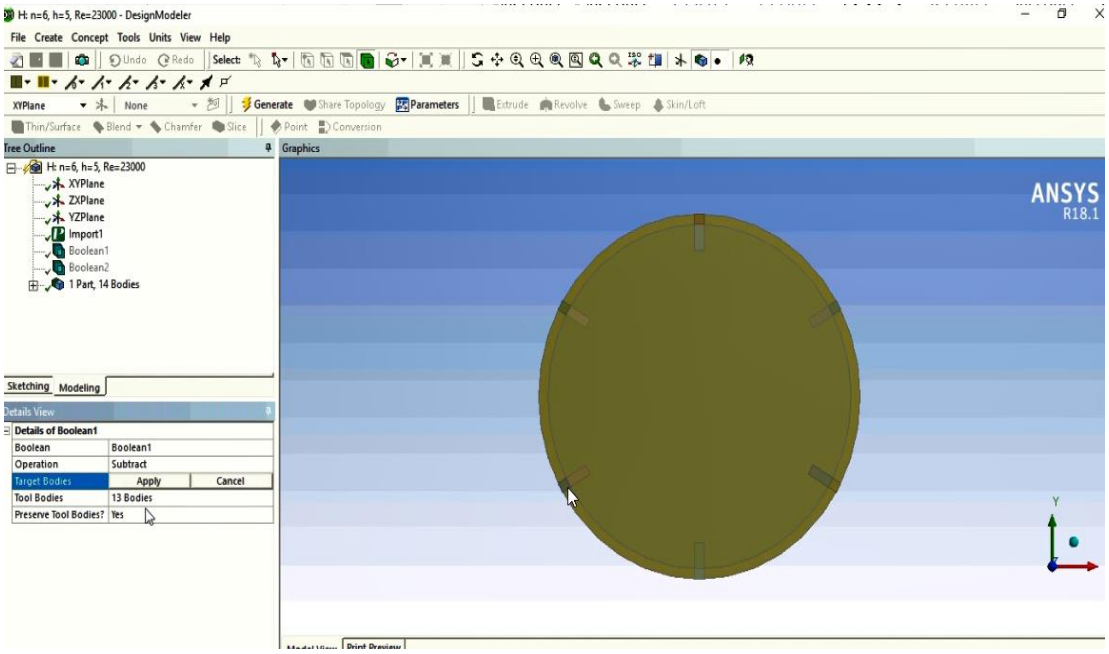

And click on generate option

Second Boolean:

Define a Boolean again and select all the fins and walls in the Tool body option.

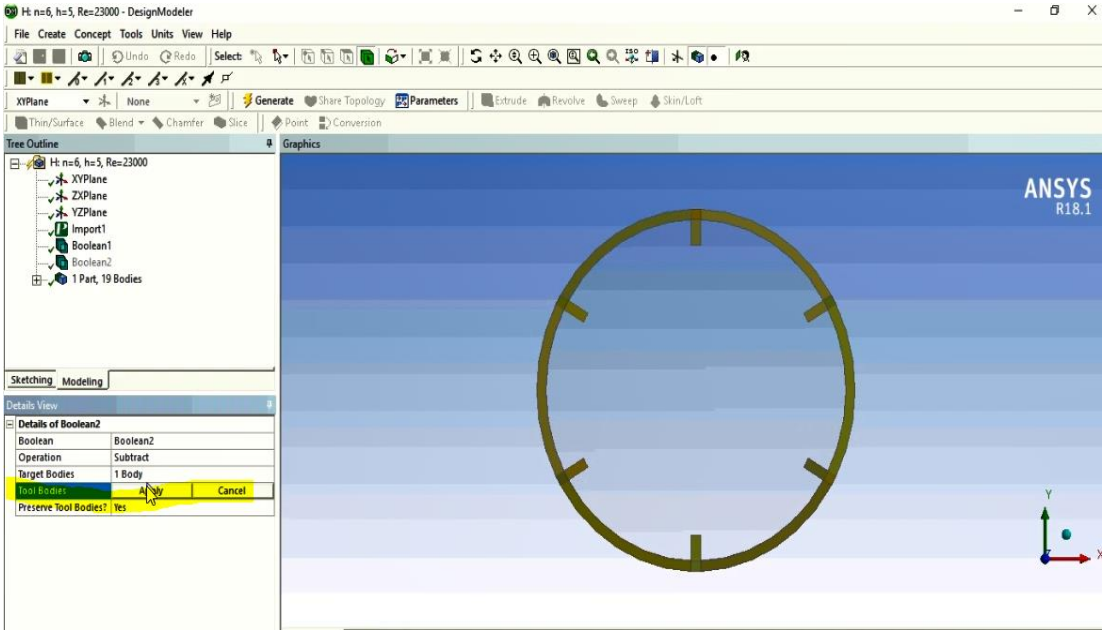

In the Target section, select the inner diameter volume

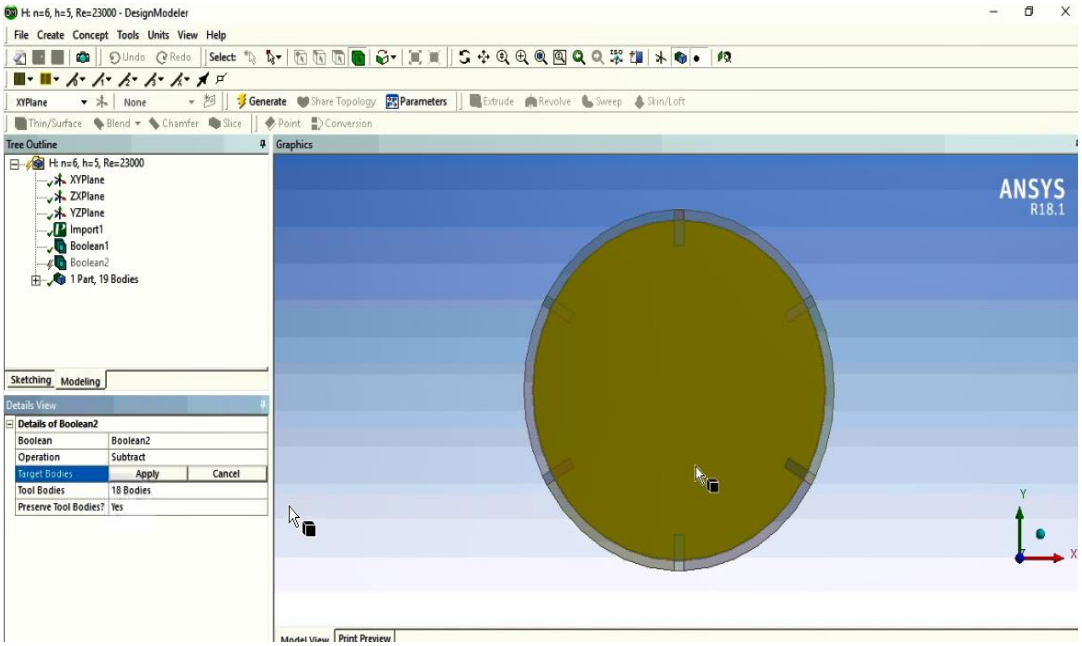

And click on generate option

Click on the inside diameter volume and select the Fluid option. Because the walls and other places are solid and there is only fluid inside the pipe.

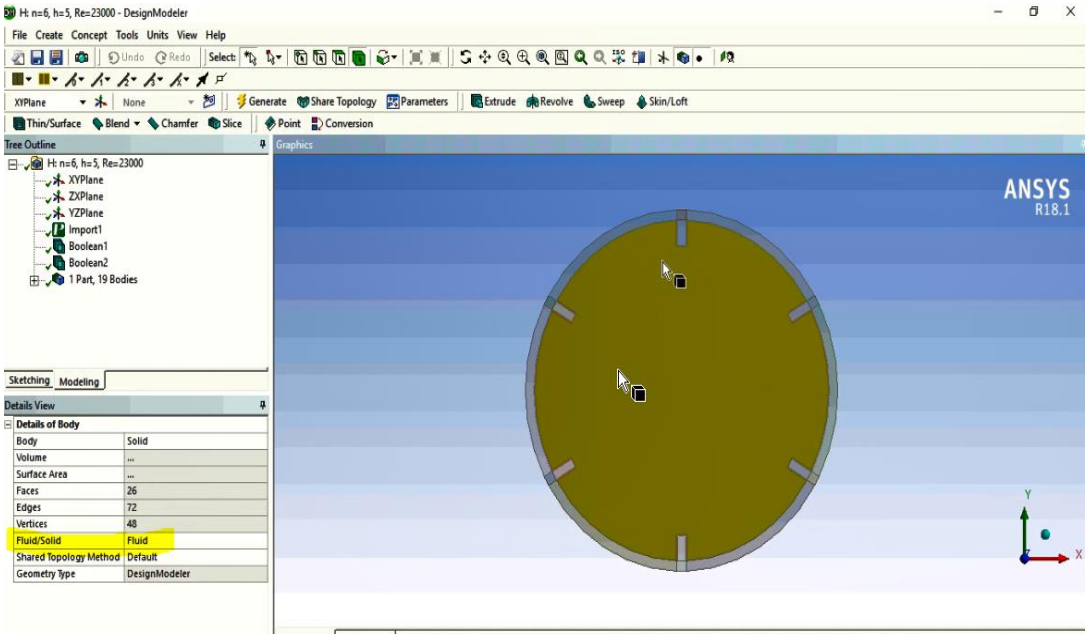

After separating the volumes, we enter the mesh section.

---

3. Mesh:

Basic settings

To mesh, first in the Sizing section, the Relevance Center was changed to Fine, and also in the Quality section, Smoothing to High, and in the Mesh Metric, the Skewness option is selected to see the accuracy of the mesh.

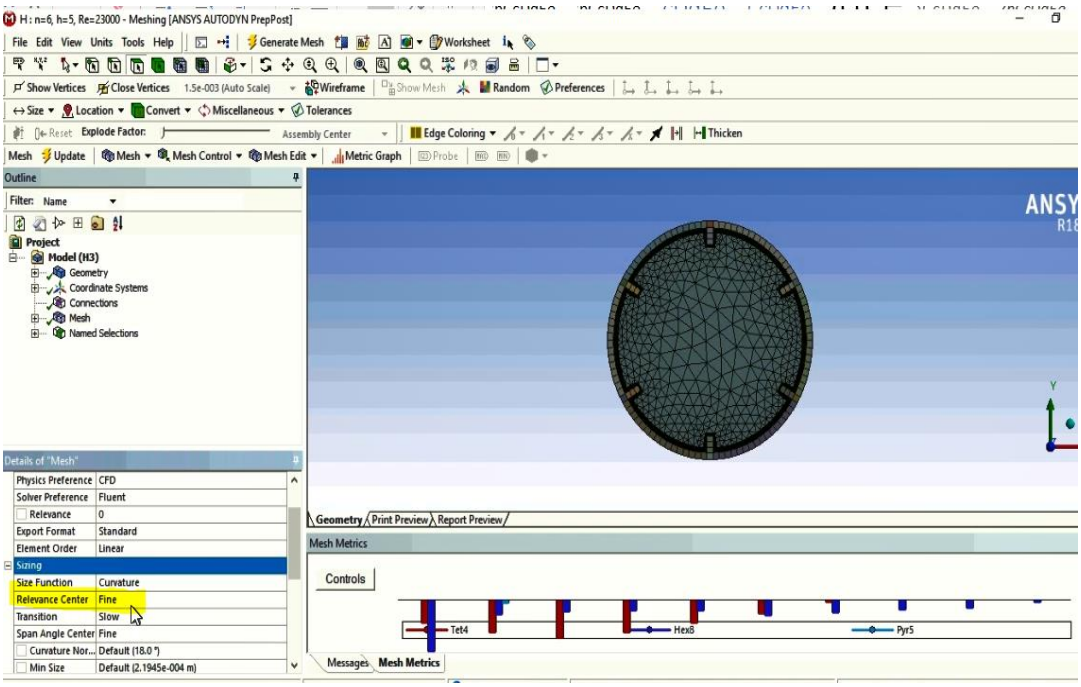

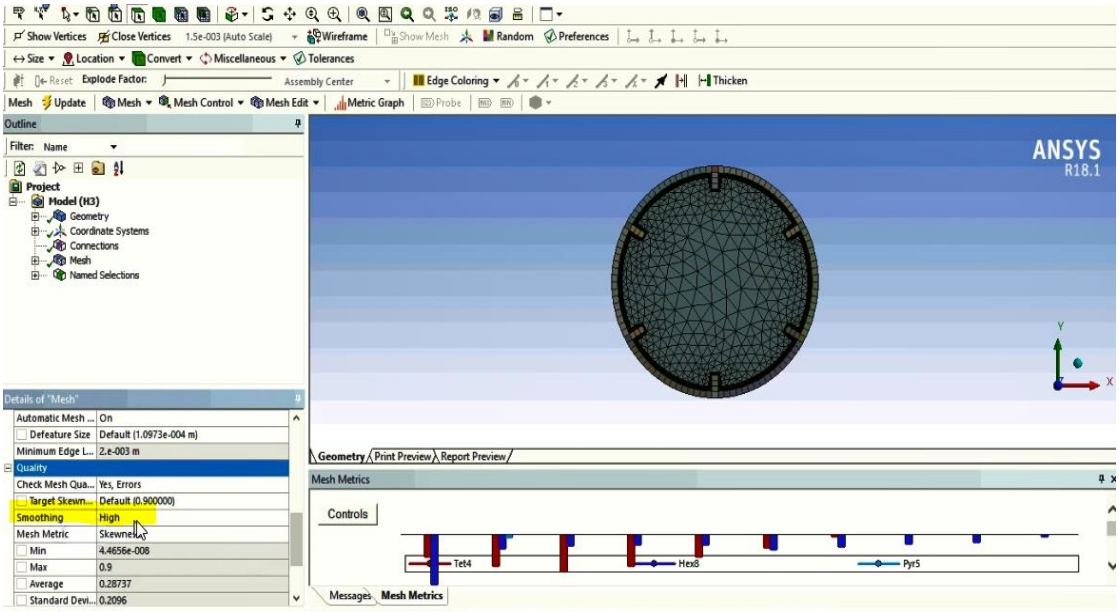

Because the flow is turbulent, the boundary layer mesh must be applied. Then, by right-clicking on the Mesh, in the Insert section, the Inflation option is selected. Because the shape is 3D, the fluid Domaine in the direction of the tube is selected for the Geometry section and the Apply option is clicked.

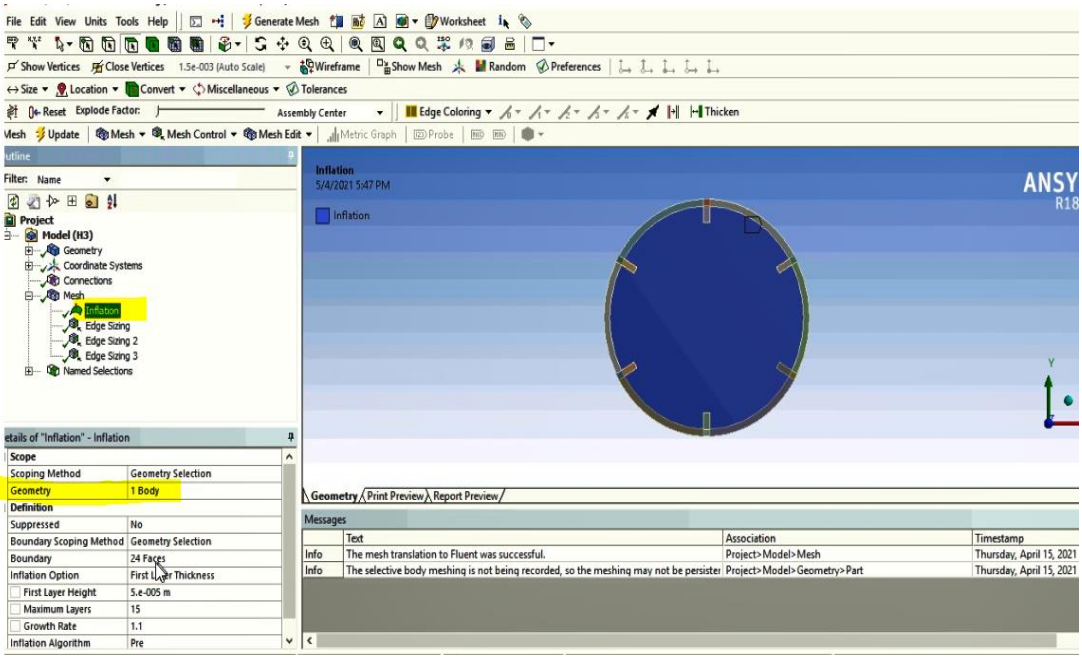

Then in the Definition section in the Boundary section, all the pages around the fluid are selected (both at the input and at the output, which is equal to 24 pages).

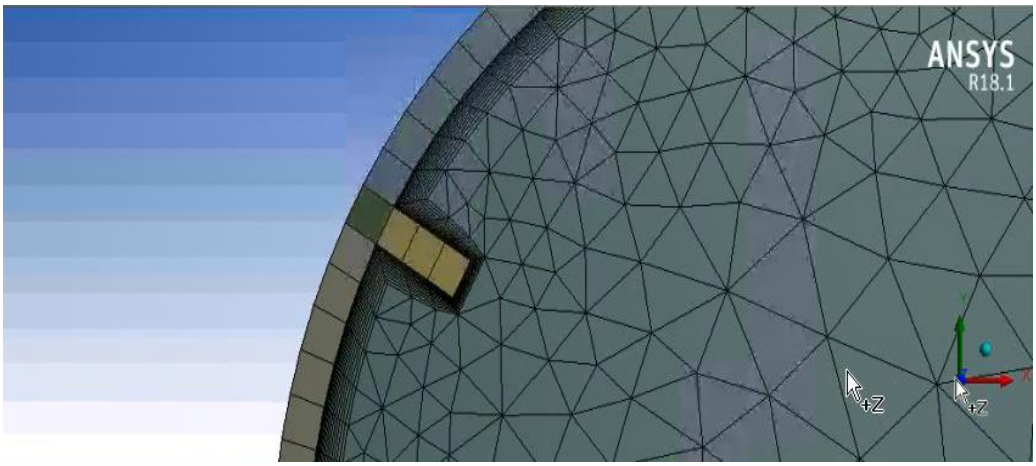

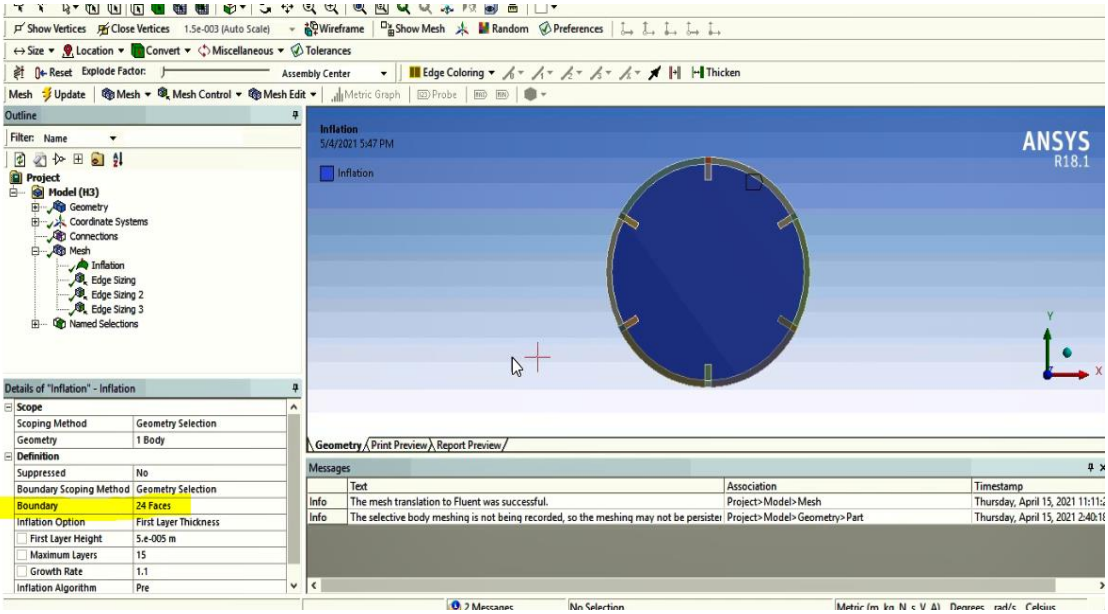

In the First Layer Height section, enter the height of the first layer a small number. In the internal flow, the following equation is used to obtain the height of the first cell.

$$\Delta y = Dy^{+}\sqrt{74}\,\mathrm{Re}_{D}^{-13/14}$$

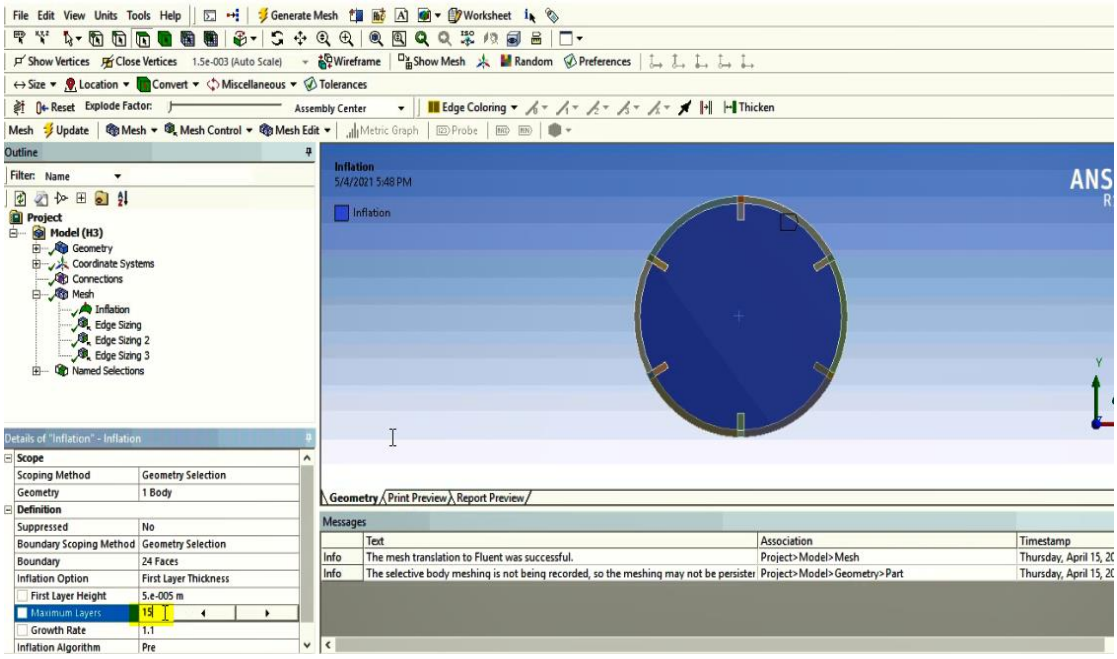

The number of layers was 15, according to Ansys software, which should be between 10-15. And the growth rate is considered 1.1.

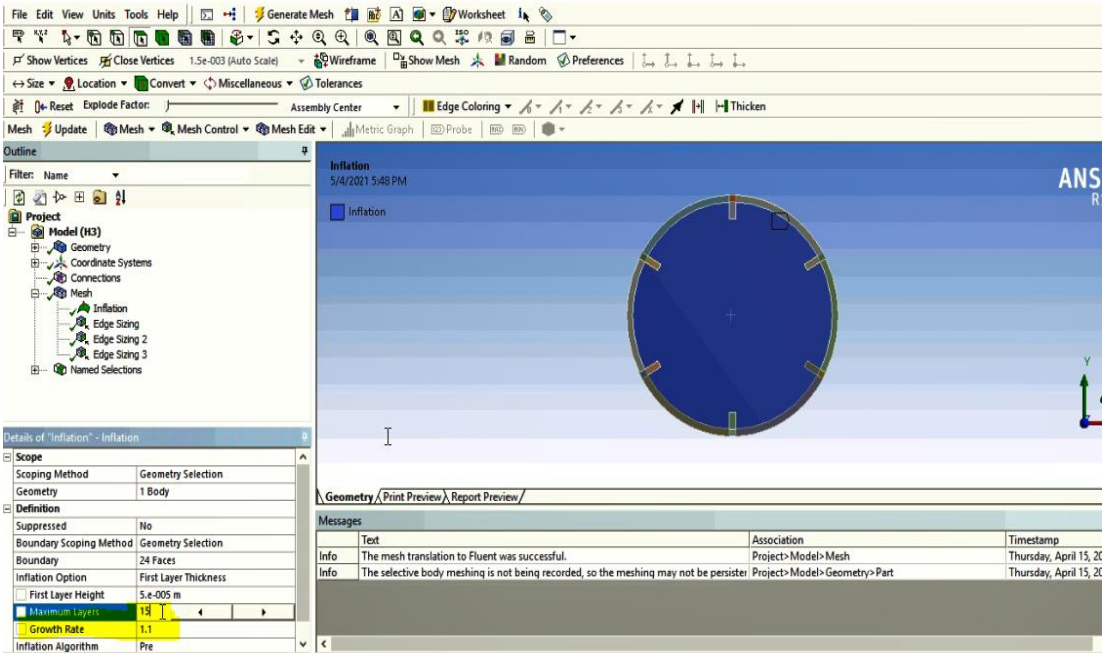

First edge sizing:

To improve the mesh using the Edge sizing option, first select the pages between the fins at the inlet and outlet of the pipe, which are 12, and in the Type field, select the Element size and enter 0.002.

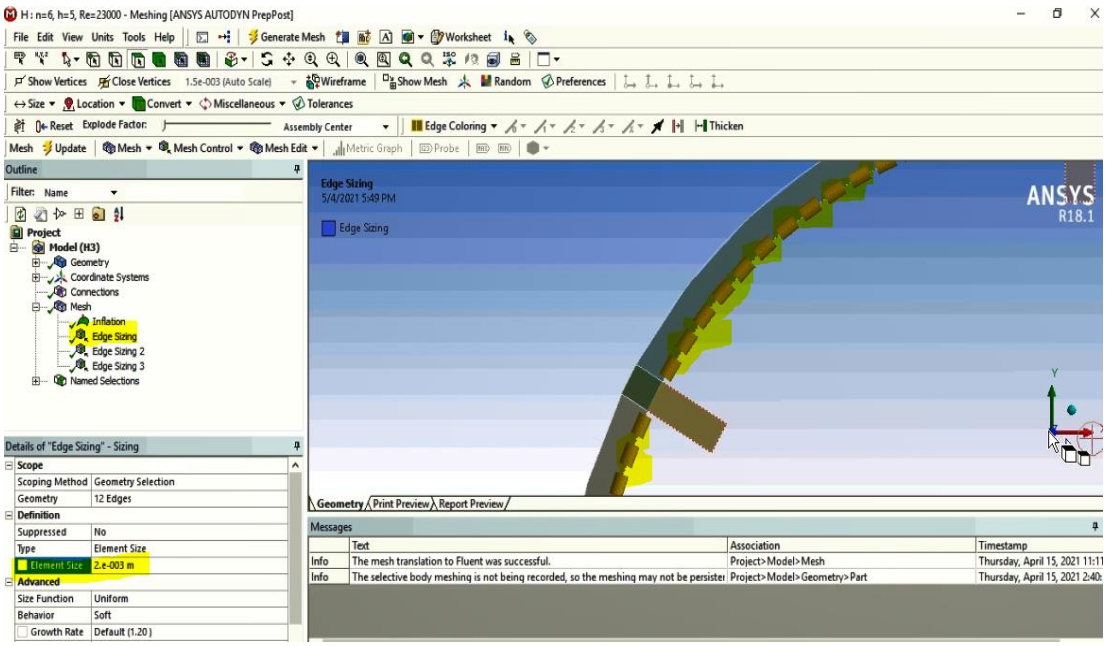

Second edge sizing:

Again, by creating a new Edge sizing, this time for the fins, we will act as before and select 24 pages at the input and output.

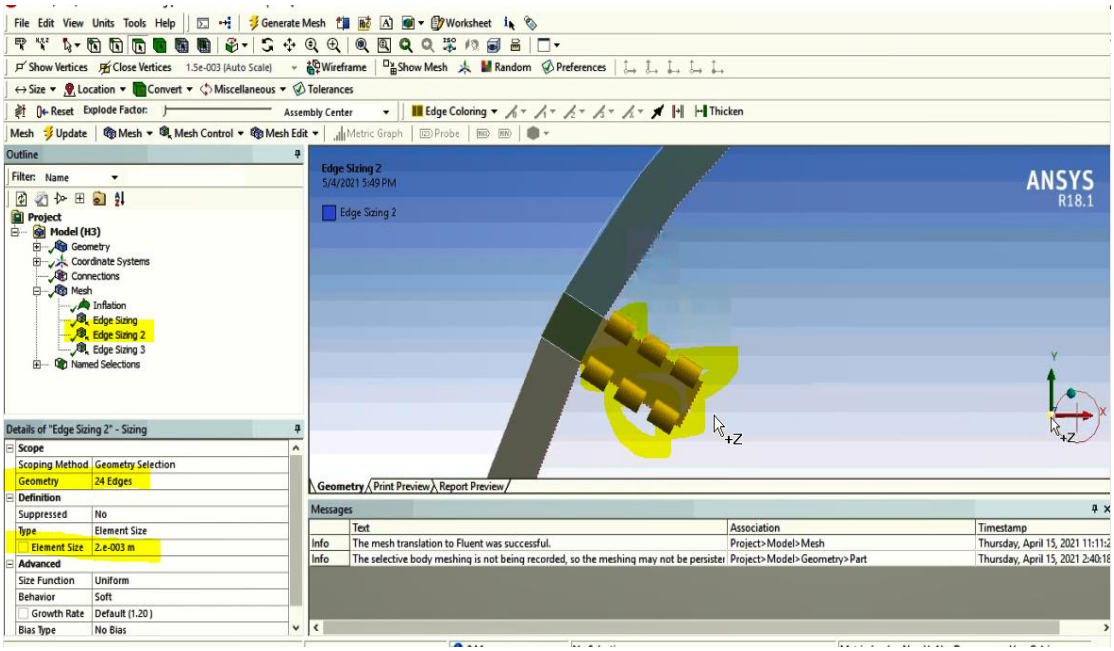

Third edge sizing:

Also, in Edge sizing 3, in the longitudinal direction, we select all the existing lines, which are 36 pages around the pipe.

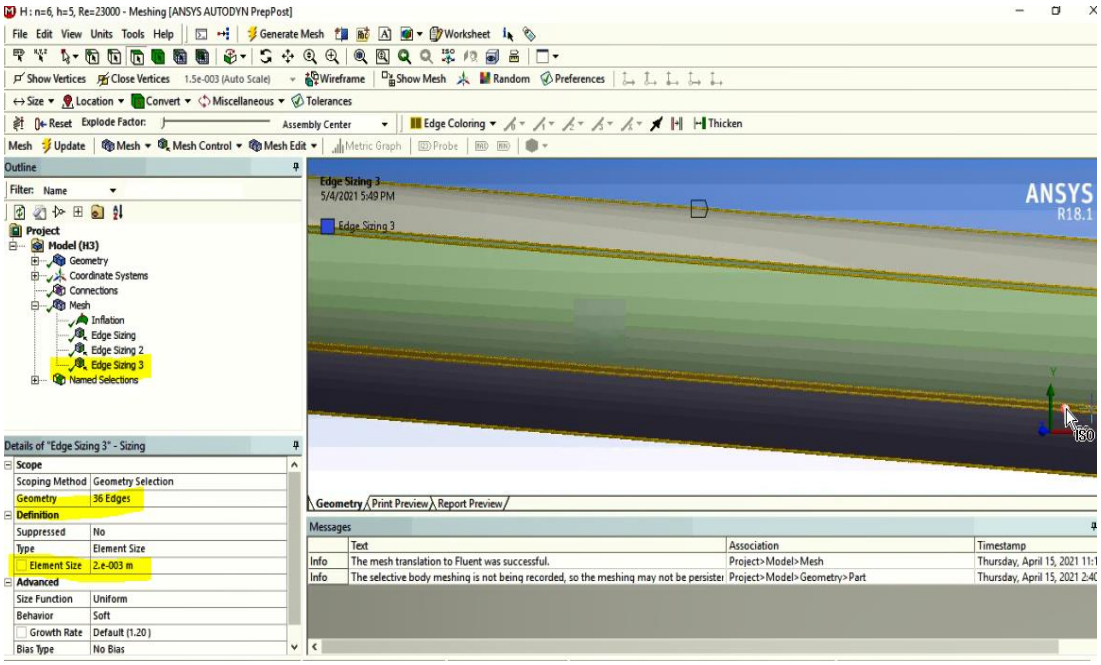

Finally, after Generate, the mesh looks like this:

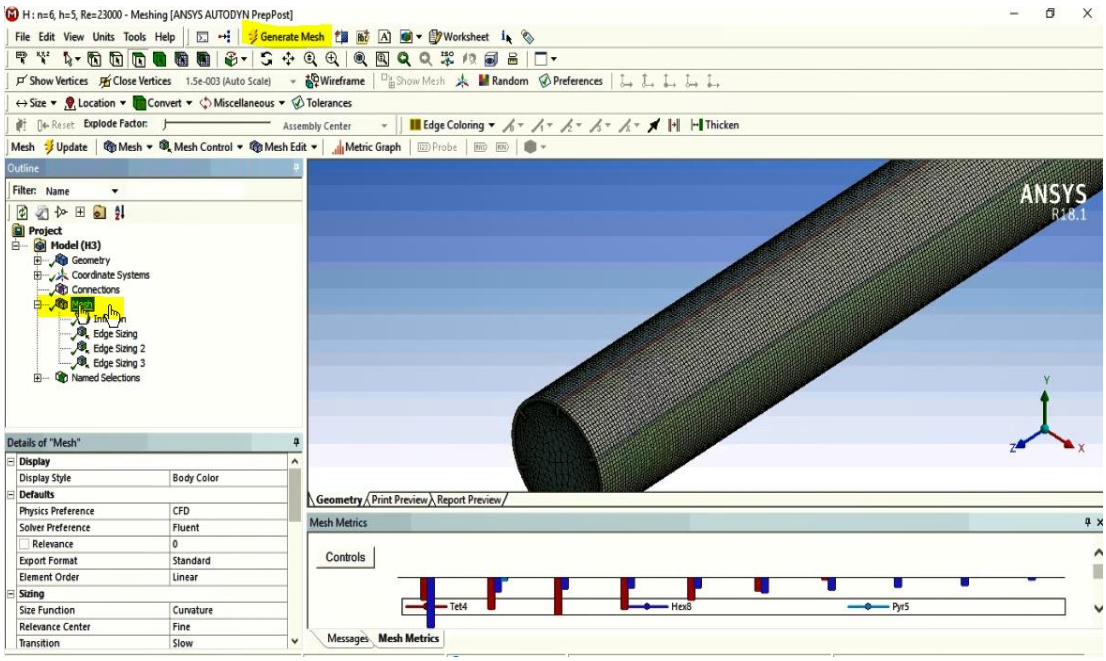

Finally, we name the pages.

By selecting the Named Selections option, the desired pages will be named. One of the front or back pages of the tube is named

Inlet and the other is called Outlet. Also, the cylindrical plate, the surrounding walls, were named wall heat flux.

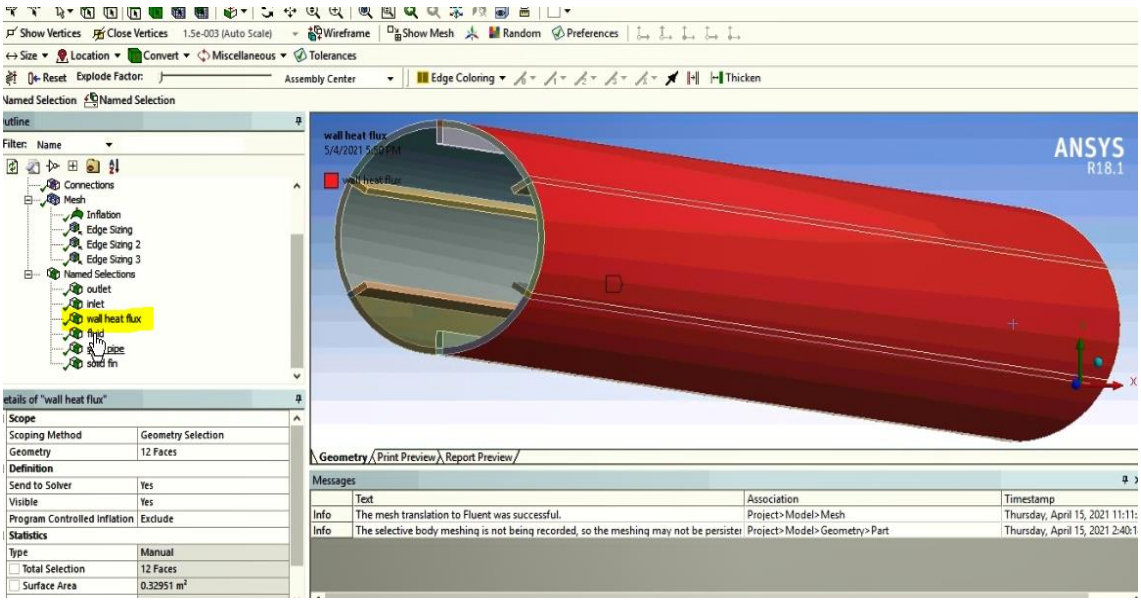

For the fluid domain, first click on the Body option and then the inner part of the cylinder is selected and named Fluid.

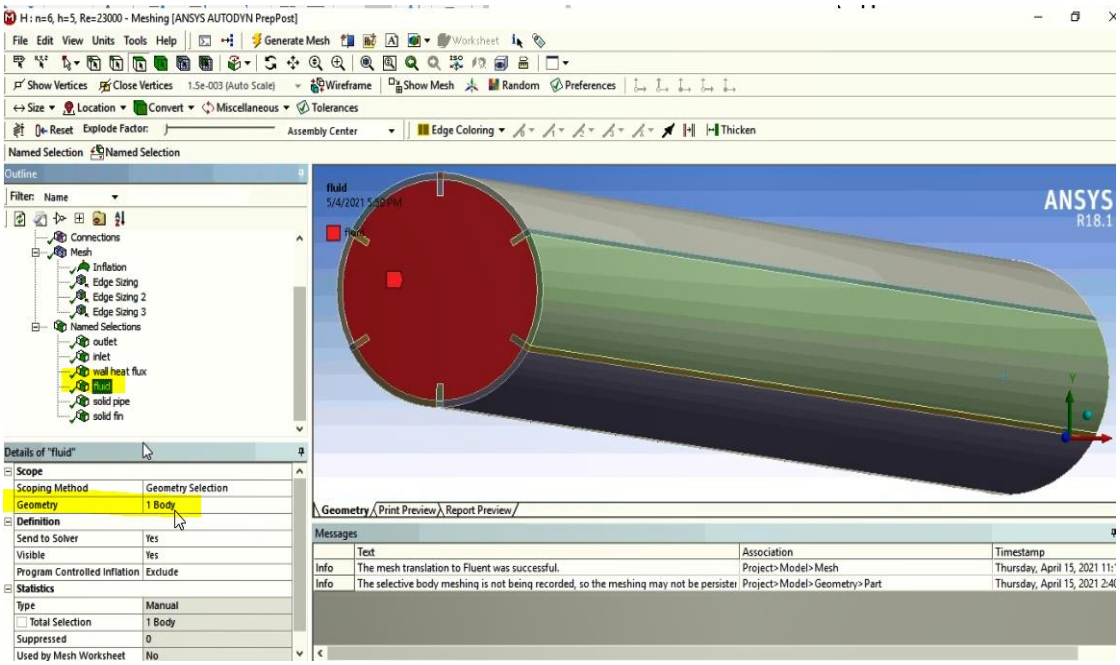

The surrounding walls are called solid pipes

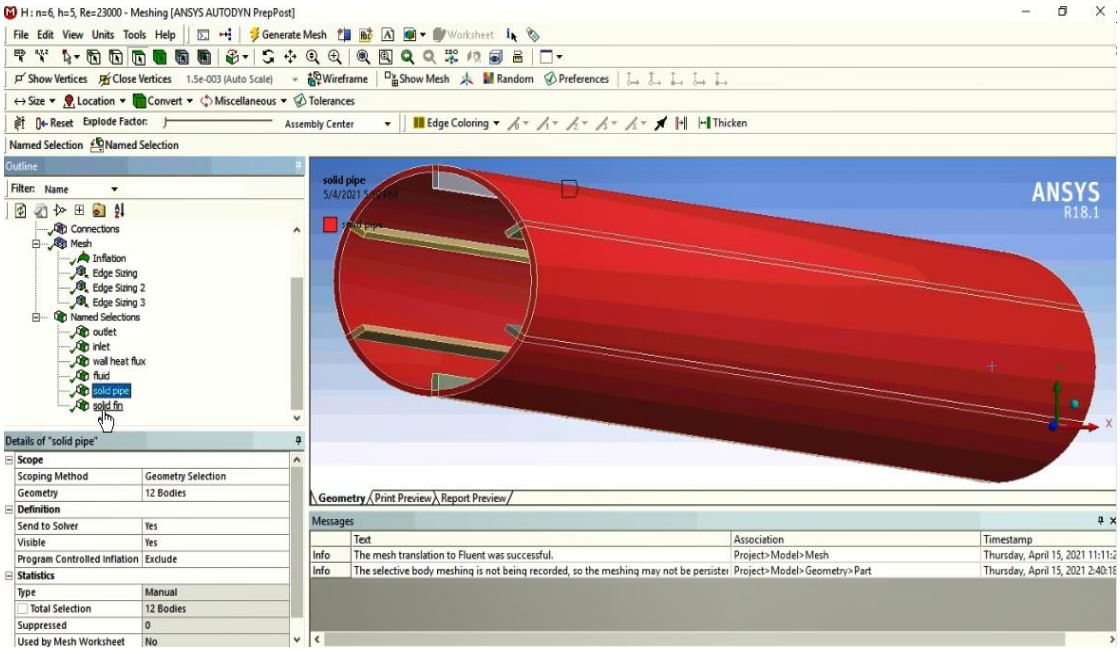

And the inner fins are also called Solid fin.

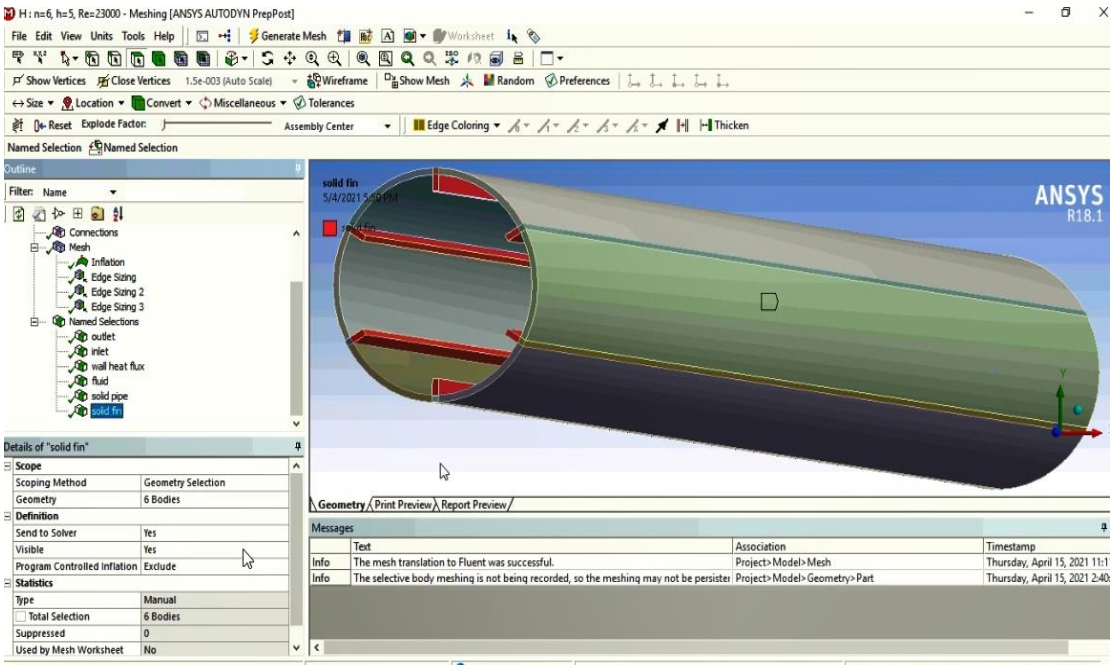

4. Setup

When Mesh file imported into fluent:

4.1. General:

First, in this section, by clicking on the Check option, the mesh is verified.

In the Type section, select the Pressure based option, in the Velocity Formulation section, select the Absolute option, and in the Time section, select the Steady option (because the solution is not time dependent). The software also shows the input in blue and the output in red.

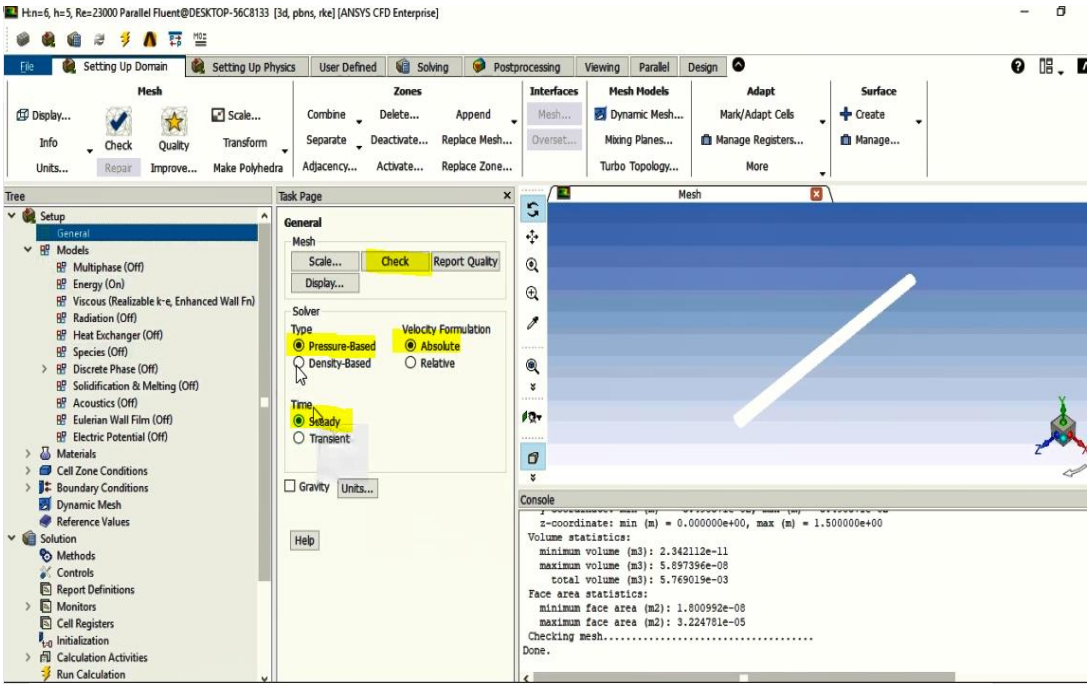

4.2. Models:

In this section, the Energy option is activated because the energy equation wants to be solved.

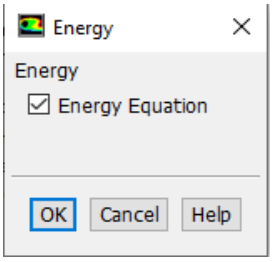

In this case, the K-epsilon option is selected. In the K-epsilon Model section, the Realizable option is selected. The Enhanced Wall Treatment option is usually selected in the Near-Wall Treatment section. Then, in the Enhanced Wall Treatment Options section, select the Thermal Effects option to observe the temperature effects on the wall.

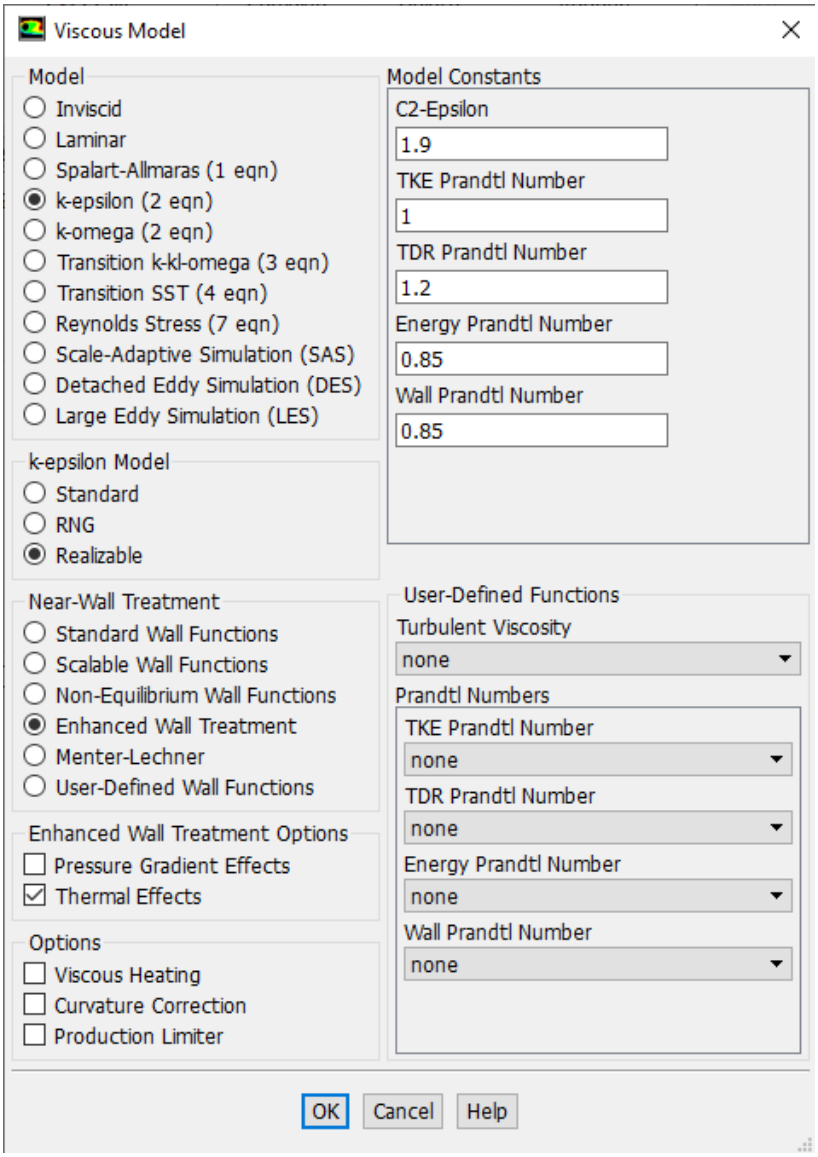

In the Inlet section and in the Momentum section, select the absolute speed and enter the input speed in the x direction according to the problem data in turbulent flow at $3.6 m/s$. At the bottom, in the Turbulent Intensity section, we enter the current turbulence intensity of 5%, which is obtained by entering the Reynolds number in the formula for turbulence intensity. In the Turbulent Viscosity Ratio section, a value of 10 is entered. And in the Thermal section, the temperature enters 300 K.

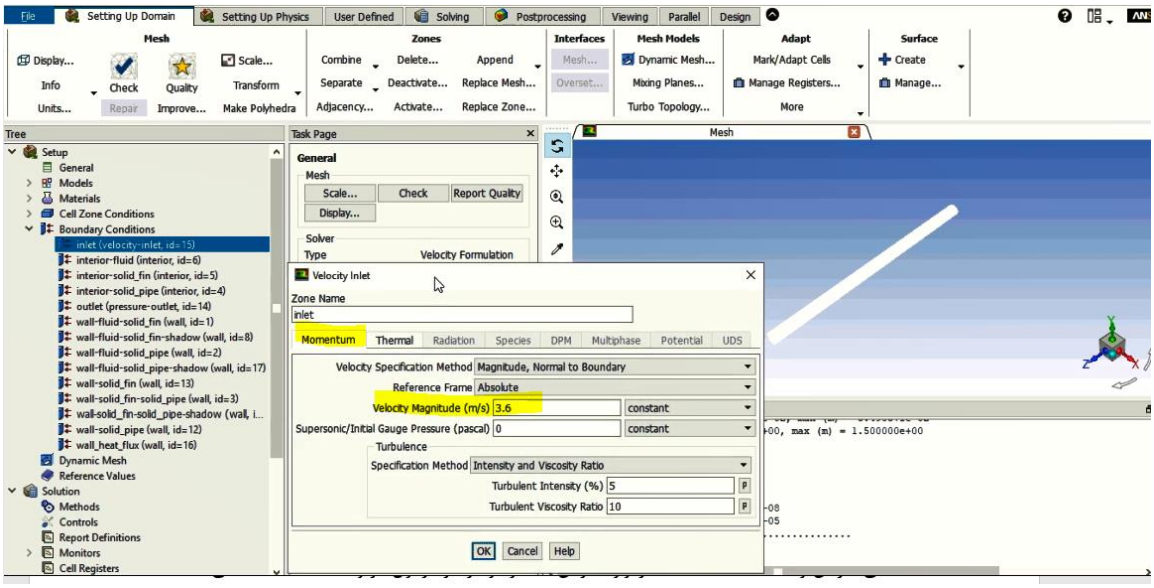

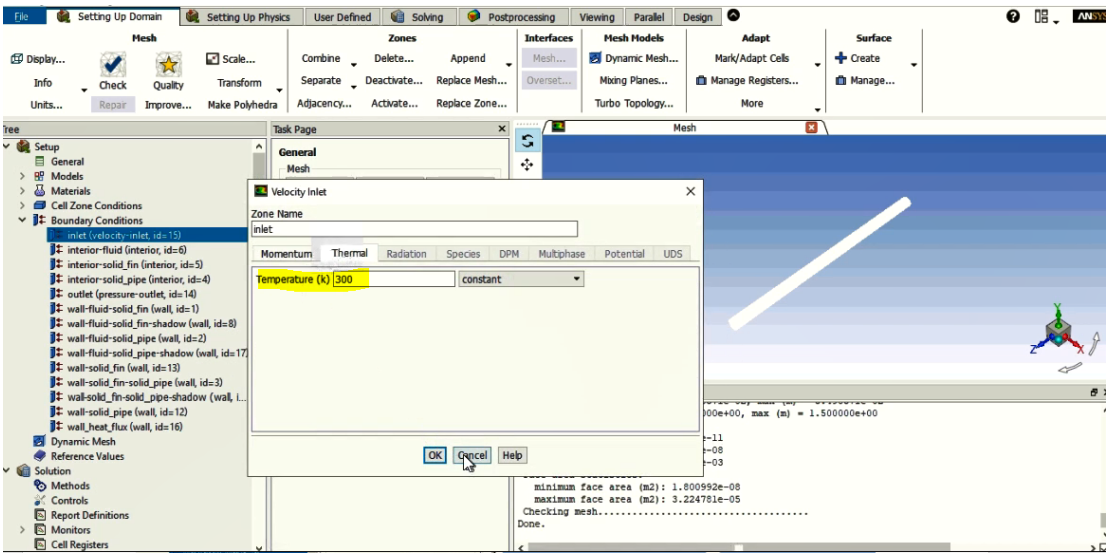

In the Outlet section, the software considers the output as a pressure outlet.

We have a variable flux in the outer wall. We call the variable flux profile in the Heat flux section

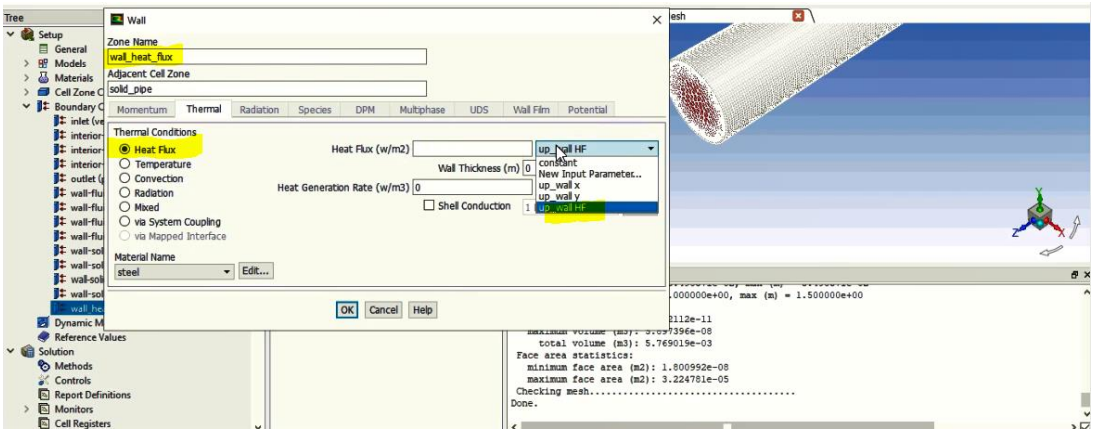

To call the profile, the file option is selected, then the read option and then the profile option is selected. And then in the Boundary conditions section for wall heat flux is called next to the heat flux option.

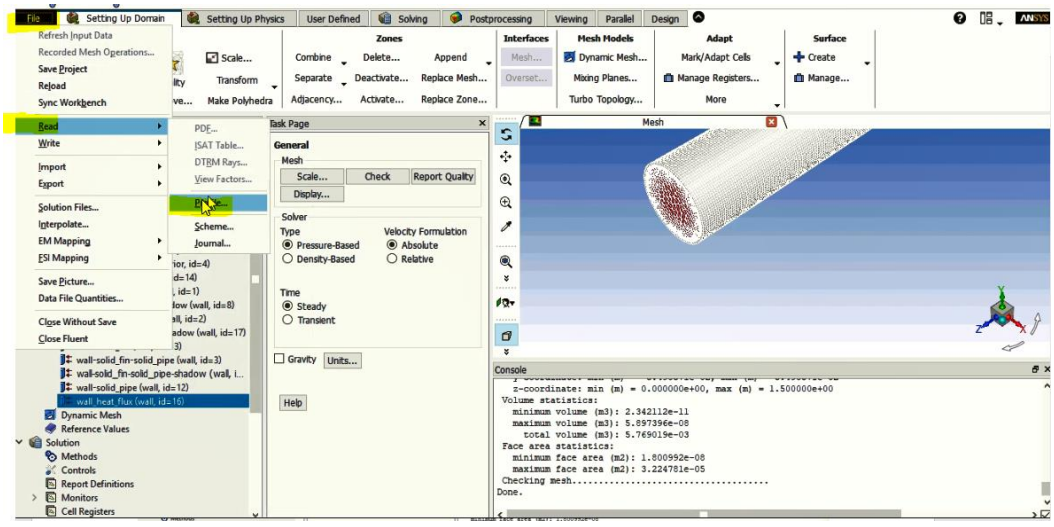

Other boundary conditions are all coupled.

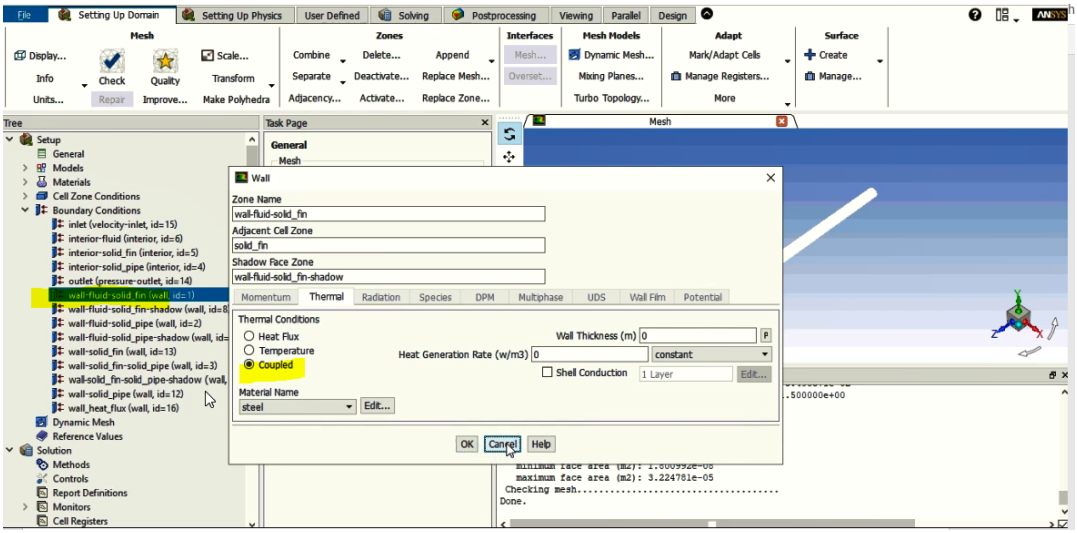

4.6. Solution:

In the Methods section and the Spatial Discretization menu, the Second Order Upwind option is selected for Momentum to solve the pressure more accurately. For turbulent kinetic energy, turbulent dissipation rate, and Energy, First Order Upwind is selected.

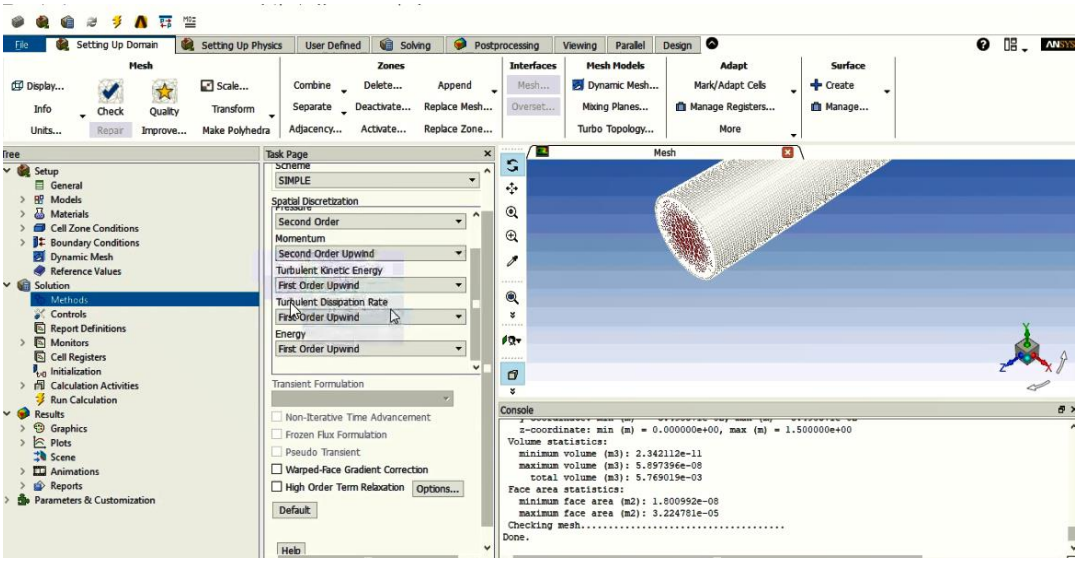

In the Controls section, there are coefficients called Under Relaxation, which remain the software default.

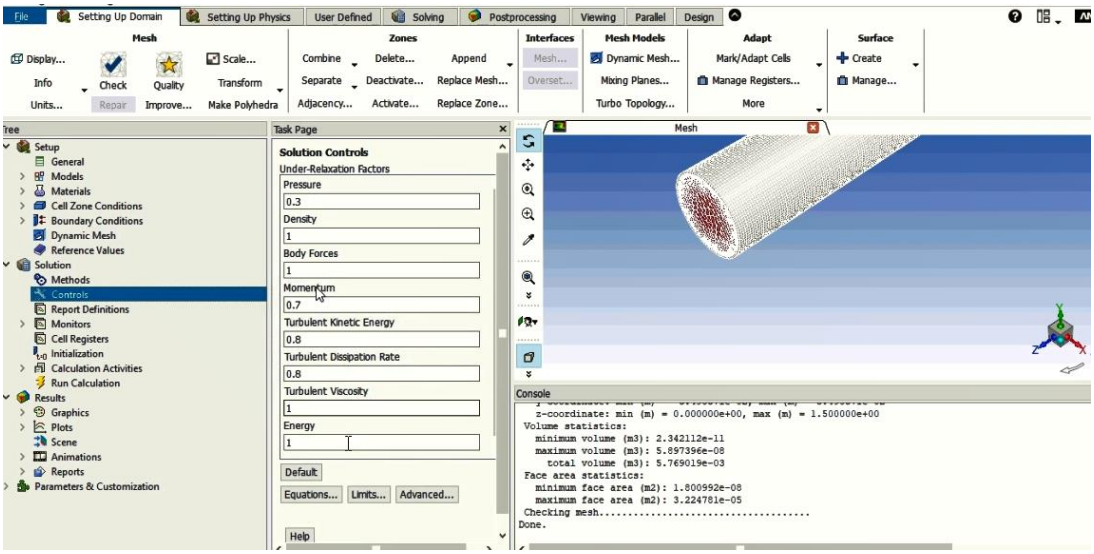

In the Monitor section, in the Residual section, all residuals enter 0.0001, except for the energy equation, which enters 1E-6.

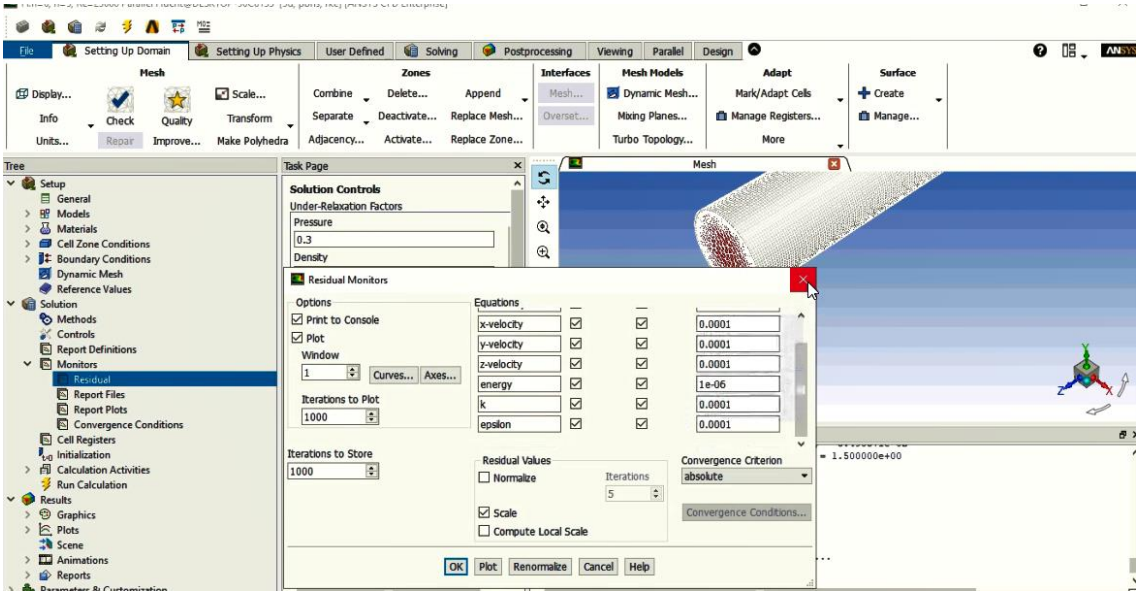

Initialization is the initial solution. Initial solutions enter the project through the Hybrid Initialization option.

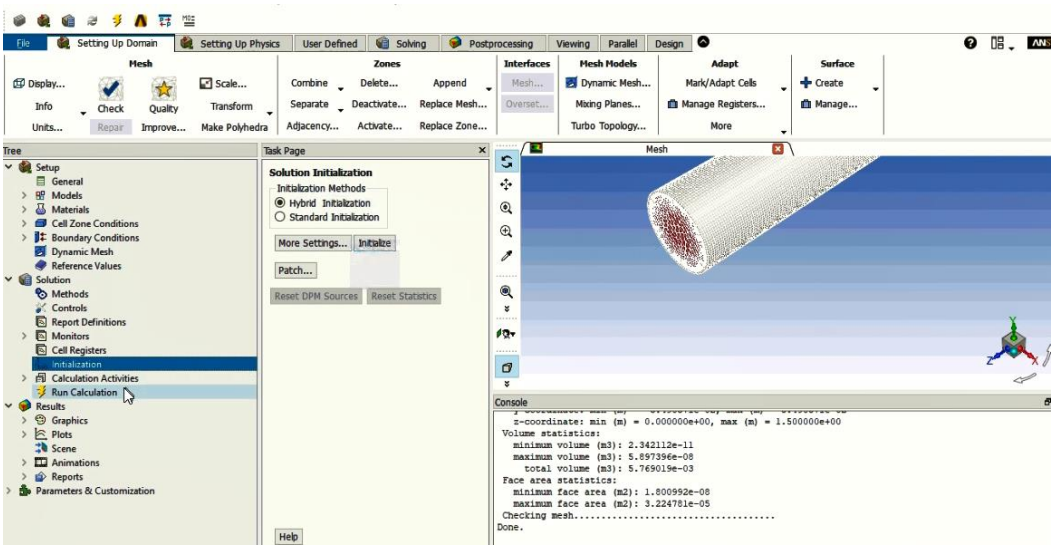

In the Run Calculation section, the value of Number of Iterations is entered as 1000 and then the Calculate option is clicked.

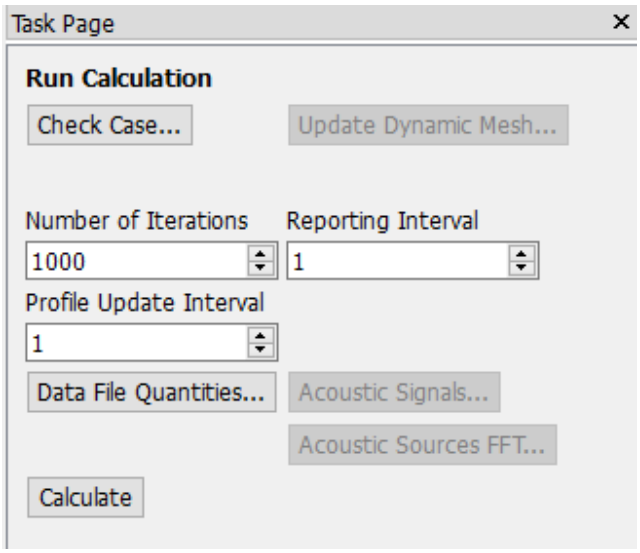

The convergence diagram for this particular case is as follows

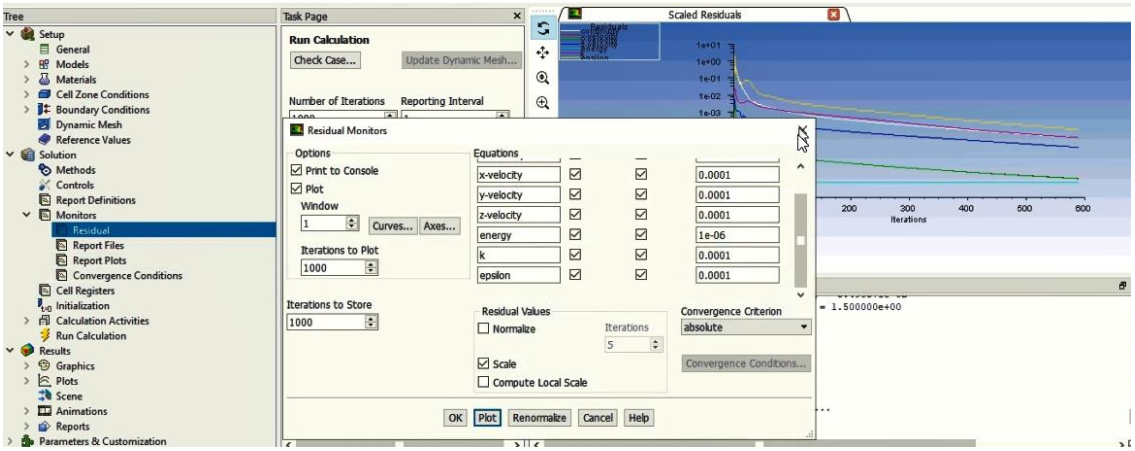
Tree
Setup
General
Models
Materials
Cell Zone Conditions
Boundary Conditions
Dynamic Mesh
Reference Values
Solution
Methods
Controls
Report Definitions
Monitors
Residual
Report Files
Report Plots
Convergence Conditions
Cell Registers
Initialization
Calculation Activities
Run Calculation
Results
Graphics
Plots
Scene
Animations
Reports
Parameters & Customization
Task Page
Run Calculation
Check Case...
Update Dynamic Mesh...
Number of Iterations
Reporting Interval
Residual Monitors
Options
Print to Console
Plot
Window
Curves...
Axes...
Iterations to Plot
Iterations to Store
Equations
x-velocity
y-velocity
z-velocity
energy
k
epsilon
Residual Values
Normalize
Scale
Compute Local Scale
Convergence Criterion
absolute
Convergence Conditions...
OK
Plot
Renormalize
Cancel
Help
Scaled Residuals
Iterations

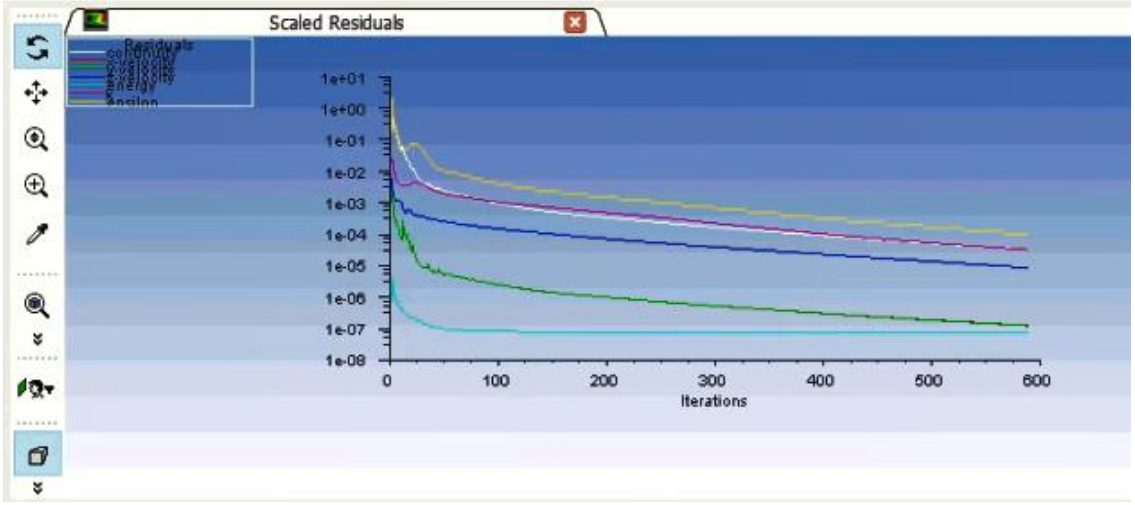
Scaled Residuals
Residuals
continuity
x-velocity
y-velocity
z-velocity
energy
k
epsilon
1e+01
1e+00
1e-01
1e-02
1e-03
1e-04
1e-05
1e-06
1e-07
1e-08
0
100
200
300
400
500
600
Iterations

8 Appendix (B)

Tables

Appendix (B) Tables

Table (1) parameters of Parabolic Trough Collector in this study

Focal length : Rim angle 120 degree: 868.246mm Rim angle 80 degree : 1745mm
Aperture width 5700mm
Absorber inner radius 66mm
Absorber outer radius 70mm
Glass cover inner radius not considered
Glass cover outer radius not considered
Material of the absorber : steel Material of the fins : steel
Material of the glass envelope not considered
Transmittance of glass cover not considered
Coating absorbance not considered
Glass cover emissivity ___not considered

Table (2) Properties of Al_2O_3 E. Bellos and C. Tzivanidis [11]

Properties	Value
ρ(kg/m^3)	4000
C_p (J/kgK)	773
k (W/mK)	40

Table (3) Physical properties of TP304H steel.(absorber and fins material) Y. Wang et.al[9]

Temperature/ ºC	20	100	200	300	400	500	600	700
Linear thermal expansion coefficient/10^{-6} ºC^{-1}	_	17.1	17.4	17.8	18.3	18.8	19.1	19.4
Conductivity/W/(m K)	12.1	12.6	13.0	13.8	14.7	16.3	18.4	20.1
Elastic modulus/105 MPa	1.97	1.93	1.85	1.78	1.69	1.61	1.54	1.45
Density/kg/m3	7860							
Specific heat capacity/J/(kg K)	475							

Table (4) — Saturated Liquid Properties of SYLTHERM 800 Fluid (SI Units) Dow Oil and Gas[50]

Temp. °C	Specific Heat KJ/Kg.K	Density kg/m3	thermal Conductivity W/m K	Viscosity mPa•s	Pressure kPa
50	1.660	908.18	0.1294	5.96	0.20
100	1.745	864.05	0.120	2.99	4.00
150	1.830	819.51	0.1106	1.70	26.1
200	1.916	773.33	0.1012	1.05	94.6
250	2.001	724.24	0.0918	0.69	242.1
300	2.086	670.99	0.0824	0.47	495.5
350	2.172	612.33	0.0729	0.33	780.9
400	2.257	547.00	0.0635	0.25	1373

Table (5) Performance Evaluation Criteria PEC results for different Re number, fins number and two arrangements

Type a	Re	Nu	PEC	% PEC		Type b	Re	Nu	PEC	% PEC
n=2	18600	332.5452	1.006248	0.624827		n=2	18600	343.6914	1.039775	3.977505
	23000	395.133	1.0061	0.61			23000	407.8759	1.038862	3.886228
	28000	454.4474	1.006002	0.60021			28000	468.593	1.038278	3.827791
n=4						n=4				
	18600	353.8505	1.04493	4.492976			18600	357.5639	1.056541	5.654115
	23000	419.3878	1.042387	4.238677			23000	423.502	1.05304	5.304024
	28000	481.4866	1.041876	4.187558			28000	485.9193	1.051858	5.185773
n=6						n=6				
	18600	365.583	1.05626	5.625958			18600	367.1191	1.060845	6.084535
	23000	432.2544	1.050615	5.061474			23000	433.8904	1.054766	5.47663
	28000	495.3455	1.047871	4.787076			28000	497.0725	1.05253	5.252954

Table (6) ANSYS Fluent solver setting

Solver	Pressure based, Steady	
Viscous model	K-epsilon, Realizable, Enhanced wall treatment	
Solution methods	Pressure-velocity coupling	SIMPLE
Spatial Discretization	Gradient	Least Squares Cell Based
	Pressure	Second Order
	Momentum	Second Order Upwind
	Energy	First Order Upwind
	TKE	First Order Upwind
	Turbulent dissipation rate	First Order Upwind

Table (7) Physical attributes of heat transfer fluid (nano fluid)

Material	φ	ρ **(kg/m^3)**	C_p***(J/kg.K)***	***K*** **(w/m.K)**	μ**(kg/m.s)**
Sylthern/Al_2O_3	4%	803.2	155.6	0.0827	0.52

الخلاصة

ان التأثير الكبير لاستخدام الموائع النانوية مع السطوح الممتدة الطولية يعطي تحسين جيد للخواص الحرارية للموائع النانوية في الأنبوب الممتص المستخدم في منظومات الجامع للإناء الطبقي. لذلك فان هذه المنظومة تعتبر واحدة من مصادر الحرارة الفعالة الواعدة التي تستخدم الاشعاع الشمسي. الحرارة المتحصلة من خلال هذه المنظومة تتحول الى طاقة كهربائية من خلال التوربينات التقليدية. هذه الدراسة تقدم حسابات عددية لجريان مضطرب ثلاثي الأبعاد باستخدام طريقة مونتي كارلو لتتبع الأشعة الساقطة والمنعكسة وطريقة الحجوم المحددة لحل المعادلات. ان المائع المستخدم لنقل الحرارة في هذه الدراسة هو ثلاثي أوكسيد الألمنيوم (الألومينا) / سيلثيرم ٨٠٠ كمائع نانوي يجري داخل الأنبوب المسؤول عن نقل الحرارة, والمقارنة بين مجموعة من الحالات التي تتضمن أعداد مختلفة من السطوح الممتدة الطولية مثبتة على السطح الداخلي للأنبوب ومرتبة بطريقتين ولثلاثة حالات حسب رقم رينولدزمحدد بالإضافة الى اختبار نسبة التركيز للفيض الحراري باستخدام طريقة مونتي كارلو لاقتفاء أثر الأشعة. ان تأثير استخدام السطوح الممتدة بارتفاع (٥ ملم) وعرض (٢ ملم) وبثلاثة أعداد (٢ , ٤ , ٦) وتنظيمها حسب الترتيب (a ,b) لكل حالة من الحالات الثلاثة قد تم استخدامها في هذه الدراسة. القيم التي تم استخدامها لعدد رينولدز في هذه الدراسة هي (١٨٦٠٠ , ٢٣٠٠٠ و ٢٨٠٠٠) تباعا". بالنسبة لزاوية حافة الطوق المستخدمة للمرايا الجامعة للحرارة هي (١٢٠º) وهي الزاوية التي تحقق درجة حرارة خروج أعلى للمائع الحراري وبنسبة تركيز تبلغ (٨٢.٤٧) وان النسبة الحجمية للمائع النانوي هي (٠.٠٤) . تم عرض التأثير على كل من درجة حرارة الخروج للمائع النانوي , رقم نسلت , معامل الاحتكاك و معيارية حساب الأداء للأنبوب الممتص للحرارة. ان ما تم ملاحظته من خلال النتائج ان كفاءة الأنبوب الماص للحرارة قد ازدادت بشكل كبير بالمقارنة مع الكفاءة الحرارية للأنبوب الخالي من الزعانف. النتائج المتحصلة من الدراسة أظهرت بأن استخدام المائع النانوي مع الزعانف يمكن أن تزيد الأداء الهيدروليكي للأنبوب الممتص وأن الحالة التي تم فيها استخدام (٦) زعانف مع الترتيب من فئة (b) قد أظهرت أفضل أداء حراري من الحالة ألتي تتضمن الترتيب (a) وأن التحسن في معيارية حساب الأداء قد بلغت (٦.٠٨٤٥%) عند استخدام رقم رينولدز (١٨٦٠٠) و (٦) زعانف عند اعتماد الترتيب (b).

جمهورية العراق
وزارة التعليم العالي والبحث العلمي
جامعة بابل
كلية الهندسة
قسم الهندسة الميكانيكية

تأثير الزعانف الداخلية باستخدام المائع النانوي على انتقال الحرارة خلال الجامع الحوضي للقطع المكافئ

رسالة
مقدمة إلى كلية الهندسة / جامعة بابل
كجزء من متطلبات نيل درجة
الماجستير في الهندسة /الهندسة الميكانيكية /القدرة

من قبل

مجاهد خلف بدر مزعل

اشراف

أ . د فاروق حسن علي

أ. د . م محسن شيخ الإسلام

2022